

**STUDIES ON OPTICAL AND X-RAY EMISSION
PROCESSES IN LASER PRODUCED PLASMA**

PRAMOD GOPINATH

**THESIS SUBMITTED
IN PARTIAL FULFILMENT OF THE REQUIREMENTS
FOR THE AWARD OF THE DEGREE OF
DOCTOR OF PHILOSOPHY**

**INTERNATIONAL SCHOOL OF PHOTONICS
COCHIN UNIVERSITY OF SCIENCE AND TECHNOLOGY
KOCHI 682 022, INDIA**

APRIL 2006

*Dedicated
to my
beloved parents*

***Studies on Optical and X-ray Emission Processes in
Laser Produced Plasma***

Ph.D Thesis in the field of Photonics

Author

Pramod Gopinath
Research Fellow
International School of Photonics
Cochin University of Science and Technology
Kochi 682 022, INDIA
E-mail: pramodmenon@gmail.com

Research Supervisor

Dr. V P N Nampoori
International School of Photonics
Cochin University of Science and Technology
Kochi 682 022, INDIA
E-mail: vpnnampoori@cusat.ac.in

International School of Photonics
Cochin University of Science and Technology
Kochi 682 022, INDIA
www.photonics.cusat.edu

April 2006

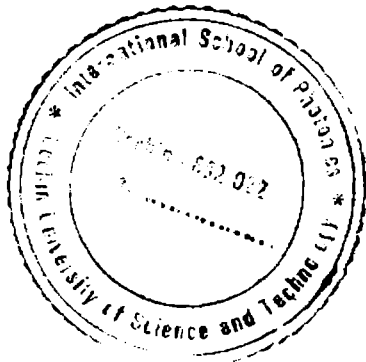
Front Cover


Photograph of Plasma induced in 2D-parabola thruster

Certificate

Certified that the research work presented in the thesis entitled **“Studies on Optical and X-ray Emission Processes in Laser Produced Plasma”** is based on the original work done by Mr. Pramod Gopinath under my guidance in the International School of Photonics, Cochin University of Science and Technology, Kochi 682 022 and has not been included in any other thesis submitted previously for the award of any degree.

Kochi
April 07, 2006





Dr. V.P.N. Nampoori
(Supervising Guide)

Declaration

Certified that the work presented in the thesis entitled, “**Studies on Optical and X-ray Emission Processes in Laser Produced Plasma**” is based on the original work done by me under the guidance of Prof. V.P.N. Nampoori in the International School of Photonics, Cochin University of Science and Technology, Kochi 682 022 and has not been included in any other thesis submitted previously for the award of any degree.

Kochi

April 07, 2006



Pramod Gopinath

Preface

Developments in laser technology over the past few years have made it possible to do experiments with focused intensities of 10^{19} - 10^{21} Wcm^{-2} . Short-pulse high-intensity lasers are able to accelerate protons and heavier ions to multi-MeV energies during their interaction with solid targets, gas jets and clusters. When such a laser radiation is focused at the intensity above 10^{15} Wcm^{-2} , local electric field strength will be almost equivalent to that within an atom. Hence, new nonlinear optical phenomena will be expected in the field of light matter interaction. Most of the research in the material interaction using high power lasers, especially related to plasma interaction, has been directed to the short pulse x-ray generation. Nanosecond laser interactions with solid targets also generate plasmas which emit radiation mainly in the optical region, the understanding of which is far from satisfactory. This thesis deals with a detailed study of some of the dynamical processes in plasmas generated by nanosecond and femtosecond lasers.

Ablation plasma is produced almost instantaneously when an intense laser beam interacts with a solid target. Due to its thermal pressure the plasma expands away along the target normal. This process of plasma formation and expansion is a highly complicated one and requires considerable amount of research for a proper understanding. The plasma plume contains different species characteristic of the target material like atoms, molecules, ions, clusters and free electrons. The presence of different species will be revealed by their characteristic line emissions. Attempts have been made to study the dynamics of these species in the plasma by optical emission spectroscopy, during the course of the thesis work. Plasma parameters like electron temperature and electron density have also been estimated from the line emissions.

X-rays are generated from the plasma produced by the interaction of an ultra-short laser with a solid target. The process of x-ray emission from laser generated plasmas is receiving greater attention by the research community. In this thesis, studies on hard x-ray emission from laser produced plasma are presented.

Results obtained during the course of the research have been organized into six chapters as described below.

Chapter 1 gives a brief introduction to laser produced plasma. The generation and evolution of plasma by the irradiation of lasers of different pulse duration and the different regimes in which they emit radiation are detailed in this chapter. The various models of the plasma expansion and the different equilibrium conditions in the plasma are explained along with some applications of laser produced plasmas.

A detailed description of the experimental techniques used in the study of the emission from plasma is given in **Chapter 2**. The Q-switched Nd:YAG laser is used to generate plasma from solid targets like silicon carbide and copper. The laser is focused on the surface of the target material kept in a vacuum chamber maintained at the required pressure. The optical emission from the plasma are recorded through a monochromator-photomultiplier tube assembly connected to a Boxcar Averager and interfaced with a computer. For the time-resolved studies of the plasma, a gated integrator is used. The signal is observed using a digital storage oscilloscope and the temporal profiles are acquired in a personal computer. In the case of X-ray emission studies, a Ti:Sapphire femtosecond laser is used and a crystal detector is used for detection of the x-ray. The signal is recorded using a multi-channel analyzer interfaced to a computer. The details of instrumentation are given in this chapter.

Silicon carbide is a ceramic material suited for high temperature, high power, high frequency and high radiation environment. The growth of SiC thin films through pulsed laser deposition has been receiving great attention in recent times among researchers. This evoked our interest to study the plasma generated on SiC targets by the irradiation of a laser, the details are described in **Chapter 3**. This plasma gives strong emission in the optical region. Different species present in the plasma have been identified. Species corresponding to the different ionized states of Si are observed in the plasma. Time-resolved and space-resolved studies of these species are discussed in this chapter. The emissions from such species also depend on the pressure in the chamber and the laser intensity. Electron density is estimated from the stark broadening parameter of Si I and electron temperature is estimated from the relative intensities of the different species in the plasma.

Studies on the emissions from the plasma generated from a Cu target is described in **Chapter 4**. At higher chamber pressures, the ionization of the ambient gas has been observed. The emissions corresponding to the ambient ionization show a spatial and temporal dependence of their intensities. Emissions corresponding to the excited neutral atom of Cu and singly ionized Cu are also observed and their dependence on the laser intensity is also studied. The velocities of the different emitters are obtained from their temporal profiles at various distances. It is also observed that during the initial phase of the plasma expansion the major emissions are due to the ionized species of the ambient molecules and only later does the characteristic emission of the target species evolve.

Chapter 5 describes the study of the x-ray emission from plasma generated by a femtosecond laser. The x-ray emission spectrum shows strong bremsstrahlung emission and is in the hard x-ray region. The temperatures obtained from the intensity–energy plot gives strong dependence on the polarization of the incident laser

light. The x-ray emission has been found to be due to the hot electron production in the femtosecond laser generated plasmas.

The final **Chapter 6** will summarize the results obtained and the general conclusion drawn there from. Brief account of the possible future directions in R & D activities in the area of laser produced plasma is also included in this chapter.

List of publications

Journals/Books

Thesis Related

1. Evolution dynamics of laser generated plasma from silicon carbide
Pramod Gopinath, Riju C Issac, Geetha K Varier, S S Harilal, Binoy Paul, V P N Nampoore and C P G Vallabhan
Optics and Optoelectronics, O P Nijhawan, A K Gupta, A K Mishra and Kehar Singh (Editors), Narosa Publishing House, New Delhi, p1044-1046 (1999)
2. Prompt electron emission and collisional ionization of ambient gas during pulsed laser ablation of silver
Riju C Issac, Geetha K Varier, **Pramod Gopinath**, S S Harilal, V P N Nampoore, C P G Vallabhan
Applied Physics A **67**, 557-561(1998)
3. Twin peak distribution of electron emission profile and impact ionization of ambient molecules during laser ablation of silver target
Riju C Issac, **Pramod Gopinath**, Geetha K Varier, V P N Nampoore, C P G Vallabhan
Applied Physics Letters **73**, 163-165 (1998)
4. Dynamics of laser produced silver plasma under film deposition conditions studied using optical emission spectroscopy
Riju C Issac, K Vasudevan Pillai, S S Harilal, Geetha K Varier, C V Bindhu, **Pramod Gopinath**, P Radhakrishnan, V P N Nampoore, C P G Vallabhan
Applied Surface Science **125**, 227-235 (1998)

5. Time resolved study of CN band emission from plasma generated by laser irradiation of graphite.
S S Harilal, Riju C Issac, C V Bindhu, **Pramod Gopinath**, V P N Nampoore, C P G Vallabhan
Spectrochimica Acta Part A **53**, 1527-1536 (1997)
6. Spatial and Pressure dependence of temporal profiles of Cu⁺ in laser produced plasma from Copper target
Pramod Gopinath, Binoy Paul, V P N Nampoore and C P G Vallabhan
(to be communicated)
7. Dynamics of the plasma generated by the irradiation of a nanosecond laser on Copper target.
Pramod Gopinath, Binoy Paul, V P N Nampoore, C P G Vallabhan
(to be communicated)

Other Fields

1. Nanosecond optical limiting response of sandwich-type neodymium dypthalocyanine in a co-polymer host
B. Aneeshkumar, **Pramod Gopinath**, Jayan Thomas, C. P. G. Vallabhan, V. P. N. Nampoore and P. Radhakrishnan
Synthetic Metals, **143**, 197-201 (2004)
2. Thermal lens spectrum of organic dyes using optical parametric oscillator
Achamma Kurian, K P Unnikrishnan, Sajan D George, **Pramod Gopinath**, V P N Nampoore and C P G Vallabhan,
Spectrochimica Acta Part A, **59**, 487-491 (2003)
3. Optical-limiting response of rare-earth metallo-phthalocyanine doped copolymer matrix.
B.Aneeshkumar, **Pramod Gopinath**, Jayan Thomas, C. P. G. Vallabhan, V. P. N. Nampoore, and P. Radhakrishnan,
Journal of Optical Society of America B **20** (7) 1486-1490 (2003)
4. Effect of pH on quantum yield of fluorescein using dual beam thermal lens technique
Achamma Kurian, Nibu A George, Sajan D George, K P Unnikrishnan, Binoy Paul, **Pramod Gopinath**, V P N Nampoore and C P G Vallabhan
Journal of Optics, **31**, 29-35 (2002)

5. **Studies on optical loss coefficient in plastic waveguides**
K Geetha, **Pramod Gopinath**, K P Unnikrishnan, S Thomas Lee, C P G Vallabhan, V P N Nampoore, P Radhakrishnan
Proceedings of SPIE-The International Society for Optical Engineering, **4904** (Optical Fiber and Planar Waveguide Technology II), 382-390 (2002)
6. **Study of energy transfer in organic dye pairs using thermal lens technique**
Achamma Kurian, K P Unnikrishnan, **Pramod Gopinath**, V P N Nampoore and C P G Vallabhan,
Journal of Nonlinear Optical Physics & Materials, **10**, 415-421 (2001)
7. **Realization of optical logic gates using thermal lens effect.**
Achamma Kurian, K P Unnikrishnan, **Pramod Gopinath**, Binoy Paul, V P N Nampoore and C P G Vallabhan ,
Proceedings of SPIE-The International Society for Optical Engineering, **4595** (Photonic Systems and Applications), 100-106 (2001)
8. **Nonlinear absorption and optical limiting in solutions of some rare earth substituted phthalocyanines**
K P Unnikrishnan, Jayan Thomas, Binoy Paul, **Pramod Gopinath**, V P N Nampoore, C P G Vallabhan
Journal of Nonlinear Optical Physics & Materials, **10**, 113-121 (2001)

Conferences

1. **Studies on laser induced plasma from Cu-Al multiple target**
Pramod Gopinath, Binoy Paul, Dilna S, Sreeja R, V P N Nampoore, C P G Vallabhan
Proc. National Laser Symposium (Post Deadline Papers), December 19-21, 2001, CAT, Indore
2. **Dynamics of the ambient molecules during laser ablation of a solid target.**
Pramod Gopinath, Binoy Paul, K P Unnikrishnan, V P N Nampoore, C P G Vallabhan
Proc. PLASMA-2000, 5-8 December 2000, Saha Institute of Nuclear Physics, Calcutta
3. **Spectral Emission from Cu⁺ in Laser Produced Copper Plasma-Spatial and Pressure Dependence**
Pramod Gopinath, Binoy Paul, V P N Nampoore, C P G Vallabhan
Proc. National Laser Symposium, 15-17 December 1999, University of Hyderabad

4. Collisional ionization of ambient molecules during laser ablation of Copper
Pramod Gopinath, Riju C Issac, Binoy Paul, Geetha K Varier, V P N Nampoori, C P G Vallabhan
Proc. National Laser Symposium, 14-16 December 1998, IIT Kanpur

5. Temporal variations of electron density and temperature in a laser produced plasma from silicon carbide
Pramod Gopinath, Riju C Issac, Geetha K Varier, C V Bindhu, S S Harilal, V P N Nampoori, C P G Vallabhan
Proc. National Laser Symposium, 10-12 December, 1997, PRL, Ahmedabad

6. Spatio-temporal evolution of laser ablated SiC plasma
Pramod Gopinath, Riju C Issac, S S Harilal, Geetha K Varier, C V Bindhu, V P N Nampoori, C P G Vallabhan
Proc. XII National Symposium on Plasma Science & Technology, 2-5 December, 1997, IPR, Gandhinagar.

Acknowledgements

It is with profound gratitude that I express by sincere thanks to my supervising guide, Prof. V.P.N.Nampoori, for the motivation and support, which ultimately led to the completion of this thesis.

I am grateful to Prof. G. Ravindrakumar of Tata Institute of Fundamental Research, Mumbai for allowing me to carry out the X-ray emission studies in his group.

I sincerely acknowledge the support, advice and inspiration given to me by Prof. C P Girijavallabhan, all through my research career at CUSAT. I am grateful to Prof. V M Nandakumaran, Prof. P Radhakrishnan, Prof. R Pratap and Mr. M Kailasnath for their timely support and advice.

It is a pleasure to express my sincere thanks to my seniors, Dr. Riju C Issac, Dr. S S Harilal, Dr. Geetha K Varier, Dr. Bindhu C V and Dr. Shelly M John, who had helped me a lot during the initial stages of my research program.

I extend my sincere thanks Dr. Rajeev P P, Dr.Sudeep Banerjee, Dr. Arvinder Sandhu and Dr. Vinod Kumarappan, of TIFR for helping me in carrying out the X-ray emission studies.

I sincerely thank Dr. Deepthy for the support, encouragement and help given to me during the final stages of this work.

My sincere thanks to all my friends and colleagues at ISP, Dr. Binoy, Dr. Aneesh, Dr. Prasanth, Dr. Unnikrishnan, Dr. Jayan Thomas, Dr. Ajith kumar, Dr. Santhosh

Chidangil, Dr. Nibu, Dr. Bindu Murali, Jibu, Premkishore, Dr. Sajan, Dr. Achamma, Dr. Annieta, Dr. Thomas Lee, Dr. Sureshkumar, Dr. Pravitha, Dr. Rajesh S. , Geetha, Santhi, Rekha, Dilna, Sr. Ritty, Rajesh M, Vinu, Manu, Jijo, Thomas, Dann, Lyjo, Litty, Jayasree, Sheeba, Parvathy, Saritha and Sajeev for all their help and support. I would also like to thank Ms. Hema B Nair, Ms. Maya and all other administrative staff members of ISP for their timely help.

I remember with deep sense of gratitude, the support from my parents, brothers Praveen and Premjith, in-laws and all other relatives. I have no words to express my gratitude to my wife Kala and my son Adithya, for their encouragement and patience during the successful completion of this work.

Thanks to the Almighty God

Pramod Gopinath

Contents

CHAPTER 1: LASER PRODUCED PLASMA -AN INTRODUCTION	1	
1.1	Introduction	1
1.2	Basic Plasma Physics	3
1.2.1	Plasma in nature	3
1.2.2	Definition of Plasma	4
1.2.3	Debye shielding	4
1.2.4	Plasma oscillations	5
1.2.5	Temperature and equilibrium	7
1.2.6	Local thermodynamic equilibrium	8
1.2.7	Coronal equilibrium	9
1.2.8	Fundamental emission processes in plasma	10
1.3	Laser ablation models	11
1.4	Plasma expansion model	13
1.5	Absorption mechanisms	16
1.5.1	Inverse bremsstrahlung absorption	16
1.5.2	Resonance absorption	17
1.5.3	Brunel effect	19
1.6	Interaction of ultra-short pulses with matter	20
1.7	Hot electrons	22
1.8	Femtosecond interactions	23
1.9	Laser plasma X-ray sources	24
	References	26

CHAPTER 2: EXPERIMENTAL TECHNIQUES	31
2.1 Introduction	31
2.2 Optical emission studies	32
2.2.1 Laser source	32
2.2.2 Plasma chamber and vacuum system	33
2.2.3 Monochromator-PMT assembly	33
2.2.4 Boxcar Averager / Integrator	34
2.2.5 Digital storage oscilloscope	35
2.2.6 Experimental setup	35
2.3 X-ray emission studies	37
2.3.1 Laser system	37
2.3.2 Experimental setup	39
2.4 Summary	42
References	43

CHAPTER 3: LASER PRODUCED PLASMA FROM SILICON CARBIDE	45
3.1 Introduction	45
3.2 Experimental	48
3.3 Results and Discussion	48
3.3.1 Identification of different species	48
3.3.2 Space resolved studies	52
3.3.3 Time of flight studies	54
3.3.4 Laser energy dependence	58
3.3.5 Pressure dependence	59
3.3.6 Electron Density Measurement	63
3.3.7 Electron Temperature Measurement	66
3.4 Summary	69
References	70

CHAPTER 4: LASER PRODUCED PLASMA FROM COPPER TARGET – SPECTRAL STUDIES	73
4.1 Introduction	73
4.2 Experimental	77
4.3 Results and Discussion	78
4.3.1 Spatial variation of Cu I	78
4.3.2 Spatial variation of Cu II	82
4.3.3 Pressure dependence of Cu II	87
4.3.4 Ionization of the ambient molecule	92
4.4 Summary	95
References	96
CHAPTER 5: STUDIES ON HARD X-RAY EMISSION FROM LASER PRODUCED PLASMA	99
5.1 Introduction	99
5.2 Experimental	103
5.3 Results and Discussion	105
5.4 Summary	115
References	116
CHAPTER 6: CONCLUSION AND FUTURE SCOPE	119

Chapter 1

Laser Produced Plasma - An Introduction

1.1 Introduction

The past few years have witnessed a dramatic upsurge in short pulse technology with its concomitant high achievable peak powers. This has been brought about the development of chirped-pulse amplification(CPA) [1,2]. Now table top terawatt lasers are to be found in many universities and national laboratories, and the first petawatt laser has been developed at Lawrence Livermore National Laboratory in USA, with others being proposed elsewhere. With these high power lasers, focused intensities between 10^{19} - 10^{21} W cm⁻² have been achieved [3]. These lasers allow the creation of laboratory plasmas with solid-state density and unusual properties (quite unlike, for example, classical laser-produced plasmas, which are produced using pulses of nanosecond duration). It is possible to produce states of the medium with relaxation times (e.g., time of expansion, collision time, life time of excited states, etc.) exceeding the laser pulse duration. The reason for the current interest in high intensity laser-plasma interactions is their relevance to a number of diverse fields e.g., advanced concepts of plasma high energy particle accelerators [4], laser-induced nuclear photophysics, astrophysics and, inertial confinement fusion [5]. The question of carrying out nuclear physics using laser source has been addressed by a number of authors using high repetition rate, femtosecond lasers [6-8], and by using single shot

Chapter 1

ultrahigh intensity lasers such as the petawatt laser at the NOVA facility and VULCAN [9,10]. There have been reports of photonuclear reactions using the γ -ray beams generated by the bremsstrahlung from the energetic electrons produced by the 50 TW VULCAN at intensities of about 10^{19} W cm⁻²[11].

At low laser energy densities, small quantities of neutral and ionized species become detectable with the most sensitive diagnostics. Repeated irradiation of the surface, at laser energy densities above the threshold limit, results in a significant material removal and the appearance of the luminous plasma plume. Pulsed laser deposition of thin films is a major application of the plasma produced by conventional lasers with pulse width in the nanosecond and picosecond regime. The processes taking place at the target have been investigated, both theoretically and experimentally, by many researchers and are available in literature [12-17]. Thermal effects play a major role in pulsed laser ablation and it has been extensively studied by Kelly et. al [18]. At comparatively low laser intensities, the vapourization from the extreme outer surface and boiling from an extended near surface region take place whereas at high laser intensities, additional effects like phase explosion [18-22] and sub surface heating [23]. A large number of model calculations are made for the study of laser-matter interaction processes [24-29]. These studies include models of laser-solid interaction, plume ionization and heating through laser absorption, hydrodynamic and collisional descriptions of the plume transport, dynamics of cluster formation, effect of ambient gas on plume evolution, etc. Different diagnostic tools have been used to investigate the laser produced plasma like time-of-flight mass spectroscopy [30], quadrupole mass spectroscopy [31], Ion probes [32], optical spectroscopy [33,34], etc

In order to understand the physics behind the laser-matter interaction, we will look at the basics of plasma physics in the following sections.

1.2 Basic Plasma Physics

1.2.1 Plasma in nature

It is often been said that 99 % of the matter in the universe is in the plasma state; that is, in the form of an electrified gas with the atoms dissociated into positive ions and negative electrons. We live in the 1% of the universe in which plasmas do not occur naturally. The reason for this is seen from the Saha equation, which tells us the amount of ionization to be expected in a gas in thermal equilibrium:

$$\frac{n_i}{n_n} \approx 2.4 \times 10^{21} \frac{T^{3/2}}{n_i} e^{-U_i/kT} \quad (1.1)$$

Here n_i and n_n are respectively, the density of ionized atoms and of neutral atoms, T is the gas temperature in K, k is the Boltzmann's constant, and U_i is the ionization energy of the gas. For ordinary air at room temperature, we may take $n_n \approx 3 \times 10^{25} \text{ m}^{-3}$, $T= 300\text{K}$ and $U_i = 14.5 \text{ eV}$. The fractional ionization $n_i / (n_n + n_i) \approx n_i / n_n$ is very low:

$$\frac{n_i}{n_n} \approx 10^{-122} \quad (1.2)$$

As the temperature is raised, the degree of ionization remains low until U_i is only a few times kT . Then n_i / n_n rises abruptly, and the gas is in the plasma state. Further increase in temperature makes n_n less than n_i and the plasma eventually becomes fully ionized. This is the reason plasma exist in astronomical bodies with temperature of millions of degrees, but not on the earth. The natural occurrence of plasmas at high temperatures is the reason for the designation "the fourth state of matter".

Chapter 1

1.2.2 Definition of Plasma

A plasma is defined as a quasineutral gas of charged and neutral particles which exhibits collective behaviour. In a plasma, as the charges move around, they can generate local concentrations of positive and negative charge, which give rise to electric fields. Motion of charges also generates currents, and hence magnetic fields. These fields affect the motion of other charged particles far away. Therefore, elements of plasma exerts a force on one another even at large distances i.e., motions depend not only on local conditions but also on the state of the plasma in the remote regions as well. This behaviour is termed as the “collective behaviour” of plasma. Plasmas are characterized by an overriding tendency to be neutral. The number of positive and negative charges per unit volume cannot be exactly equal; else there would be no electric fields at all. Since the opposite charge densities need differ only by a very small quantity to create the electric field, for all purposes these densities can be treated as being equal. This approximation is known as the “quasineutrality”. The plasma is “quasineutral”, i.e., neutral enough so that one can take

$$n_i \approx n_e \approx n \quad (1.3)$$

where n_e is the electron number density, n_i is the ion density and n is a common density called the plasma density.

1.2.3 Debye Shielding

A fundamental characteristic of the behavior of a plasma is its ability to shield out electric potentials that are applied to it. When a positively charged object is placed in a plasma, the mobile electrons are attracted to it and form an electron cloud covering the charge; similarly, a negatively charged object will repel electrons, leaving an ion

cloud for shielding. The thickness of these clouds is of the order of the Debye length λ_D , defined by

$$\lambda_D = \left(\epsilon_0 kT / ne^2 \right)^{1/2} \quad (1.4)$$

The Debye length does provide a measure of the distance over which the influence of an individual charged particle is dominant. If the dimensions L of a system are much larger than λ_D , then whenever local concentrations of charge arise or external potentials are introduced into the system, these are shielded out in a distance short compared with L , leaving the bulk of the plasma free of large electric potentials or fields. A criterion for an ionized gas to be a plasma is that it be dense enough that λ_D is much smaller than L . The picture of Debye shielding is valid only if there are enough particles in the charge cloud. Clearly, if there are only one or two particles in the sheath region, Debye shielding would not be a statistically valid concept. The number of particles, N_D in the “Debye sphere” is given by [35]

$$N_D = n \frac{4}{3} \pi \lambda_D^3 = 1.38 \times 10^6 T^{3/2} n^{-1/2} \quad (\text{T in K}) \quad (1.5)$$

In addition to $\lambda_D \ll L$, “collective behaviour” requires $N_D \gg 1$.

1.2.4 Plasma oscillations

Just as the Debye length represents a typical length for collective action, the plasma frequency or rather, its reciprocal – is a typical time. The plasma frequency is the resonance frequency for collective oscillations of the electrons about their equilibrium positions. If we consider all the electrons in a slab of plasma, of unit cross-section and length L , to be displaced simultaneously from their equilibrium positions by a distance x (where $x \ll L$), the amount of displaced charge is $e n_e x$. The slab now has a surface charge $+\sigma$ at one end and $-\sigma$ at the other, where $\sigma = e n_e x$. The electric field produced within the slab by this charge is σ/ϵ_0 . Each electron therefore

Chapter 1

experiences a force $e \sigma / \epsilon_0$, or $e^2 n_e x / \epsilon_0$, and its equation of motion, if one neglects collisions and thermal energy is,

$$M\ddot{x} + \frac{e^2 n_e}{\epsilon_0} x = 0 \quad (1.6)$$

This is the equation of undamped simple harmonic motion and has the solution

$$x = a \sin \omega_p t \quad (1.7)$$

where the angular frequency ω_p is given by

$$\omega_p^2 = \frac{e^2 n_e}{\epsilon_0 m} \quad (1.8)$$

The plasma frequency in Hz is given as

$$\nu_p = \frac{\omega_p}{2\pi} = \left(\frac{e^2 n_e}{4\pi^2 \epsilon_0 m} \right)^{1/2} \quad (1.9)$$

where n_e is in m^{-3} . For the laboratory plasmas, with n_e in the range 10^{20} - 10^{24} m^{-3} , we have ν_p between 10^{11} and 10^{13} Hz, which puts the plasma frequency in the far infrared region. The plasma oscillation is not just a resonance oscillation of one electron bound to a nucleus, of the type dealt with in classical absorption/dispersion theory; it is a collective motion of free electrons, and the restoring force exists only because all the electrons are displaced together. This collective behaviour tends to disappear if the electron motions are randomized by collisions, a necessary condition for which is

that the time between collisions exceeds the oscillation period, or the collision frequency ν_C be much smaller than ν_p .

1.2.5 Temperature and equilibrium

The equilibrium distribution of energy among the different states of an assembly of particles is determined by the parameter T defining the temperature for that particular form of energy. A plasma is said to be in thermal equilibrium when electrons, ions and radiation are strongly coupled to each other and share the same temperature. The distributions appropriate to kinetic, excitation and ionization energy are given by Maxwell, Boltzmann and Saha respectively and the distribution of radiative energy is governed by the Planck function. The Maxwellian distribution of electron velocities is given by

$$f_e = n_e \left(\frac{m}{2\pi kT_e} \right)^{3/2} \exp \left[-\frac{mv^2}{2kT_e} \right] \quad (1.10)$$

The populations N_u and N_l of two ionic bound levels, u and l, with statistical weights g_u and g_l , respectively, are given by the Boltzmann equation

$$\frac{N_u}{N_l} = \frac{g_u}{g_l} \exp \left[-\frac{\Delta E_{u,l}}{kT} \right] \quad (1.11)$$

where $\Delta E_{u,l}$ is the energy difference between the two levels and T is the thermodynamic temperature of the plasma. The population of ionization states is given by the Saha equation

$$\frac{N(Z+1)n_e}{N(Z)} = \frac{g_0(Z+1)}{g_0(Z)} \left[\frac{2\pi m kT}{h^2} \right]^{3/2} \exp \left[-\frac{\chi_0(Z)}{kT} \right], \quad (1.12)$$

Chapter 1

which gives the ratio between the population densities of two ionization states with charges Z and $Z+1$, and statistical weights $g_0(Z)$ and $g_0(Z+1)$, respectively. The subscript '0' refers to the ground state of the ion and, in TE, it is, by far, the most populated one; $\chi_0(Z)$ is the ionization potential of the ion with charge Z , n_e is the electron density, m is the electron mass and h is the Planck's constant.

Complete thermodynamic equilibrium exists when all forms of energy distribution mentioned above are described by the same temperature parameter. Statistically, for every photon emitted, a photon of the same frequency must be absorbed, for every excitation by electron collision (collision of the first kind) there must be a de-excitation by electron collision (collision of the second kind), etc. In practice this situation cannot be fully realized. However large and dense the plasma, photons must leak out from the edges of the plasma. A close approach to thermodynamic equilibrium requires that such losses be small compared to the total energy.

1.2.6 Local thermodynamic equilibrium

The form of energy most likely to be out of balance with the others is the radiation energy, since radiative equilibrium requires the plasma to be optically thick at all frequencies. Many plasmas can be described by a state known as local thermodynamic equilibrium, or LTE, in which it is possible to find a temperature parameter for every point that fits the Boltzmann and Saha relations for the populations of the excited and ionic states and the Maxwell distribution of velocities among the electrons. The criterion for LTE is that collisional processes must be much more important than radiative, so that the shortfall of radiative energy does not matter. More precisely, an excited state must have a much larger probability of de-

excitation by an inelastic collision than by spontaneous radiation. This requires a high electron density. In numerical form the criterion for LTE is given as

$$n_e \gg 1.6 \times 10^{12} T^{1/2} (\Delta E)^3 \text{ cm}^{-3} \quad (1.13)$$

where T is the electron temperature in K and ΔE is the energy difference in eV between the state in question and any neighbouring state to which it can make transitions [36].

1.2.7 Coronal equilibrium

In the absence of LTE it is still possible to estimate relative populations, but only if the relevant collisional cross-sections and radiative transition probabilities are known. The next most important approximation after LTE is described as coronal equilibrium, since it is applicable to the sun's corona where temperature is high ($\sim 10^6$ K) and electron density is low ($\sim 10^8 \text{ cm}^{-3}$). In this case collisional excitation and ionization are balanced respectively by radiative de-excitation and recombination. By comparing the ionization and recombination rates one obtains the basic equation which governs ionization processes in coronal equilibrium

$$n_e N(Z) S(T_e, Z, 0) = n_e N(Z+1) \alpha_{fb}(T_e, Z+1, 0), \quad (1.14)$$

where $S(T_e, Z, 0)$ is the collisional ionization coefficient and $\alpha_{fb}(T_e, Z+1, 0)$ is the radiative recombination coefficient. The above equation leads to the important result that, in a coronal plasma, the population of the ionization state does not depend upon the electron density and is given by

$$\frac{N(Z+1)}{N(Z)} = \frac{S(T_e, Z, 0)}{\alpha_{fb}(T_e, Z+1, 0)} \quad (1.15)$$

Chapter 1

Once again it is assumed that most of the ions are in their ground state and therefore both the ion populations and the coefficients are relative to the ground level. Also, it is assumed that electrons have a Maxwellian velocity distribution with a characteristic temperature, T_e .

1.2.8 Fundamental Emission Processes in Plasma

Once the plasma has gained thermal energy, radiation is emitted via free-free, free-bound and bound-bound mechanisms. In the first mechanism, free electrons interacting with the Coulomb potential of the ions, radiate in a continuum electromagnetic spectrum, giving rise to the so-called bremsstrahlung emission. The second process, known as recombination, is the transition from initial free electron states to bound electron states and produces a continuum electromagnetic spectrum. The third emission mechanism produces a line spectrum as a result of transitions between discrete (bound) levels of ionized atoms [37].

Free-free transitions correspond to loss or gain of energy by an electron in the field of an ion. This type of radiation is to be expected classically from any charged particle constrained to follow a curved path, since the particle is necessarily accelerated in the process, it is otherwise known as bremsstrahlung, meaning 'braking radiation'. There are no characteristic edges associated with it. For $h\nu \gg kT$ its importance increases with increasing wavelength, small energy changes being more probable than large ones, and at long wavelengths it approaches the black body function.

Transfers between different ionic states for both atomic and molecular species are classified under the name of bound-free transitions. Transitions between a bound and an unbound, or free, state give rise in both emission and absorption to radiation continua extending in the short wavelength direction from the line series

limits. In absorption a radiative transition from a bound state to a free state is known as photoionization. The inverse process of radiative recombination occurs when an ion captures an electron and makes a radiative transition to a bound state. This so-called bound-free continuum is characterized by discontinuities or edges in both the absorption and emission coefficients whenever $h\nu$ becomes large enough to reach the next bound level.

When an atom or ion makes a transition from one bound state to another of lower energy, the energy of the emitted photon is well defined. In the absence of perturbations, the transition gives rise to a spectral line whose profile depends upon the spontaneous life time of the upper state, and on the distribution of velocities of the emitting atoms, which causes a distribution of Doppler shifts. Collisions, electric fields and magnetic fields may perturb the initial and final states of the emitting atoms and the perturbations affect the spectral line profile. In a cool partially ionized gas, much of the line emission is in the infrared and visible regions of the spectrum. As the temperature increases, atoms can be raised to more energetic excited states and thus tend to emit lines of shorter wavelengths. At around 10 eV nearly all the atoms will be ionized and multiple ionizations of many-electron atoms occur. These result in the emission of shorter wavelengths in the UV and x-ray regions of the spectrum.

1.3 Laser ablation models

Pulsed laser ablation is classified according to the interaction processes, the heating rate and the laser power density. The various processes include normal vapourization, normal boiling, phase explosion, sub-surface heating, etc. The phenomenon of vapourization is predominant when the laser pulse duration is in microseconds or longer and when the laser power density is $\leq 10^6 \text{ W cm}^{-2}$. The electron phonon energy transfer takes place on a time scale of ~ 0.1 picoseconds and the absorbed energy is rapidly converted into heat. Heat dissipation is very fast compared to the

Chapter 1

duration of the laser pulse. Normal vapourization can operate essentially at any fluence and pulse length. The target undergoes normal vapourization from the extreme outer surface. Nucleation in the vapour plume does not enter into the picture. Since the vapour pressure is non-zero at all temperatures exceeding 0 K, it follows that for normal vapourization the surface temperature is not fixed.

In the second type, which requires that the pulse length be sufficiently long for heterogeneous bubble nucleation to occur, the target undergoes normal boiling from a zone extending from the surface to a depth related to the absorption length. In this case, the surface temperature is fixed and the temperature gradient at and beneath the surface is zero.

The third type, called phase explosion, requires that the laser fluence be sufficiently high and the pulse length sufficiently short that the target reaches $\sim 0.90 T_{ic}$ (T_{ic} being the thermodynamic critical temperature) at and beneath the surface. At laser intensities of the order of GW cm^{-2} or higher, obtained by nanosecond or even shorter laser pulses, instead of the combined effect of melting and vapourization, the process of phase explosion occurs. Homogeneous bubble nucleation therefore occurs, and the target makes rapid transition from superheated liquid mixture to a mixture of vapour and equilibrium droplets. As with boiling one can expect that at and beneath the surface, the temperature gradient will be zero. Much of the historical work were done by Martynyuk [22,38,39] and by Fucke and Sydel [40,41], and the terms *phase explosion* and *explosive boiling* were both introduced.

The subsurface heating model was apparently first postulated in 1972 in the work by Dabby and Paek[23], was first applied by Gagliano and Paek [42], and was reinvestigated numerically by various authors. The basis of this model is that a laser pulse heats the near surface region but, as a result, atoms are vapourized from the surface and carry away heat. The target therefore losses the ideal exponential

temperature profile and develops a modified profile such that it is hotter by as much as 3000 K just beneath the surface [43]. As a result the pressure is much greater beneath the surface and a type of explosion, leading to similar results as phase explosion, occurs.

1.4 Plasma expansion model

When the radiation from an intense laser with sufficient energy is focused on a target, plasma is generated. This process of laser induced optical breakdown involves radiative heating of free electrons within the solid by the intense laser pulse. The electrons couple very strongly to the incident radiation and by absorbing the energy; they are strongly accelerated, and collide with ions, neutral atoms and molecules. This process is known as inverse bremsstrahlung. The energy absorbed by the electrons increase their kinetic energy in turn increase the electron temperature. As the ionization is increased further, the electron density increase to such a value that, the plasma becomes opaque to the laser radiation and hence it never reaches the target to generate plasma and the target material becomes decoupled from laser radiation. Because of the heating which follows the absorption of energy by inverse bremsstrahlung, the plasma is driven rapidly away from the target surface; resulting in the decrease of electron density making the laser reach the target.

The effusion model assumes that the particles of the target material fly freely from the target surface. During expansion into the ambient, the atoms and ions attain very high velocities of the order of 10^5 - 10^6 cm s⁻¹. The time taken by these species to travel specific distances above the target surface is a measure of the velocity of these species. For truly thermal emission at low number densities, when the particles disperse without collisions, the velocity distribution function has the form of a “half-range” Maxwellian i.e. the velocities normal to the surface take only positive values, and there is no recondensation at the surface. At higher number densities, collisions

Chapter 1

amongst the emitted particles lead to an altered velocity distribution function which is commonly approximated as being a “full-range” Maxwellian in a center-of-mass coordinate system. Effectively, the exponential part of the distribution function for the velocity component normal to the surface (v_x) changes from

$$\exp\left(-\frac{mv_x^2}{2kT_s}\right), \quad v_x \geq 0, \quad (1.16)$$

to

$$\exp\left(-\frac{m(v_x - u_k)^2}{2kT_k}\right), \quad -\infty < v_x < \infty, \quad (1.17)$$

where v_x is still the x-velocity as seen from the target surface; u_k , the centre-of-mass velocity similar to the velocity of sound; T_k is about 70% of T_s for a monatomic species. The Knudsen layer is defined as the region within a few mean free paths of the target surface in which the change from the first equation to the second occurs as a highly non-equilibrium collision process. For even higher number densities, the downstream boundary of the Knudsen layer acts like the throat of a nozzle. Still further collisions occur, leading to the well-known phenomena of the adiabatic expansion, which is described by a relation similar to the second equation but with u_k exceeding the velocity of sound and the temperature being less than T_k . Moreover when Knudsen layer formation is a highly nonequilibrium collision process, unsteady adiabatic expansion is an equilibrium phenomenon. Beyond Knudsen layer boundary the system is better described by the formalism of unsteady adiabatic expansion. At still farther distances, in situations with three spatial dimensions, or in situations with short enough pulse widths, a stage is reached where there is no further interaction, the so called freezing length.

The ablated species expands into vacuum adiabatically due to the large pressure difference between the ablation spot and vacuum. The scenario is slightly different when the expansion is in the presence of an ambient gas [44-50]. The interaction of the plasma plume with the ambient gas includes the formation of a shock front [51-54]. In shock wave model of plasma expansion, the ejected material acts like a piston which compresses the gas ahead of it and forms a shock wave. Most of the gas phase reactions happen at the shock layer [55]. The shock wave is basically a density discontinuity which moves very rapidly compressing the ambient molecules in front of the wave to form a denser layer thereby generating high temperatures. The position of the shock front (R_{sw}) within the assumptions pertaining to strong explosions is given by

$$R_{sw} \approx \xi \left[\frac{Et^2}{\rho(\infty)} \right]^n \tag{1.18}$$

where $\xi \approx 1$. The values of both ξ and n depend on the symmetry of the problem. $n= 1/5$ for spherical expansion, $n = 1/4$ for cylindrical symmetry for the shock front and $n=1/3$ for plane waves, $\rho(\infty)$ is the undisturbed density of the ambient gas and E is the sum of the kinetic energy of the shock wave and the thermal energy of the vapour plume.

A classic drag-model shows better agreement at low pressures and early times. The ejected pulse of ablation products is regarded as an ensemble that experiences a viscous force proportional to its velocity through the background gas. The equation of motion, $a = -\beta v$, giving

$$v = v_0 e^{-\beta t} = v_0 - \beta z \tag{1.19}$$

$$x = x_f (1 - e^{-\beta t}) \tag{1.20}$$

where β is the slowing coefficient and $x_f = v_0 / \beta$ is the stopping distance of the plume. The drag model predicts that the plume will eventually come to rest, due to resistance from collisions with the background gas, while shock model predicts continued propagation.

1.5 Absorption mechanisms

As the laser light propagates in the plasma several mechanisms can account for transfer of energy from the electromagnetic wave to the plasma, according to the interaction regime.

1.5.1 Inverse bremsstrahlung absorption

The electrons, while oscillating under the action of the laser electric field, collide with the ions giving rise to transfer of electromagnetic energy to the plasma. The fraction of absorbed laser energy after a propagation over a distance L in a uniform plasma is given by

$$\alpha_{ab} = 1 - \exp[-k_{ib}L], \quad (1.21)$$

where,
$$k_{ib} = 3.10 \times 10^7 Z n_e^2 \ln \Lambda \omega_L^{-2} \left[1 - \left(\frac{\omega_p}{\omega_L} \right)^2 \right]^{-1/2} (T_e (eV))^{-3/2} \text{ cm}^{-1}$$

(1.22)

is the inverse bremsstrahlung coefficient, i.e. the imaginary part of the laser wave vector k , and $\ln \Lambda$ is the Coulomb logarithm for the electron-ion collisions.

It is clear that collisional absorption is higher for lower temperatures, higher densities, higher Z plasmas. Consequently, in the case of interaction with inhomogeneous plasmas most of the absorption takes place in the proximity of the critical density n_c , provided that the density scale length is not too short. In fact, several processes can lead to shortening of the density profile near n_c thus strongly reducing inverse bremsstrahlung absorption. On the other hand, for sufficient large scale lengths, strong absorption may occur in the well underdense plasma preventing laser energy from reaching the critical density layer.

At high laser intensities the electron-ion collision frequency is dominated by the oscillatory motion of the electrons in the laser electric field. In fact, the effective electron velocity is in this case given by

$$v_{eff} = \sqrt{v_{th}^2 + (eE_L/m\omega_L)^2}, \quad (1.23)$$

where E_L is the laser electric field. Due to the strong dependence of the cross-section of electron-ion collisions on the electron velocity, $\sigma_{ei} \approx 4\pi Z^2 e^4 m^{-2} v_{th}^{-4}$, the inverse bremsstrahlung coefficient reduces to the effective value

$$k_{ib}^{eff} = k_{ib} \left[1 + \frac{3}{2} \left(\frac{v_q}{v_{th}} \right)^2 \right]^{-1} \quad (1.24)$$

where $v_q = eE_L/m\omega_L$ is the electron quiver velocity.

1.5.2 Resonance absorption

Laser radiation obliquely incident on a plasma with a component of the electric field in the plane of incidence can excite resonant longitudinal plasma oscillations at the

Chapter 1

critical density surface. The damping of the excited electron waves lead to conversion of electromagnetic laser energy into thermal energy. The turning point for a light wave impinging on a plasma density gradient at an incident angle θ , occurs at a density n_e^{tp} given by the classical theory

$$n_e^{tp}(\theta) = n_e \cos^2(\theta) \quad (1.25)$$

Therefore, the component of laser electric field parallel to the density gradient has to tunnel through the plasma to reach the critical density region and drive resonantly electron plasma waves. Consequently, there is an optimum angle of incidence that maximizes the absorption. In fact, for $\theta \rightarrow \pi/2$ the electromagnetic wave has to tunnel through too large distance and the plasma wave is not driven efficiently. On the other hand, for $\theta \rightarrow 0$ the component of laser electric field parallel to the density gradient vanishes and once again the electron wave is not driven efficiently. The resonance absorption coefficient maximizes at $\approx 50\%$ for an angle of the incidence given by $\sin(\theta) \approx 0.8(\omega_L L/c)^{-1/3}$, where L is the density scalelength and ω_L is the laser angular frequency[56].

There is a simple way to show the dependence of the resonance absorption on laser polarization. By expressing the plasma dielectric constant in terms of the electron density,

$$\epsilon = 1 - \left(\frac{\omega_p}{\omega_L}\right)^2 = 1 - \frac{n_e}{n_c} \quad (1.26)$$

The Poisson equation in a plasma, $\bar{\nabla} \cdot (\epsilon \bar{E}) = 0$, can be written as follows:

$$\bar{\nabla} \cdot \bar{E} = -\frac{\bar{\nabla} \epsilon \cdot \bar{E}}{\epsilon} = \frac{\bar{\nabla} n_e \cdot \bar{E}}{n_c - n_e} \quad (1.27)$$

On the other hand, $\bar{\nabla} \cdot \bar{E} = -4\pi e \delta n_e$, where δn_e is the electron density perturbation of the plasma wave. By equating the right member of the last two equations, we have

$$\delta n_e = \frac{\bar{\nabla} n_e \cdot \bar{E}}{4\pi e (n_e - n_c)} \quad (1.28)$$

The last equation shows in particular that ‘s’ polarized laser radiation, for which $\bar{\nabla} n_e \cdot \bar{E} = 0$, cannot drive langmuir waves, while for ‘p’ polarized radiation, for which $\bar{\nabla} n_e \cdot \bar{E} \neq 0$, the electron density perturbation of the plasma wave increases when the critical density is approached.

1.5.3 Brunel effect

Very intense laser radiation, obliquely incident on a metallic surface or a sharply bounded overdense plasma, pulls electrons into the vacuum and drives them back into the plasma with a velocity

$$v_q = \frac{eE_L}{m\omega_L} \quad (1.29)$$

Since the electric field inside the plasma is zero, one can see that a large part of the kinetic energy acquired by the electrons in vacuum is lost when electrons re-enter the plasma [57]. This mechanism is more efficient than the usual resonance absorption for $v_q/\omega_L > L$, L being the density scale length. Since the absorption due to the Brunel effect is proportional to v_q/c , it plays an important role at relativistic laser

Chapter 1

intensity and is of particular interest in femtosecond interactions where sharply bounded plasmas are achieved

1.6 Interaction of ultra-short laser pulses with matter

A very high electric field amplitude can be achieved in the focal spot, much higher, for example, than the magnitude of atomic field (e.g., the field acting on an electron in the first Bohr orbit of the hydrogen atom)[58]:

$$E_a = e/r_b^2 = m_e^2 e^5 \hbar^{-4} = 5.1 \times 10^9 \text{ V cm}^{-1}, \quad (1.30)$$

where, $r_b = \hbar^2/m_e e^2 = 5 \times 10^{-9} \text{ cm}$ is the Bohr radius. This high electric field amplitude can be achieved in a linearly polarized laser beam with intensity

$$I_a = cE_a^2/8\pi = 3.4 \times 10^{16} \text{ W cm}^{-2}. \quad (1.31)$$

Laser – matter interactions occurring at intensities $I > I_a$ will result in direct ionization of the material and the production of highly stripped ions. The parameter characterizing the ionization process in a strong field is known as the Keldysh parameter [59]. It equals the ratio of the ionization potential I_i to the electron oscillation energy in a laser electric field ϵ_{os}

$$\Gamma = I_i / 2\epsilon_{os} \quad (1.32)$$

For ionization of a K-shell electron from an atom with charge Z , one obtains $I_i = Z^2 I_H$, where $I_H = m_e e^2 / 2 \hbar^2$ is an ionization potential for hydrogen. The oscillation energy

$$\epsilon_{os} = e^2 E_0^2 (1 + \alpha^2) / 4 m_e \omega_0^2, \quad (1.33)$$

where ω_0 is the laser frequency and α is the polarization parameter ($\alpha = 0$ for linear polarization and $\alpha = 1$ for circular polarization). It is convenient to represent Γ and ϵ_{os} as functions of the laser parameters in the form

$$\begin{aligned} \Gamma^2 &= 0.73 Z^2 / I_{14} \lambda_{\mu m}^2 (1 + \alpha^2) \\ \epsilon_{os} &= 9.3(1 + \alpha^2) I_{14} \lambda_{\mu m}^2 \text{ [eV]} \end{aligned} \quad (1.34)$$

where I_{14} is the laser intensity in units of $10^{14} \text{ W cm}^{-2}$ and $\lambda_{\mu m}$ is the laser wavelength in microns. For intensities $I \geq 10^{14} \text{ W cm}^{-2}$ and $\lambda \leq 1 \mu m$ one obtains from equation (1.34) that $\Gamma > 1$. This means that multiphoton ionization takes place. At $I \geq I_a$ tunnel ionization occurs. When the laser intensity is further increased ($I \gg I_a$) another physical threshold is reached, which corresponds to the oscillation energy becoming equal to the electron rest energy $E_{os} = m_e c^2$. The corresponding (relativistic) values of the laser intensity and field amplitude are

$$\begin{aligned} I_r &= 4n_e m_e c^3 = 1.14 \times 10^{19} (\lambda_{\mu m})^{-2} \\ E_r &= 2 m_e c \omega_0 / e = 12.87 E_a / \lambda_{\mu m} \end{aligned} \quad (1.35)$$

Here $n_e = m_e \omega_0 / 4\pi e^2 = 10^{21} (\lambda_{\mu m})^{-2} \text{ [cm}^{-3}\text{]}$ is the critical electron density of the plasma at the frequency ω_0 . At intensities above the relativistic threshold, plasmas with the relativistic electrons may be produced. During the very short interaction time (with pulse durations less than 100 fs) electrons cannot transfer a significant fraction of their energy to ions even at intensities $I \leq I_r$. Hence, no heating of the ions and consequently no plasma expansion occur during the pulse. The laser-matter interaction at relativistic intensities becomes strongly nonlinear. The first nonlinear effect which should be taken into account is due to the light pressure on the surface of the solid target. The light pressure at relativistic intensity $I_r = 10^{19} \text{ W cm}^{-2}$ reaches $3.3 \times 10^3 \text{ Mbar}$. This pressure is comparable to the value of the thermal pressure in the central core of a heated and compressed laser-fusion target. It can act like a piston

Chapter 1

on the surface of a solid target in conventional hydrodynamics. The light pressure can lead to direct heating of ions. It can also induce Rayleigh-Taylor instability at the plasma-vacuum interface because at this boundary the “light liquid” (photons) accelerates the heavy ions. Such an overdense plasma may be of practical interest as an ultrashort source of fast particles and x rays or, as a medium for an X-ray laser. The unique combination of high density, temperature, and short lifetime provides a promising source of pulsed x rays.

1.7 Hot electrons

Measurements of the spectrum of the X-ray radiation emitted in laser-plasma interaction experiments show evidence of the generation of suprathermal electrons. Besides the thermal Maxwellian population of electrons characterized by a temperature T_e , there is a small population which can be modeled as being distributed as a Maxwellian at a much higher temperature T_h . These electrons give rise, via bremsstrahlung emission, to hard X-ray radiation, well above the typical thermal emission from laser produced plasma. Besides its importance for the understanding of the mechanisms from which such hot electrons originate, such an emission can be useful in applications requiring harder X-rays.

Hot electrons may be produced by several mechanisms. They may be generated as a result of the inhibition of electron thermal conduction [60,61] that prevents the laser energy absorbed in the proximity of the critical density layer to propagate towards the high-density plasma regions. In this case, a thin plasma layer just beyond the critical surface can reach very high temperature, and the production of hot electrons and ions become possible. Another source of hot electrons is the resonance absorption mechanism. This absorption process produces an intense electric field parallel to the plasma density gradients, strongly localized in the proximity of the critical surface [56]. Numerical simulations show that slow electrons

that travel only a small fraction of this high-field region during a laser period, experience an oscillating electric field, which does not produce a significant increase of their kinetic energy. On the other hand, very fast electrons move across the high-field region in a very small fraction of period, experience a constant electric field. However, due to the short duration of the electric field action, the energy gain of these electrons is very small. But, electrons with an intermediate velocity, crossing the region in a fraction of period, can gain as much energy as their kinetic energy. Finally, electrons can also be accelerated up to suprathermal energies by the electric field of the intense laser radiation or by that of the plasma waves.

1.8 Femtosecond interactions

The advent of CPA has led to high power lasers capable of delivering several joules in tens of femtoseconds. These lasers can be used to study radiation-matter interaction at intensities exceeding 10^{20} W cm⁻². The characteristic time of hydrodynamic expansion of laser-produced plasma, i.e. the time taken by the plasma to expand by a length comparable with the laser wavelength, is of the order of a few picoseconds. Therefore, the use of femtosecond laser pulses enables us to study the interaction of intense optical radiation with plasmas characterized by solid density and ultra steep gradients. According to the current ionization models [62,63] at the high intensities attainable by femtosecond lasers, the time required to ionize the target is extremely short, so that the plasma becomes opaque to the impinging radiation in a fraction of a period of the laser field oscillation. In the typical experiments reported so far, the laser pulse is focused on a thick target, or a film coated on a transparent massive substrate. In principle, the plasma produced in these conditions can be divided into three regions. The first region consists of the plasma expanding in the vacuum, whose typical extent is a few hundreds of angstroms. The second, characterized by an electron density of the order of that of the solid target times the average ionization degree, extends over a length of the order of the skin depth, typically of the order of a

Chapter 1

few hundreds of angstrom. In these two regions, laser energy deposition is accounted for by different mechanisms including collisional absorption, resonance absorption, Brunel effect and anomalous skin effect. A strong electron heating is produced in a very short time, so that the electron velocity distribution is far from a Maxwellian and the plasma, despite the high intensity, is away from thermal equilibrium. The high density and the high electron kinetic energy make these plasmas bright sources of x-ray pulses, with photon energy extending up to MeV region. The third region, not directly reached by the laser electromagnetic field, is heated by thermal diffusion and extends over several thousands of angstroms.

1.9 Laser-plasma X-ray Sources

A laser-plasma X-ray source is generated by focusing a high-power laser pulse onto the surface of a target placed in vacuum. Laser pulse durations can range between a few tens of femtoseconds and tens of nanoseconds with energies ranging from a few mJ to tens of kJ with focused pulse intensities up to 10^{20} W cm⁻². However, X-ray sources can be driven at laser intensities on target as low as 10^{12} W cm⁻² easily achievable by laser systems running in a Q-switch configuration. The X-ray pulse emitted is emitted into the 4π solid angle with the angular distribution weakly peaked on the target normal. The duration of the X-ray pulse is roughly the same as that of the impinging laser pulse. The interaction of high-power femtosecond laser pulses with matter is now established as a powerful technique of generating short intense X-ray pulses with photon energies extending from a few hundreds of electron volts to MeV region. X-ray photons are emitted either by radiative de-excitation and recombination processes or by electron-ion collisions. There have been lot of reports of the soft X-ray generation [64-69] and hard x-ray generation [70-81] from the plasma produced by intense ultra short lasers. The generation of higher harmonics in femtosecond laser produced plasma is also becoming a topic of interest to many researchers [82-84]. This X-ray source can be used for studying transient processes in

chemistry, biology, and physics as well as for microlithography, microscopy of biological cells, etc. Nuclear reactions have been reported from the femtosecond laser heated deuterium clusters [85]

In the present thesis, attempt has been made to study the evolution of the plasma generated using a nanosecond laser at two different target surfaces viz., silicon carbide and copper. The generation of hard X-ray emission from a plasma created by the irradiation of a femtosecond laser on copper target is also studied.

Chapter 1

References:

1. D. Strickland and G. Mourou, *Opt. Commun.* 56 (1985) 219
2. M.A.Perry and G. Mourou, *Science* 264 (1994) 917
3. P.Maine et al. *IEEE Trans. Quantum Electron.* QE-24 (1988) 398
4. D. Umstadter, S. Y. Chen, A. Maksimchuk, G. Mourou and R. Wagner, *Science* 273 (1996) 472
5. M. Tabak, et al., *Phys. Plasma* 1 (1994) 1626
6. J.D. Kmetec, C. L. Gordon, III, J. J. Macklin, B. E. Lemoff, G. S. Brown, and S. E. Harris, *Phys. Rev. Lett.* 68 (1992) 1527
7. P.L. Shkolnikov, A.E. Kaplan, A. Pukhov, and J. Meyer-ter-Vehn, *Appl. Phys. Lett.* 71 (1997) 3471
8. G. Pretzler et al., *Phys. Rev. E* 58 (1998) 1165
9. M. H. Key et. al., *Phys. Plasma* 5 (1998) 1966
10. P.A. Norreys et.al., *Phys. Plasma* 6 (1999) 2150
11. K.W.D. Ledingham et al, *Phys. Rev. Lett.* 84 (2000) 899
12. D B Chrisey and G K Hubler (Eds.) *Pulse laser deposition of thin films*, John Wiley and Sons, New York (1994) and references there in
13. T P Hughes, *Plasmas and Laser Light*, Adam Hiller (1975)
14. J.C. Miller and R.F. Haglunds (Eds.) *Laser Ablation: Mechanisms and Applications*, Springer-Verlag, (1991)
15. R.K. Singh and J. Narayan, *J. Appl. Phys.* 68 (1990) 233
16. K L Saegner, *Processing of Advanced Materials* 2 (1993) 1
17. R.W. Dreyfus, *J. Appl. Phys.* 69 (1991) 1721
18. R. Kelly, J.J.Cuomo, P.A. Leary and J.E. Rothenberg, *Nucl. Instr. Meth. Phys. Res. B* 7/8(1985) 755
19. R. Kelly, A. Miotello, B. Brare, A. Gupta and Casey, *Nucl. Instr. Meth. Phys. Res. B* 65 (1992) 187
20. R. Kelly, *Nucl. Instr. Meth. Phys. Res. B* 46 (1990) 441

21. R. Kelly and A. Miotello, Nucl. Instr. Meth. Phys. Res. B 122 (1997) 374
22. M M Martynyuk, Sov. Phys. Tech. Phys. 19 (1974) 793
23. F.W.Dabby and U.C. Paek, IEEE J. Quantum. Electro. QE-8 (1972) 106
24. J.N.Leboeuf, K.R.Chen, J.M.Donato, D.B. Geohegan, C.L.Liu, A.A. Poretzki and R.F. Wood, Appl. Surf. Sci. 96-98 (1996) 14
25. G.J. Pert, J. Plasma Phys. 35 (1986) 43
26. S. I. Anisimov, B.S.Luk'yanchuk and A. Luches, Appl. Surf. Sci., 96-98 (1996) 24
27. X.L.Mao, W.T. Chen, M.Caetano,M.A.Shannon and R.E.Russo, Appl. Surf. Sci., 96-98 (1996) 126
28. J.H. Bechtel, J. Appl. Phys. 46 (1975) 1585
29. K.H.Song, X Xu, Appl. Phys. A 65 (1997) 477
30. A. Vertes, P. Juhasz, P. Jani and A. Czitrovsky, Int. J. Mass. Spectrom. Ion Process 83 (1988) 45
31. J.F. Friichtenicht, Rev. Sci. Instrum. 45 (1974) 51
32. W. Demtroder and W. Jantz, Plasma Phys. 12 (1970) 691
33. S.R.Foltyn, R.E. Muechausen, R.C.Estler, E. Peterson, W.B. Hutchinson, K.C. Ott, N.S.Nogar, K.M.Hubbard, R.C. Dye and X.D. Wu, Mater. Res. Soc. Symp. Proc. 191 (1990) 205
34. D.B. Geohegan, Appl. Phys. Lett. 60 (1992) 2732
35. F.F. Chen, *Introduction to Plasma Physics and Controlled Fusion*, Second Edition, Vol. 1, Plenum Press, New York (1984)
36. A.P.Thorne, *Spectrophysics*, Chapman and Hall Ltd, London (1974)
37. H.R. Griem, *Plasma Spectroscopy*, McGraw-Hill, New York (1964)
38. M.M. Martynyuk, Sov. Phys. Tech. Phys. 21 (1976) 430
39. M.M. Martynyuk, Russ. J. Phys. Chem. 57 (1983) 494
40. W. Fucke and U. Seydel, High Temp.- High Press. 12 (1980) 419
41. U. Seydel and W. Fucke, J. Phys. F 8 (1978) L157
42. F.P.Gagliano and U.C. Paek, Appl. Opt. 13 (1974) 274

Chapter 1

43. D. Bhattacharya, R.K. Singh and P.H. Holloway, *J. Appl. Phys.* 70 (1991) 5433
44. S.S.Harilal, R.C.Issac, C.V.Bindhu, V.P.N.Nampoori and C.P.G. Vallabhan, *J. Appl. Phys.* 80 (1996) 3561
45. S.S.Harilal, R.C.Issac, C.V.Bindhu, V.P.N. Nampoori and C.P.G.Vallabhan, *J. Appl. Phys.* 81 (1997) 3637
46. Y.I.Lee, K.Song, H.K.Cha, J.M.Lee, M.C.Park, G.H.Lee and J. Sneddon, *Appl. Spectrosc.* 51 (1997) 959
47. Z. Paszti, Z.E.Horvath, G.Peto, A.Karacs and L. Guzzi, *Appl. Surf. Sci.* 109/110 (1997) 67
48. X.Y.Chen, S.B. Xiong, Z.S.Sha, Z.G.Liu, *Appl. Surf. Sci.* 115 (1997) 279
49. D.B. Koopman, *Phys. Fluids* 15 (1997) 1959
50. B.Y.Man, X.T. Wang and G.T. Wang, *Appl. Spectrosc.* 51 (1997) 1910
51. D.A.Freiwald, *J. Appl. Phys.* 43 (1972) 2224
52. W.K.A.Kumudini, Y.Nakayama, Y.Nakata, T. Okada and M.Maeda, *J. Appl. Phys.* 74 (1993) 7510
53. S.J.Lee, K.Imen and S.D.Allen, *J. Appl. Phys.* 74 (1993) 7044
54. X.Y.Chen, S.B.Xong, Z.S.Sha and Z G Lin, *Appl. Surf. Sci.* 115 (1997) 279
55. R.W.Dreyfus, *Appl. Surf. Sci.* 86 (1995) 29
56. W.L.Kruer, *The Physics of laser Plasma Interactions*, Addison Wesley, New York (1988)
57. F. Brunel, *Phys. Rev. Lett.* 59 (1987) 52
58. E.G.Gamaly, *Laser and Particle Beams* 12 (1994) 185
59. L.V.Keldysh, *Zh. Eksp. Teor. Fiz* 47 (1964) 1945
60. L. Spitzer, *Physics of fully Ionized Gases*, Interscience, New York, (1962)
61. R.C.Malone, R.L.Mc Crory and R.L. Morse, *Phys. Rev. Lett.* 34 (1975) 751
62. S.Augst, D.Strickland, D. Mayerhoff, S.L. Chin and J. Eberly, *Phys. Rev. Lett.* 63 (1989) 2212
63. M.Protopapas, C. H. Keitel, P.L. Knight, *Rep. Progr. Phys.* 60 (1997) 389

64. D.G.Stearns, O.L. Landen, E.M. Campbell and J.H. Scofield, *Phys. Rev. A* 37 (1988) 1684
65. J.F.Pelletier, M. Chaker and J.C. Kieffer, *J. Appl. Phys.* 81 (1997) 5980
66. T. Nishikawa, H. Nakano, N. Uesugi and T. Serikawa, *Appl. Phys. B* 66 (1998) 567
67. H. Nakano, Y. Goto, P. Lu, T. Nishikawa and N. Uesugi, *Appl. Phys. Lett.* 75 (1999) 2350
68. A. Shimoura, T. Mochizuki, S. Miyamoto, S. Amano and T. Uyama, *Appl. Phys. Lett.* 75 (1999) 2026
69. S.S.Harilal, C.V.Bindhu and H.J. Kunze, *J. Phys. D: Appl. Phys.* 34 (2001) 560
70. J.D.Kmetec, *IEEE J. Quantum Electron.* 28 (1992) 2382
71. B.N. Chichkov, C. Momma, A. Tunnermann, S. Meyer, T. menzel and B. Wellegehausen, *Appl. Phys. Lett.* 68 (1996) 2804
72. P. Zhang et al, *Phys. Rev. E* 57 (1998) R3746
73. M. Yoshida, Y. Fujimoto, Y. Hironaka, K.G. Nakamura, K. Kondo, M. Ohtani and H. Tsunemi, *Appl. Phys. Lett.* 73 (1998) 2393
74. C. Gahn, G. Pretzler, A. Saemann, G.D. Tsakiris, K.J. Witte, D. Gassmann, T. Schatz, U. Schramm, P. Thirolf and D.Habs, *Appl. Phys. Lett.* 73 (1998) 3662
75. J. Yu, Z.Jiang, J.C.Kieffer, A. Krol, *Phys. Plasmas* 6 (1999) 1318
76. T.D.Donnelly et al, *J. Phys. B: At. Mol. Opt. Phys.* 34 (2001) L313
77. P.P.Rajeev, P.Taneja, P. Ayub, A.S. Sandhu and G.R. Kumar, *Phys. Rev. Lett.* 90 (2003) 115002
78. J. Zheng, K.A. Tanaka, T.Sato, T. Yubuuchi, T. Kurahashi, Y. Kitagawa, R. Kodama, T. Norimatsu and T. Yamanaka, *Phys. Rev. Lett.* 92 (2004) 165001

Chapter 1

79. R.M. Stevenson, L.J.Suter, K.Oades, W.Kruer, G.E. Slark, K.B.Foumier, N. Meezan, R. Kauffman, M.Miller, S.Glenzer, C. Niemann, J. Grun, J.Davis, C.Back and B.Thomas, *Phys. Plasmas* 11 (2004) 2709
80. R.J.Mason, E.S. Dodd and B.J. Albright, *Phys. Rev. E* 72 (2005) 015401(R)
81. M.Hagedorn, J.Kutzner, G.Tsilimis and H. Zacharias, *Appl. Phys. B* 77 (2003) 49
82. D. von der Linde, *Notions and Perspectives of Nonlinear Optics*, Ole Keller (Ed) World Scientific, Singapore (1995)
83. G.Veres, J.S. Bakos, I.B.Foldes, K.Gal, Z.Juhasz,G.Kocsis and S. Szatmari, *Europhys. Lett.* 48 (1999) 390
84. H.A.Salih, R.P. Sharma and M. Rafat, *Phys. Plasmas* 11 (2004) 3186
85. T. Ditmire, J. Zweiback, V.P. Yanovsky, T.E.Cowan, G.Hays amd K.B. Wharton, *Nature*, 398 (1999) 489

Chapter 2

Experimental Techniques

2.1 Introduction

With the invention of high-power pulsed lasers, the study of laser-matter interactions has assumed many new dimensions among which the phenomenon of laser ablation has a major role both in fundamental studies and in technological applications. The interaction of laser radiation with solids is a very complex process. It includes light absorption and plasma formation in the vicinity of the target, thermalization of the ablation products due to collisions among themselves and with ambient gas molecules, evolution and propagation of the plume, and the eventual deposition of the ablative products on suitable substrates situated at a distance from the target. For the characterization of the photo fragmented species in a plasma, many diagnostic tools are used including laser induced fluorescence[1], absorption spectroscopy [2], mass spectroscopy [3], optical emission spectroscopy [4], time resolved spectroscopy[5], streak photography[6], ICCD photography[7], etc. In the present work, plasma formed at the target surface is characterized by optical emission spectroscopy. This chapter gives a comprehensive account of the experimental technique for the analysis of laser produced plasma both in the optical domain as well as in the X-ray domain.

2.2 Optical emission studies

2.2.1 Laser Source

The laser used is an electro-optically Q-switched Nd:YAG laser (Quanta Ray DCR 11) having a fundamental output of 1.06 μm . The optical cavity in the DCR -11 is an unstable resonator. In a stable resonator the ray of light is traveling close to the optical axis and is reflected toward the optical axis by its cavity mirrors. Stable resonators can only extract energy from a small volume near the optical axis of the resonator, which limits the energy of the output. Conversely, unstable resonators can have large beam diameters. Thus they can efficiently extract energy from active media whose cross-sectional area is large, like that of a typical Nd:YAG laser rods. The output coupler in an unstable resonator is a small high reflector mounted on a clear substrate which lies on the optical axis of the resonator. Energy escapes from the resonator by diffracting around this dot, which gives the 'diffraction coupled resonator' its name [8]. The diffraction coupled resonator delivers a 'doughnut' shaped beam profile at 9 ns pulse width (FWHM) with a power stability of $\pm 4\%$. The laser beam has a typical line width of $< 1\text{ cm}^{-1}$ with 220 MHz spacing between the longitudinal modes and a beam divergence of $< 0.5\text{ mrad}$. The high peak power of the Q-switched pulse permit frequency conversion in nonlinear crystals like KD^*P . The 1064 nm fundamental interacts with the crystal to produce 532 nm wavelength. This can be double again by passing through a second crystal to yield 266 nm. It can also be mixed in KD^*P with residual 1064 nm to produce a 355 nm radiation.

The fundamental wavelength of laser with pulse duration of 9 ns and energy of 275 mJ, when focused on to a solid target, produces power densities of the order of 10^{10} W cm^{-2} at the focal spot. The laser also provides trigger outputs to synchronize oscilloscope, energy meter, boxcar, etc.

2.2.2 Plasma Chamber and Vacuum System

The essential constituent of the experimental setup is a plasma chamber with optical view ports and provision for vacuum pumps. The chamber consists of a bottom plate, body of the chamber and a top plate. Two optical viewing ports of diameter 10 cm are introduced for emission diagnostics of the plasma and a third window having a diameter of 4 cm is used as laser inlet. The base of the chamber is a mild steel disk plated in soft chromium having thickness of 1.5 cm and diameter 35 cm. A central hole with diameter 12 cm allows the plasma chamber to be in contact with the diffusion and rotary pumps. The body of the chamber is 18 cm high with three glass windows. The top plate of the chamber is a disk with thickness of 1.5 cm and diameter 35 cm made of mild steel and coated with soft chromium.

The vacuum system consists of a rotary pump followed by a diffusion pump. The system is fitted with a needle valve and the chamber can be maintained at pressures ranging from atmospheric pressure to 2×10^{-5} mbar. For accurate measurement of pressure inside the chamber, pirani and penning gauges are used.

2.2.3 Monochromator–PMT Assembly

Monochromators are widely used for analyzing the light emitted from any source. The specifications for the performance of a monochromator include dispersion and the stray light levels. Generally the dispersion is given in nm/mm, where the slit width is expressed in mm. The monochromator used in the present study is Spex Model 1704, which is a 1 m scanning spectrometer having a maximum resolution 0.05\AA [9]. The monochromator covers a spectral range 350-950 nm using a grating with 1200 grooves per mm blazed at 500 nm and spectral band pass 0.1\AA . The entrance and exit slits on the front of the spectrometer are controlled by micrometer screws above the slits. The scan rate of the monochromator is adjusted by using microprocessor controlled Spex

Chapter 2

Compudrive (CD 2A) arrangement. Spex compudrive has a keyboard control over the spectrometer. The main advantage of CD2A compudrive is that we can programme the start and end positions of the scan, rate, repetitive scan, delay between repetitions, etc [10]. The output of the Spex monochromator is coupled to a thermoelectrically cooled photomultiplier tube (Thorn EMI, Model KQB 9863 with a rise time of 2ns). The photomultiplier tube is a very versatile and sensitive detector of radiant energy in the ultra-violet, visible and near-infrared regions of the electromagnetic spectrum.

2.2.4 Boxcar Averager / Integrator

A small part of the signal pulse may be required to analyse the signal. To recover such a signal buried in noise, some form of averaging process is required and for that, some kind of multi-point averager or a Fourier transform analyzer is necessary. Signals of such transient nature, triggered by repetitive pulses from the excitation source can be analyzed in this form. This is achieved by a boxcar integrator, which essentially is an instrument used to recover complex repetitive signals hidden in noise. The boxcar used for the present study is a Stanford Research Systems (SR 250) module. It essentially has a gate generator, a fast gated integrator and an exponential averaging circuit. Triggered by the pulse from the laser, the gate provides an adjustable delay from few ns to 100 ms, before it generates continuously adjustable gate of 2ns to 15 ms [11]. The signal at the gate is integrated by the fast gated integrator and is normalized by the gate width to provide a voltage proportional to the part of the input signal pulse level at the gate. This signal is further amplified according to the front panel sensitivity setting. By fixing the delay and the gate width so that only the voltage from the part of the signal pulse alone is measured, it is possible to temporally separate out the PMT signal due to the emission of the particular species from the other unwanted signal components contained in the signal pulse, thus improving the signal to noise ratio of detection. This module also has a computer interface module SR 245. This module is a versatile module capable of providing a variety of the scanning, counting and

communications function typically required in the laboratory. It is remotely programmable via both RS232 and GPIB rear panel connectors and can be used with laboratory computers. Eight front panel analog ports can be programmed as inputs or outputs with a range of ± 10.24 volts. Two front panel digital input/output bits are provided for general use as well as an eight-bit digital input/output port accessible via an internal 20 pin dual in-line connector[12].

2.2.5 Digital Storage Oscilloscope

A digital storage oscilloscope (DSO, Tektronix TDS 220), which is a 100 MHz two channel real time oscilloscope, was used to monitor the signal from the photomultiplier tube. The oscilloscope can be triggered both internally and externally. In the present work, it was triggered using Nd:YAG laser pulses. The pulse shapes can be digitally stored and plotted. The DSO is necessary for measuring time delays of the different species in the plasma. It is also useful while setting the gate delay and gate width using the gated integrator.

2.2.6 Experimental Setup

When high intensity laser light is focused on a solid target, the target surface will get vapourized and plasma is formed at the surface. The schematic of the experimental setup is given in figure 2.1. The laser used in the experiment to produce plasma is a Q switched Nd:YAG laser (Quanta Ray DCR 11) operated at the fundamental wavelength of 1064 nm with pulse width 9 ns and repetition frequency 10 Hz. The laser pulse energy is measured with a calibrated laser energy meter (Delta Developments). The targets used are discs of diameter 1.5 cm and thickness 2-3 mm approximately, which is kept inside the plasma chamber. The targets were rotated about an axis parallel to the laser beam and frequently translated during irradiation in order to avoid multiple hits at the same location for long time. Multiple hits at the

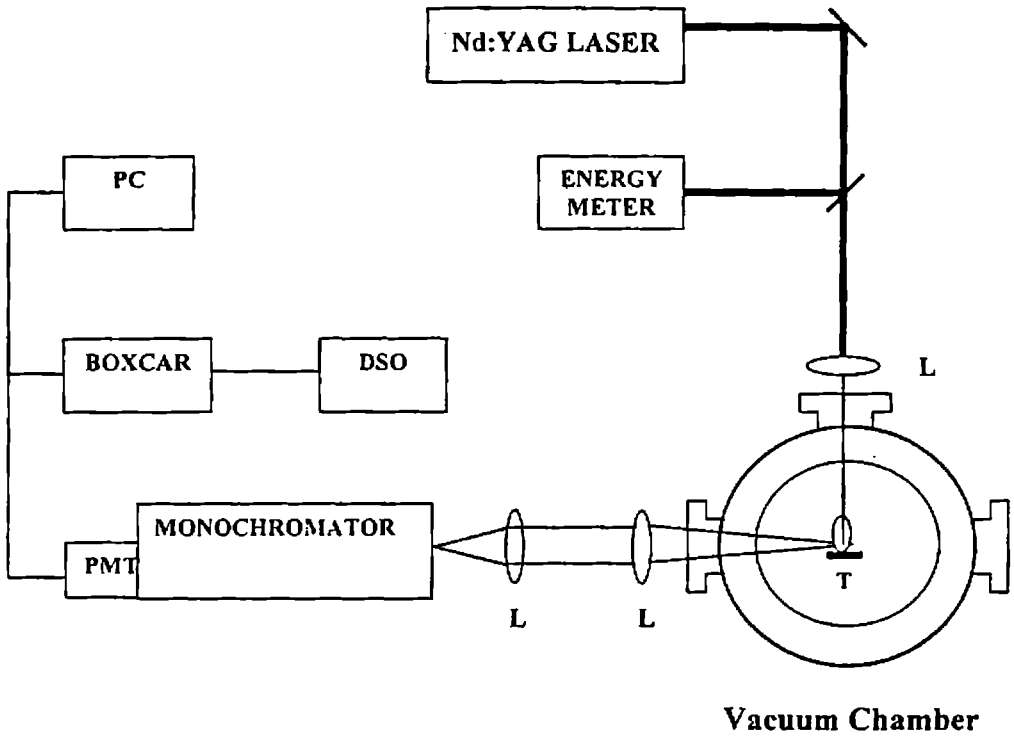


Figure 2.1: Block diagram of the experimental setup. L-Lens, T-Target, PC-Personal Computer, DSO-Digital Storage Oscilloscope, PMT-Photomultiplier Tube

same location will cause pitting of the target, thereby causing change in laser spot size and hence change the intensity at the focal spot. A convex lens of focal length 60 cm focuses the laser beam to the target. Laser beam hits the target surface normally. The chamber is connected to rotary and diffusion vacuum pumps and maintained at the required pressure. The lowest pressure which can be attained in the chamber is 2×10^{-5} mbar. The bright plasma emission was viewed through a side window at right angles to the plasma expansion direction. The section of the plasma was imaged onto

the slit of a monochromator using appropriate collimating and focusing lenses so as to have one to one correspondence with the sampled area of the plasma and the image. The recording of the spectrum was done by using a photomultiplier tube, which was coupled to a boxcar averager/ integrator which is computer interfaced. The averaged output from the boxcar averager was also fed to a digital storage oscilloscope for monitoring.

Space resolved studies of plasma were done along the expansion direction of the plasma. Plasma from the required sections was imaged on to the slit of the monochromator by a pair of lenses, a collimating lens and a focusing lens. The collimating lens could be translated continuously in the horizontal plane in the direction of the axis of the expansion of the plasma to examine different parts of the plasma plume at different distances from the target. The time of flight signals are monitored on the digital storage oscilloscope having an input impedance of 50Ω .

Time resolved emission spectroscopy can be used to measure the expansion velocities of atomic, molecular and ionic species. Time resolved analysis of the plasma emission is carried out by scanning the gate of the boxcar averager through the required temporal regions by adjusting the delay.

2.3 X-ray emission studies

2.3.1 Laser System

The laser system used for the X-ray generation studies is Titanium:Sapphire (Ti:S) system based on the principle of chirped pulse amplification. The system is schematically represented in Figure 2.2. It comprises of an oscillator (Mira Seed Laser), grating pulse-stretcher, regenerative amplifier (RGA), multipass amplifier and

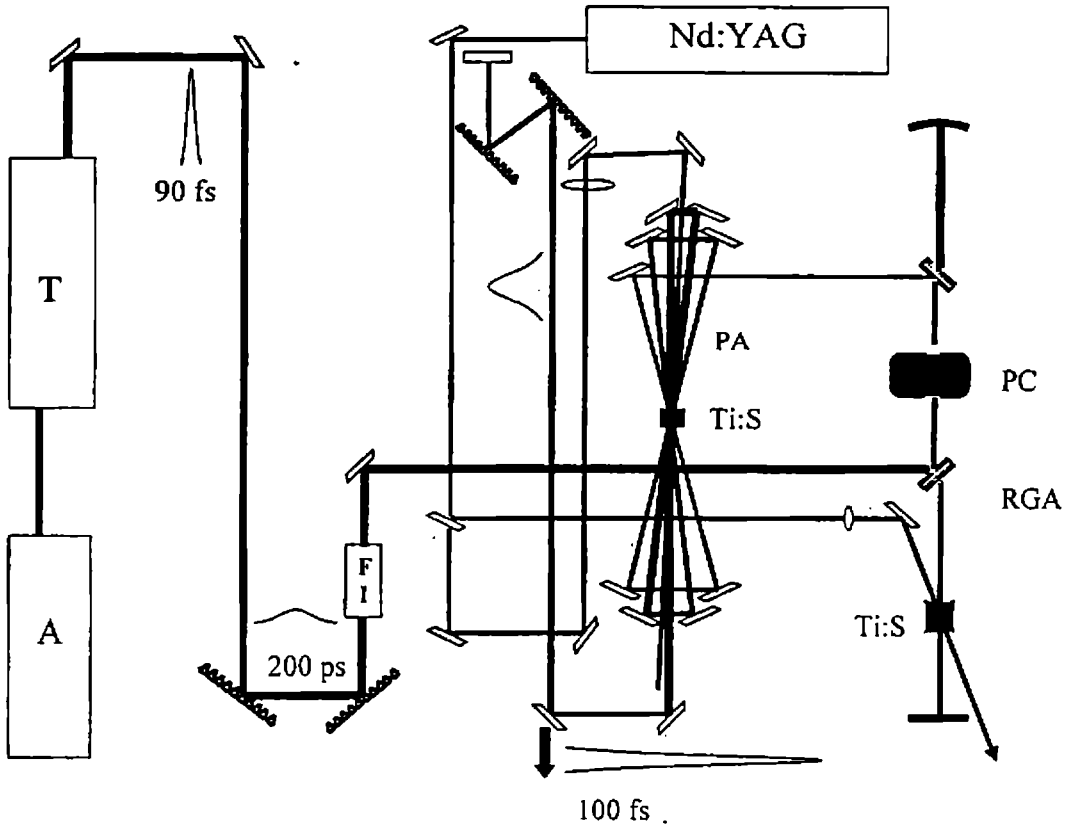


Figure 2.2 Schematic of the high intensity femtosecond Titanium:Sapphire laser. T- Ti:S Oscillator, A- Ar⁺ Pump, FI- Faraday Isolator, RGA- Regenerative amplifier, PA- Four pass amplifier, PC – Pockels Cell

a grating pulse-compressor. The oscillator produces 76 MHz pulses in a titanium sapphire (Ti:S) crystal by Kerr lens modelocking and is pumped using an Ar⁺ laser (Coherent). The average mode locked output power is 450 mW at 90 fs with a bandwidth of 20 nm. These pulses are taken to a folder-stretcher configuration, which temporally stretches the pulse to about 200 ps. The stretched pulse is then coupled into

the RGA. The latter is pumped by 80 mJ of 532 nm radiation from a 6 ns Nd:YAG laser (Continuum Surelite) operating at a repetition rate of 10 Hz. A Pockels cell selects pulses from the oscillator pulse train at 10 Hz which get amplified in the RGA from a few nJ per pulse to about 10 mJ after 11 passes in the RGA. The amplified output pulse is switched out by the Pockels cell. Further amplification is achieved by a multipass amplifier system pumped by 300 mJ from the Nd:YAG laser, which increases the pulse energy to 80 mJ. The 200 ps stretched pulse is finally compressed to about 100 fs by a grating pulse-compressor. The final output obtained from this laser system is 50-55 mJ per pulse, with pulse duration of 100 fs at a repetition rate of 10 Hz. The resulting maximum output power is 0.5 TW [13].

2.3.2 Experimental setup

The linearly polarized femtosecond laser pulses are focused on to solid targets mounted inside the vacuum chamber using a 30 cm focal length plano-convex lens, forming a plasma at the focal point. The schematic is given in figure 2.3[14]. A thin half-wave plate was introduced in the beam path to switch the polarization of the beam between horizontal (p) and vertical (s). The target is constantly rotated and translated to avoid multiple hits at the same spot by the laser pulses. A thallium doped sodium iodide (NaI (Tl)) scintillation detector was used for collecting hard X-ray emission in the range 30-500 keV. NaI (Tl) detectors are routinely used for gamma-ray spectroscopy because of their excellent photon yield, large interaction cross-section for γ -ray detection and reasonably good resolution. They are used to measure radiations in the range 10 keV – 10 MeV. The NaI (Tl) crystal is normally enclosed in an aluminium casing and is of about 2 inch size. The thallium doping facilitates metastates between the conduction band and valence band of the NaI crystal. The electrons generated by the deposition of energy from the X-ray photon de-excited from the metastates to the valence band, emitting visible light at 415 nm. A PMT

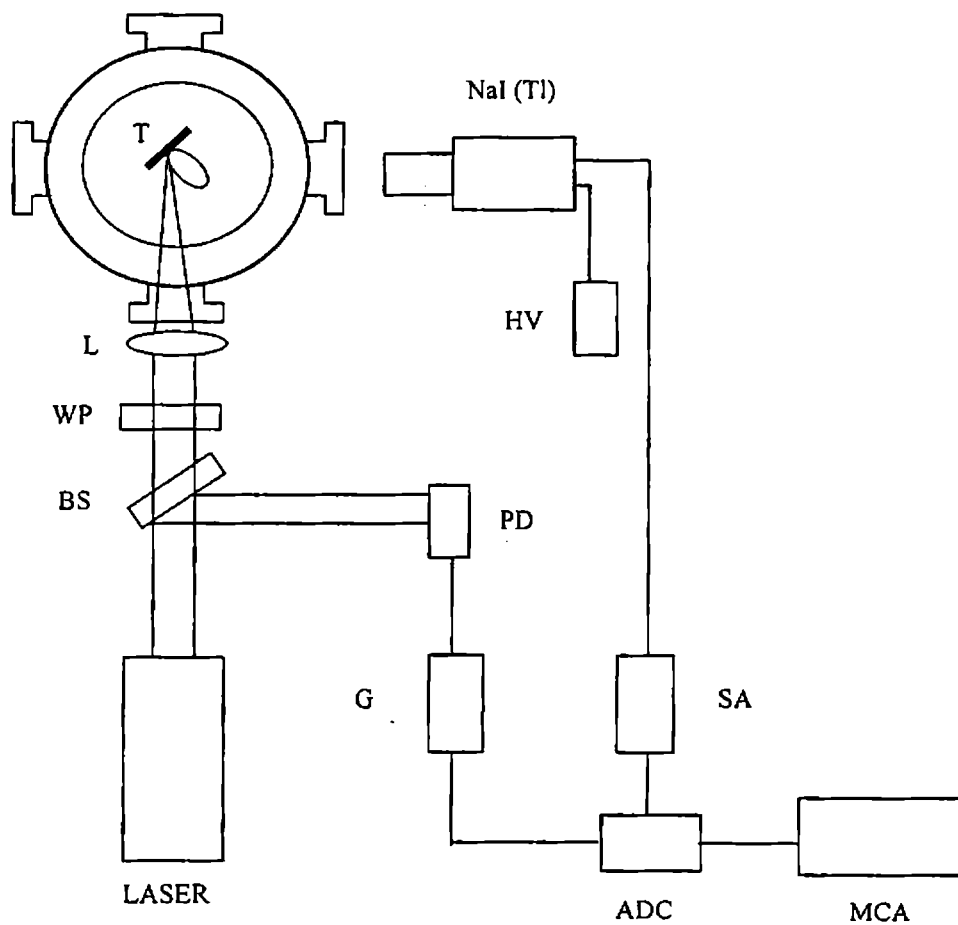


Figure 2.3 Schematic of experimental set up for X-ray detection. T- Target, L-Lens, WP- Wave Plate, BS- Beam Splitter, PD- Photo Diode, HV- High Voltage, G-Delay Gate Generator, SA- Spectroscopy Amplifier, ADC- Analog to Digital Converter, MCA- Multi Channel Analyser

attached to the crystal collects the visible photons and gives out a voltage pulse. The NaI(Tl) detector has the maximum light yield (number of photons emitted per X-ray photon) and a fair amount of linearity (the dependence of the number of visible photons or the height of the voltage pulse on the energy of the incident X-ray photon) in the energy regime that we are interested in. The Pulse Height Analysis (PHA) set-up provides the energy-dispersed X-ray yield. The pulses from the pre-amplifier of the detector are amplified again and properly shaped by a spectroscopy amplifier. Pulse shaping is performed to minimize the probability of pile-up (detailed in chapter 5) due to the long tail of the pre-amplifier output. The spectroscopy amplifier gives unipolar and bipolar outputs, with variable shaping times. The shaped pulses from the spectroscopy amplifier were fed to a Multi Channel Analyzer (MCA) through an Analog to Digital Converter (ADC). Most of the recent MCAs have built-in ADCs and it is enough to feed the unipolar pulses from the spectroscopy amplifier to the MCA directly. The pulses are height-analyzed in the MCA and are counted in different channels according to their heights. This provides the energy spectrum of the X-ray emission from the plasma.

The NaI (Tl) crystal is quite susceptible to the background radiation coming from the radioactive elements in concrete walls, cosmic rays, etc. To improve the signal to noise ratio, a time-gate is employed. A delay gate generator is triggered by a part of the laser pulse that produces plasma, which generates a time window of variable width. The emission is recorded only in this time window enabling almost back-ground free collection. Calibration of the detector is an essential aspect of any experiment as it decides the absolute photon energy corresponding to each pulse height. Well defined emission lines from radiation sources like Co^{57} , Cs^{137} , Co^{60} , etc are normally used for calibration in gamma-ray spectroscopy. Since the best spectrometer systems show nonlinearities over a wide range of channels, it is better to use calibration peaks at various points along the measured energy range. The NaI (Tl) detector was calibrated using Cs^{137} . There are two emission lines in the range

Chapter 2

considered viz. 36.6 keV and 661.6 keV. The channel numbers of the multi-channel analyzer is calibrated accordingly. With this setup, the hard X-ray emission can be recorded and subsequent analysis can be done.

2.4 Summary

Laser systems and the accessories required for the experiments have been described in this chapter. The details of the experimental setups for the optical emission studies and the X-ray emission studies are given.

References:

1. Y. Nakata, W.K.A. Kumudini, T. Okada, M. Maeda, *Appl. Phys. Lett.* 66 (1995) 3206
2. R.Mitzner, A.Rosenfeld and R. Konig, *Appl. Surf. Sci.*, 69 (1993) 180
3. H. Izumi, K. Ohata, T.Sawada, T. Morishita and S. Tanaka, *Appl. Phys. Lett.* 59 (1991) 597
4. D.B.Geohegan and D.N. Mashburn, *Appl. Phys. Lett.* 55 (1989) 2345
5. S.S.Harilal, R.C. Issac, C.V.Bindhu, V.P.N.Nampoori and C.P.G. Vallabhan, *Jpn. J. Appl. Phys.* 36 (1997) 134
6. V.Yu Baranov, O.N.Derkach, V.G. Grishina, M.F. Kanevskii and A. Yu. Sebrant, *Phys. Rev. E* 48 (1993)1324
7. D.B. Geohegan and A.A. Puretzky, *Appl. Phys. Lett.* 67 (1995) 197
8. Instruction Manual, Quanta Ray DCR 11, Nd:YAG laser
9. Instruction Manual, Spex 1704 Spectrometer (Spex, USA)
10. Instruction Manual, Spex CD 2A Compudrive (Spex, USA)
11. Instruction Manual, SR 250 (SRS, USA)
12. Instruction Manual, SR 245 (SRS, USA)
13. S. Banerjee, PhD Thesis, Tata Institute of Fundamental Research (2000)
14. P.P.Rajeev, PhD Thesis, Tata Institute of Fundamental Research (2003).

Chapter 2

Chapter 3

Laser Produced Plasma from Silicon Carbide

3.1 Introduction

Laser ablation of solid materials is becoming more and more important for elemental analysis of a wide variety of samples. It has also become a dominant technology for applications such as production of nanomaterials, deposition of thin films, welding and bonding of metal parts, micromachining of semiconductor materials, chemical analysis, etc [1- 3]. For these applications, an understanding of the relationship between the quantity and size of ablated particles versus laser irradiance is crucial in selecting the optimum process parameters. The quality of films depends on the properties of plasma produced by the laser, such as the particle velocity, temperature and number density distribution of particles in the plasma. Plasma characteristics in turn depend on laser intensity, wavelength and pulse duration, as well as on the physical and chemical characteristics of target material, and the ambient atmosphere. Laser ablation involves complex and collective mass-removal mechanisms, and identification of the relevant mechanism is the key to estimating the ablated mass accurately at a particular laser irradiance. Depending on the laser irradiance, this mass may be removed in the form of fine vapor, liquid droplets, or solid flakes due to evaporation, hydrodynamic instability, exfoliation and explosive boiling [4-8]. Evidence for phase explosion and generation of large particles during high power nanosecond laser ablation of silicon has been reported by Yoo et. al. [9]

Chapter 3

The interaction of pulsed laser ablation plumes with background gas has received increased attention due to its importance in laser deposition, nanoparticle formation and growth, cluster production, etc. Thin films deposited by pulsed laser deposition techniques have several advantages over other deposition techniques. This technique is based on the vaporization process induced by focusing high energy pulsed laser on the surface of a material. In fact, the high energetic content of ejected species allows low temperature deposition processes. Moreover, its ability to congruently transfer stoichiometry from target to the film, allows the growth of complex materials. When the energy density of the laser is higher than a threshold value, a stream of atoms, molecules and clusters is ejected from the target surface depending on the target material as well as on the laser wavelength. Such a stream, known as plume, which is composed of excited neutral and ionized species, emits radiation that can be conveniently analyzed to gather information about its composition and dynamics [10]. Since the properties of thin films are strictly related to the deposition conditions adopted, attempts to identify the precursor processes occurring during plume expansion have to be made. There exists several diagnostic techniques for the characterization of the plasma including optical emission spectroscopy, mass spectroscopy, laser induced fluorescence, Langmuir probe, photothermal deflection, Thomson scattering, fast photography, etc. Of these techniques, optical emission spectroscopy has received considerable attention for characterizing plasma as it is a relatively simple method and also because it gives in situ information on the dynamics of the specific species present in the plasma.

To specify the dynamics of plasma, we define the electron temperature as that describes the relative population distribution of atoms through the Boltzmann law, while the ionic temperature describes the ionization equilibrium between two successive ionization states. Several reports considering plasma diagnostics have been devoted to the study of temporal evolution and species spatial distribution in the plasma [11,12], shape and size of the emitting plume using bidimensional imaging

techniques[13-15] and plasma formation thresholds of different materials[16-20]. Diagnostics of silicon plasma produced by visible nanosecond laser ablation has been reported by Milan and Laserna[21].

Amorphous silicon carbide thin films are widely employed in many applications due to their chemical stability, hardness and interesting optical and electronic properties [22]. One of the major advantages offered by this material is the possibility of tailoring its optical, electrical, and structural properties by varying its stoichiometry. In a recent work, optical emission lines from the plasma generated in vacuum as well as in nitrogen ambient, by the laser ablation of sintered SiC target, were studied [23]. The time integrated and spatially resolved emission spectra were mostly dominated by atomic emission lines from silicon and carbon species, either neutral or singly ionized. Observation of CN species has also been found when the ablation process was carried out in a nitrogen gas background. Bonding configurations and optical band gap for nitrogenated amorphous silicon carbide films prepared by pulsed laser ablation has also been reported recently by Trusso et.al.[24]

In this chapter, the dynamics of laser produced plasma from a silicon carbide target has been studied. Evolution of the different species present in the plasma has been investigated using optical emission spectroscopy by monitoring their space-resolved and time-resolved emissions. The velocities of the different ionized species in the plasma as well as its variation with distance from the target have been investigated. The electron density and electron temperature which are the major characteristics for a plasma have been evaluated and their evolution studied.

Chapter 3

3.2 Experimental

The details of the experimental setup have already been discussed in Chapter 2. The fundamental radiation from a pulsed Q-switched Nd:YAG laser with a pulse repetition rate of 10Hz is focused onto a SiC target kept inside the vacuum chamber maintained at a pressure of 2×10^{-5} mbar. The target is uniformly rotated to ensure that the laser beam is incident on a new surface and also to avoid pitting of the sample. The plasma plume formed at the surface of the target is imaged onto the slit of a monochromator by a system of two lenses, such that there is a one to one correspondence between the image and the plume. The output of a photomultiplier tube which is connected to the monochromator is given to a Boxcar Averager/Gated Integrator which is interfaced to a computer. The Boxcar Averager averages the emission intensities for ten consecutive pulses. The temporal profile of the emission is also observed using a Digital Storage Oscilloscope.

3.3. Results and Discussion

3.3.1 Identification of different species

The optical emission from the plasma generated at the target by irradiation using laser is mainly in the blue region of the electromagnetic spectrum. Spectra are recorded in the wavelength range 350-550 nm at a distance of 4mm from the target surface. The different emitting species are identified from the recorded spectra by comparing the emission lines with standard reference data [25,26]. These optical emission spectra are found to have emissions due to the Si and C species corresponding to different ionization states. It includes emissions from both neutral and ionic species. Emission spectra recorded in the different wavelength ranges are shown in the figures 3.1 (a)-(d). Table 3.1 gives list of species identified from the emission spectra with their emission wavelengths. At a distance of 4 mm from the target, emission from the Si II

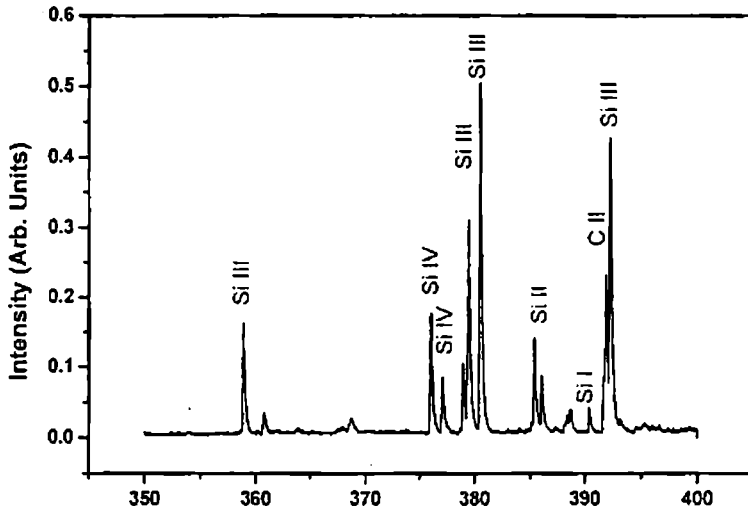


Figure 3.1(a): Emission spectrum in the wavelength range 350 - 400 nm

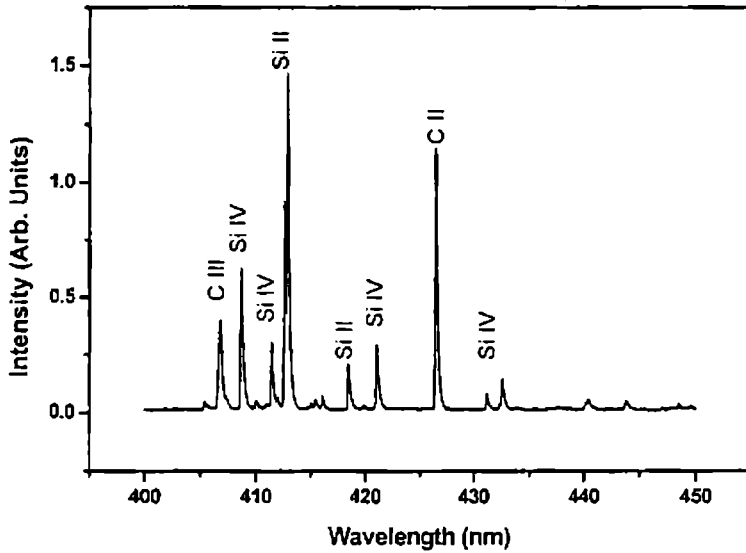


Figure 3.1 (b): Emission spectrum in the wavelength range 400 - 450 nm

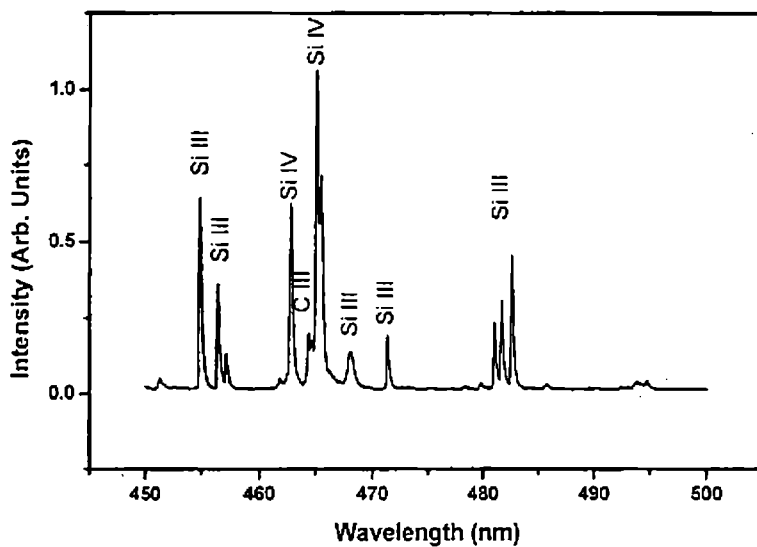


Figure 3.1 (c) : Emission spectrum in the wavelength range 450 - 500 nm

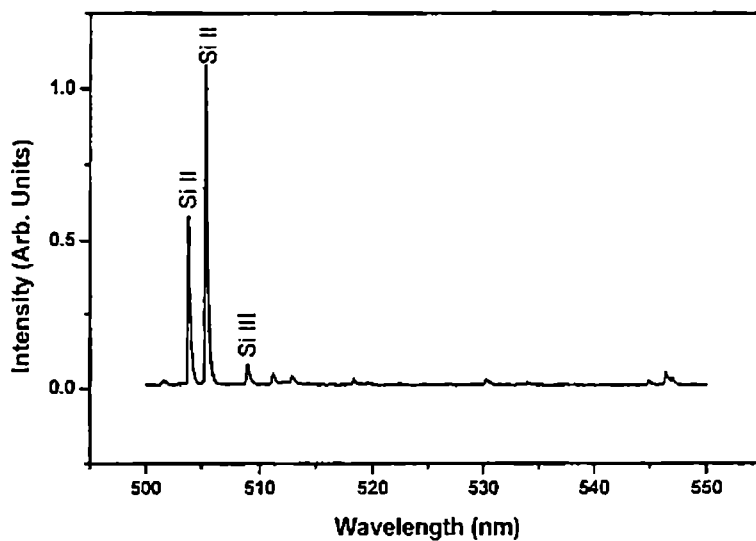


Figure 3.1 (d): Emission spectrum in the wavelength range 500 - 550 nm

Wavelength (nm)	Species	Wavelength(nm)	Species
359.04	Si III	421.24	Si IV
376.24	Si IV	426.72	C II
377.31	Si IV	431.41	Si IV
379.61	Si III	455.26	Si III
380.65	Si III	456.78	Si III
385.36	Si II	462.86	Si IV
390.55	Si I	464.74	C III
391.89	C II	465.43	Si IV
392.45	Si III	468.30	Si III
406.79	C III	471.67	Si III
408.88	Si IV	481.33	Si III
411.61	Si IV	481.97	Si III
412.80	Si II	482.89	Si III
413.09	Si II	504.10	Si II
418.33	Si II	505.59	Si II
419.07	Si II	509.14	Si III

Table 3.1: Species identified for different line emission

species at wavelength of 413.09 nm, corresponding to the transition $3s^2(^1S)3d - 3s^2(^1S)4f$, is found to be the most intense. Other emission lines corresponding to the same species (Si II) are also present in the spectrum. Emission from Si I species corresponding to $3s^23p^2 - 3s^23p4s$ transition is also observed at a wavelength of 390.55 nm. The ionization potential for 390.55 nm emission is 8.152 eV and that for the 413.09 nm emission is 16.346 eV [27]. Strong ionization of Si atoms by the high intensity laser, resulting in the different emission lines corresponding to the second ionized and third ionized species of silicon are also attributes of these spectra. However, the emission corresponding to Si I is very weak when compared to that from the ionized species such as Si II, Si III and Si IV. This is mainly due to the low

Chapter 3

transition probability for the Si I species. Ionization of carbon atoms is not that evident from the emission spectrum apart from a few lines corresponding to C II and C III. Moreover, the intensities of those lines are very small when compared to that of silicon. No emission corresponding to molecular species could be observed in the recorded spectrum. But, the presence of SiC species have been observed using time of flight quadrupole mass spectrometry by other investigators[28,29]. Since the emissions corresponding to SiC does not lie in the optical emission region considered for the present study, it could not be detected using this experimental setup.

3.3.2 Space resolved studies

Even though different emission lines corresponding to the different species mentioned above are observed in the recorded spectrum, only those emission lines corresponding to the maximum relative intensity is considered for the detailed analysis of the spectrum using time-resolved and space-resolved studies. The monochromator is fixed at these wavelengths and the space-resolved studies are conducted by imaging different regions of the plasma plume into the slit of the monochromator by moving the lens, mounted on a translation stage. The image is adjusted such that the region corresponding to 1 mm, 2mm, 3mm, etc from the target position could be imaged so that only emissions from these regions will be processed. Figure 3.2 shows the variation of the intensities of emission lines corresponding to the neutral and ionized states of Si viz. Si I, Si II, Si III and Si IV, with distance from the target. The plasma is generated by the irradiation of laser at energy of 100mJ and at a pressure of about $1-2 \times 10^{-5}$ mbar. The intensities of emission have been obtained from the temporal profiles recorded for that particular species. The emissions at 390.4nm, 413.0 nm, 455.2nm and 408.7 nm correspond to Si I, Si II, Si III and Si IV respectively.

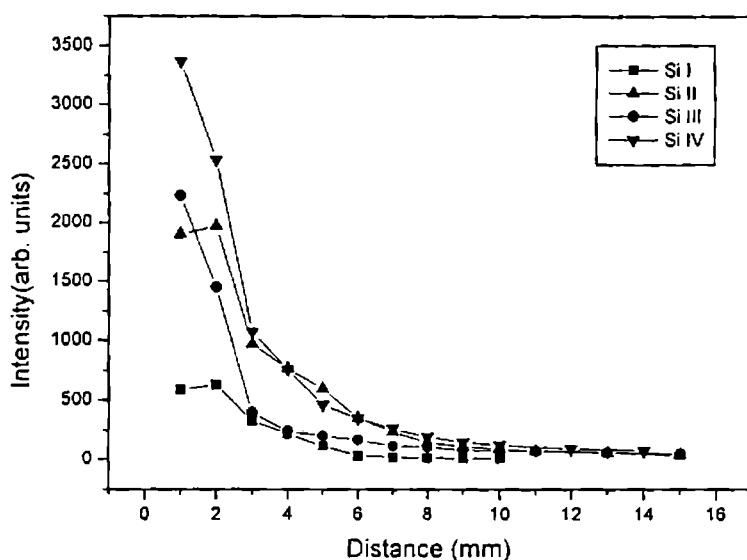


Figure 3.2: Spatial variation of intensity of Si I, Si II, Si III and Si IV

From the spatially resolved spectra, it can be deduced that the spectral intensity decreases with distance from the target surface. Due to the high expansion velocities of the leading plasma edge, the electrons and ion densities decrease very rapidly with time, thus making the plasma transparent to the laser beam. As the plasma is constantly augmented at the inner edge by the evaporated target material for the time duration of the laser pulse, a high density of ions is produced near the target surface. The area near the target surface is thus constantly absorbing the laser radiation during the time interval of the laser pulse, while the outer edge of the plasma is transparent to the laser beam [30]. Nearest to the target, intensity of the most-ionized species, viz., Si IV, is the highest. This is due to the fact that close to the target, the laser power density is quite high to produce emission species of higher ionizations and upon expansion there is a greater chance of them getting converted into lower ionization states due to collision with electrons. Nearest to the target, the

Chapter 3

intensity of the neutral species is the lowest as most of the atoms ejected out of the target are ionized. All the species are observed upto a distance of 15 mm even though the intensity is reduced considerably when compared to that at the surface of the target. We have not observed any molecular species of Si. Most of the observed lines are that of ionized atomic lines. The intensity of the monoatomic species is found to decrease exponentially with distance, which can be ascribed to the particle density decay within the observation volume [31]

3.3.3 Time of flight studies

The temporal behaviour of different species in the plasma can be studied by giving the PMT output to a digital storage oscilloscope. These temporal profiles for different species are observed by keeping the wavelength of the monochromator fixed at the

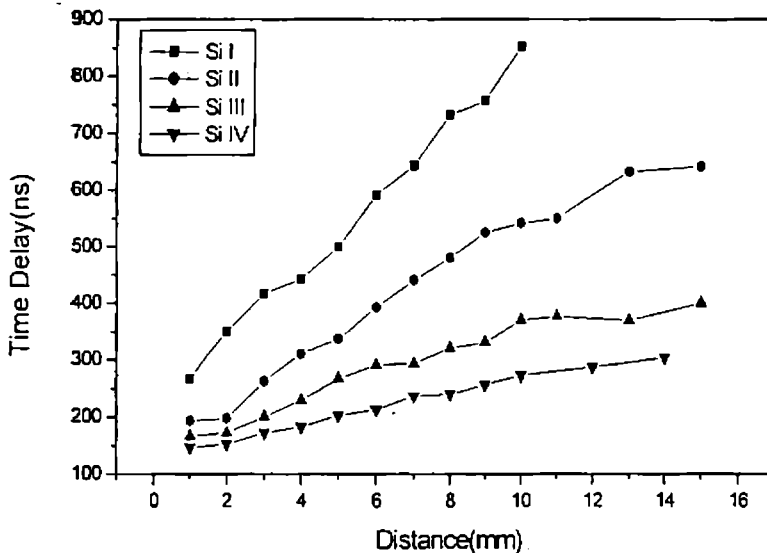


Figure 3.3: Spatial variation of time delay for Si I, Si II, Si III and Si IV

corresponding emission wavelengths. The temporal profiles attain a maximum value and then decrease. For the temporal profiles, the time delay corresponding to the peak intensity is noted. These profiles are recorded for different sections of the plasma, i.e., at different distances from the target surface. Figure 3.3 shows the variation of time delay with the distance from the target for the different species considered earlier. It is seen that time delay increases as the distance is increased. It is also observed that the time delay at a particular distance is more for the neutral or less ionized species when compared to others.

The velocity of the emitted species at different distances from the target can be obtained from the time of flight studies. In expanding plasma, the velocity of the emitted species is found to vary with the position of observation. The energy of the incident laser pulse impinging on the target is varied and the velocities for various

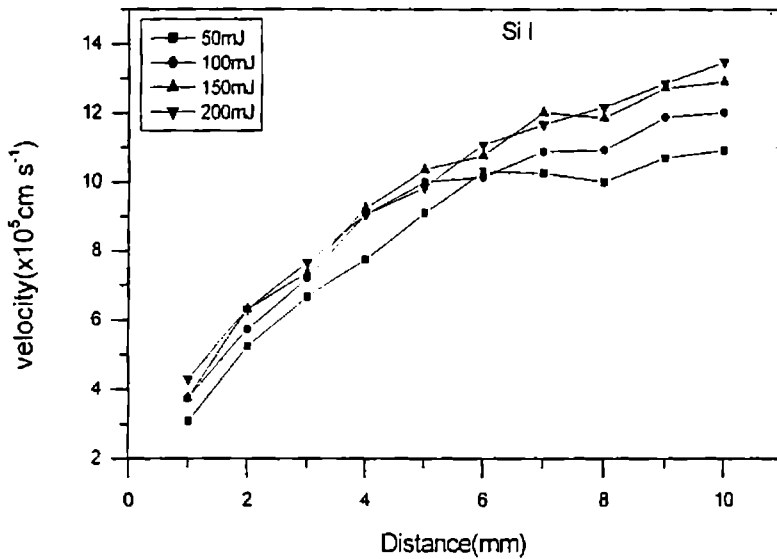


Figure 3.4: Spatial variation of velocity of Si I for different laser energies

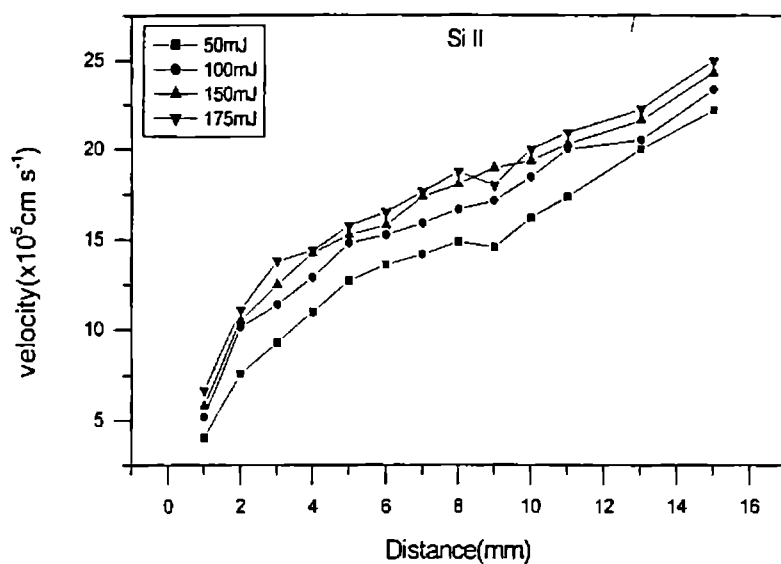


Figure 3.5: Spatial variation of velocity of Si II for different laser energies

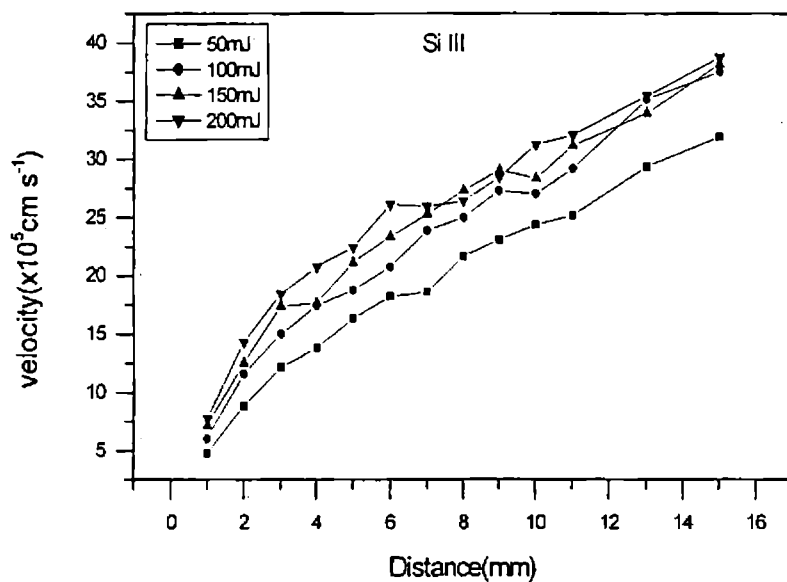


Figure 3.6: Spatial variation of velocity of Si III for different laser energies

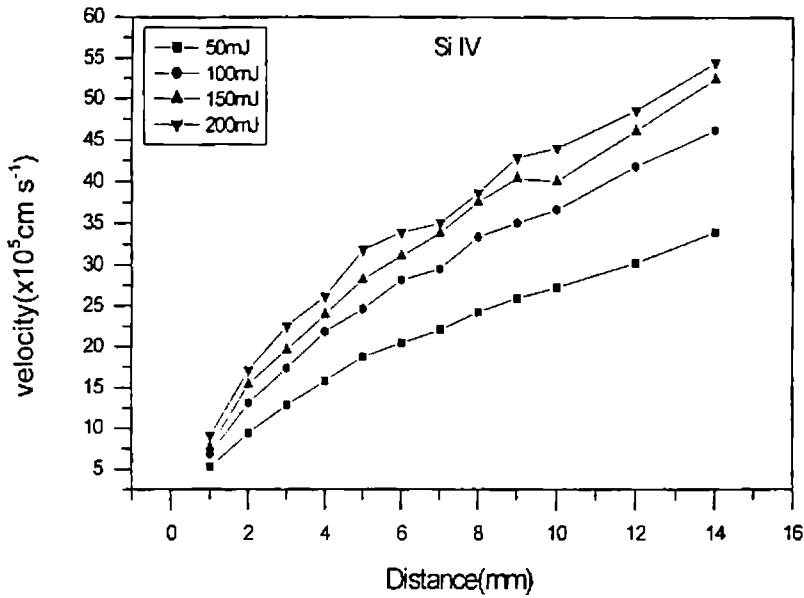


Figure 3.7: Spatial variation of velocity of Si IV for different laser energies

laser energies are plotted. Figures 3.4 and 3.5 show the variation of velocity of Si I and Si II, with distance. The velocities of the particles are found to increase with distance upto a distance of about 4 mm from the target surface, beyond which the rate of increase decreases. The plot also reveals that the velocity of the species generated by the irradiation of high energy pulses have higher velocities when compared with those generated at lower fluences. Figures 3.6 and 3.7 show the velocity distribution at different distances from the target for the species Si III and Si IV for different energies of the laser pulse. A comparison of the different plots for different species show that velocity is higher for highly charged species i.e., Si IV when compared to lower ionized species. Ion expansion velocities are expected to depend on the ion degree of ionization and a velocity increase with the ion charge has been observed for more energetic ions [32]. The ion velocity values are in reasonable agreement with

Chapter 3

previously reported velocities of neutral aluminium atoms in excimer laser-ablated plasmas [33]

3.3.4 Laser energy dependence

The intensity of emission, to a large extent, depends on the laser fluence. The intensity of emission for different ionization states is monitored as a function of laser energy. Laser energy is varied from 50 mJ to 200 mJ in steps of 25 mJ. Figure 3.8 shows the variation in the relative intensities of emission for various species of Si with change in laser fluence at a distance of 5mm from the target and at a pressure of about 2×10^{-5} mbar. It is observed that at this distance the intensity of the singly

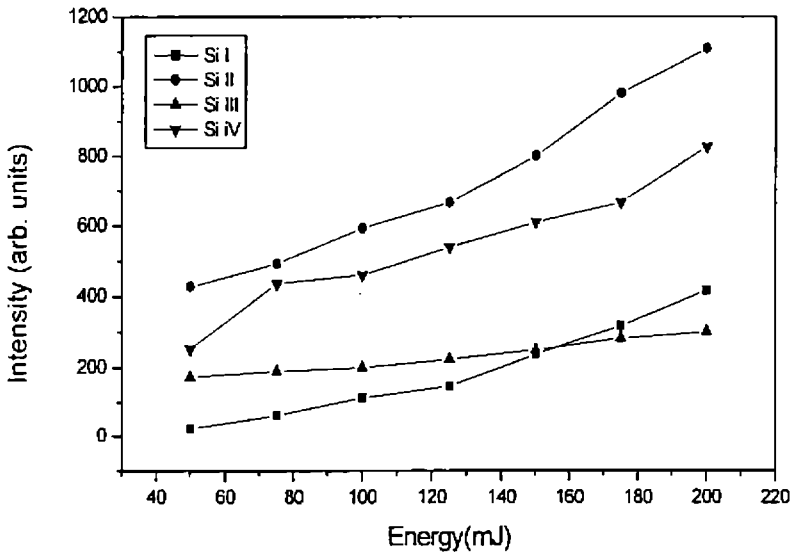


Figure 3.8: Variation of intensity with laser energy for Si I, Si II, Si III and Si IV

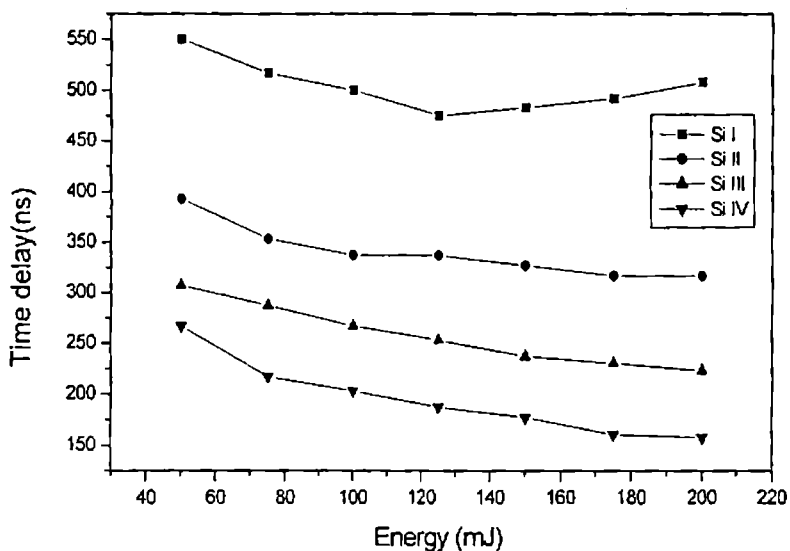


Figure 3.9: Variation of time delay with laser energy for Si I, Si II, Si III and Si IV

ionized species has maximum intensity and that due to neutral species has the lowest intensity. In all cases, the intensity of emitted species is found to increase with incident fluence. This can be attributed to the fact that more number of species of a particular ionization state is ejected from the target with increase in incident energy. From figure 3.2 it can be seen that closer to the target, intensities of highly ionized species is large when compared to others. The variation of time delay with laser energy for the different species is shown in figure 3.9. Time delay is found to decrease with laser energy for all the species and the delay for the more ionized species is found to be less compared to the lesser ionized ones.

3.3.5 Pressure dependence

The effect of pressure on the temporal profile of the emitting species is investigated

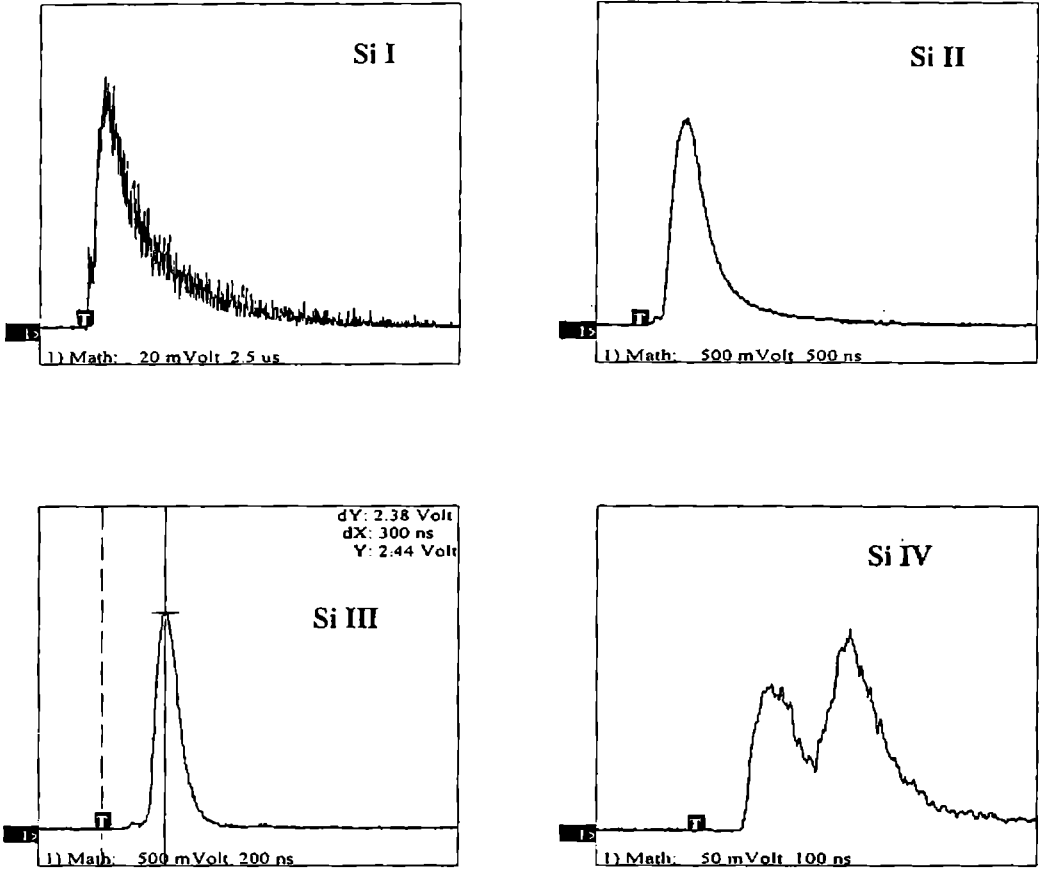


Figure 3.10: Temporal profiles of Si I, Si II, Si III and Si IV, where the temporal profile of Si IV shows a double peak structure

by varying the pressure inside the chamber in the range 2×10^{-5} mbar to 1×10^{-3} mbar. This is monitored by recording the intensity of the emitted species using a digital oscilloscope at a distance of 5 mm from the target surface and at the laser pulse energy of 150 mJ. Figure 3.10 shows the temporal profiles of Si I, Si II, Si III and Si IV. It is observed that for the pressure range considered, the temporal profile of emission corresponding to the third ionized species of Si has two peaks while other profiles have only a single peak. Figure 3.11 shows the intensity of emission from different species present in the plasma for different ambient pressure. The intensity of the lines corresponding to Si II and Si III is found to decrease with increase in pressure. In the case of Si IV, the two peaks behave differently. The first peak, which is the faster one, does not show any variation with increase in pressure whereas the peak due to the slower component decreases with increase in pressure in the chamber. Emissions from the neutral species of silicon also do not show any variation with change in pressure. The variation of the intensity peaks with time delay corresponding to different ambient pressure of the chamber is shown in figure 3.12.

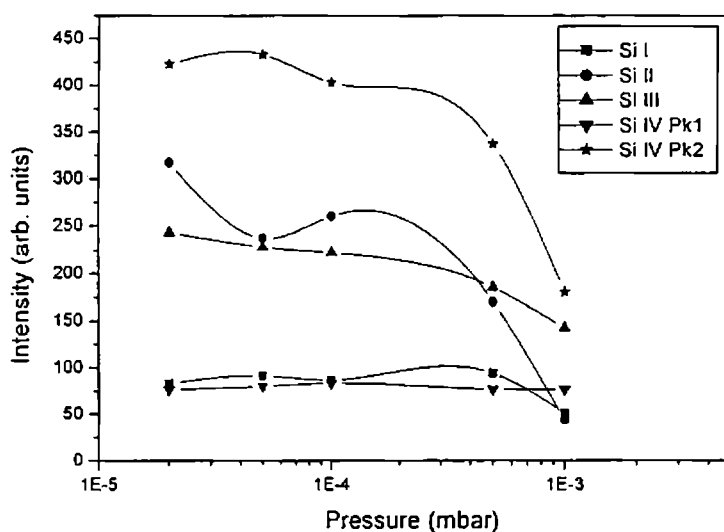


Figure 3.11: Variation of intensity with pressure for Si I, Si II, Si III and Si IV

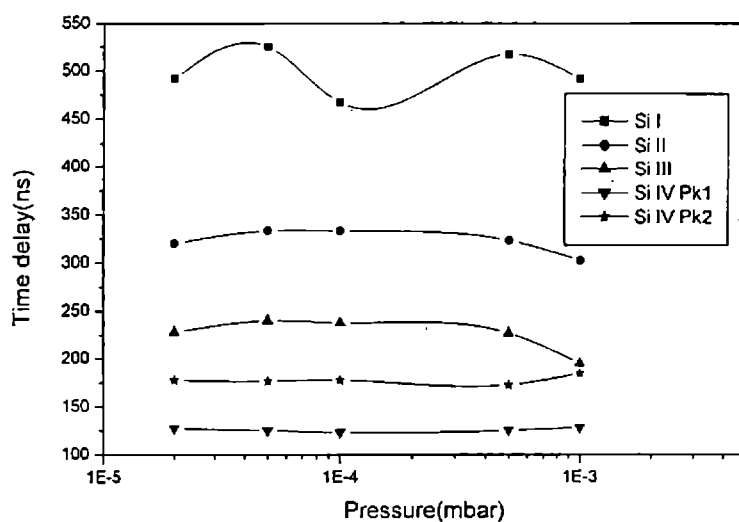


Figure 3.12: Variation of time delay with pressure for Si I, Si II, Si III and Si IV

The pressure is varied from 2×10^{-5} mbar to about 1×10^{-3} mbar. Time delay does not have a notable change with pressure. But the delays for different species are different for the pressure range considered for the present study. The time delay of emission of these species is found to decrease for the different ionization states, with the maximum delay for the neutral species of silicon and the minimum delay for the Si IV species. A remarkable observation is that the time delays for the two peaks corresponding to Si IV species are different. There is a faster component and a slower component in the temporal profile of the signal obtained at this particular wavelength corresponding to the ionized species of silicon. Even though there are two components for the temporal profile of the Si IV species, the delay is less than that of Si III species.

3.3.6 Electron density measurement

Measurement of Stark broadened line profile of an isolated atom or singly ionized species is the most commonly and accurately used spectroscopic technique to determine electron density of plasma [34]. For well-resolved transitions for which the Stark broadening coefficients have been measured or calculated, linewidth measurements can provide electron densities. Measured Stark profiles permit the determination of electron densities in plasmas of almost any chemical composition, even if the latter is not well known. The broadening of emission line is caused by the interaction of radiating atoms or ions with perturbing electrons or ions. It is principally a density effect and does not depend sensitively on temperature or on the electron velocity distribution. Stark broadening is independent of the assumption of Local Thermodynamic Equilibrium [35]. In Stark broadening method, absolute photon intensities are not required, and merely the relative line shapes and widths are sufficient to calculate electron density. Background corrections can usually be ignored because both continuum and overlapping wings from other lines are almost always practically constant over a sufficient wavelength range on both sides of the maximum. In this method, full width at half maximum (FWHM), i.e., wavelength differences between the two points where the intensity falls by a factor of 2 with respect to the maximum, is used. Full-widths of the required lines have been obtained from the tabulated Stark profiles given in Griem [34].

The full width at half maximum (FWHM) of the lines $\Delta \lambda_{1/2}$ is related to the electron density by the expression [32]

$$\Delta \lambda_{1/2} = 2W \left[\frac{n_e}{10^{16}} \right] + 3.5 \text{ \AA} \left[\frac{n_e}{10^{16}} \right]^{1/4} \left[1 - \frac{3}{4} N_D^{-1/3} \right] W \left[\frac{n_e}{10^{16}} \right] \text{ \AA} \quad (3.1)$$

where W is the electron impact parameter which can be incorporated to different

Chapter 3

temperatures, A is the ion broadening parameter and N_D the number of particles in the Debye sphere defined as [36]

$$N_D = 1.72 \times 10^{12} \frac{[T(eV)]^{3/2}}{[n_e(m^{-3})]^{1/2}} \quad (3.2)$$

The first term on the right side of equation 3.1 represents the broadening due to electron contribution and the second term is the ion correction factor. For nonhydrogenic ions, Stark broadening is predominantly by electron impact. Since the perturbations caused by ions are negligible compared to electrons, the ion correction factor can safely be neglected. Therefore equ 3.1 reduces to

$$\Delta \lambda_{1/2} = 2W \left[\frac{n_e}{10^{16}} \right] \text{ \AA} \quad (3.3)$$

Electron density is calculated by charting the stark-broadened profile of Si II atom corresponding to an emission at 385.3 nm. The emission from the plasma at a distance of 2 mm from the target is used for the present study and the energy of the laser pulse is fixed at 150 mJ. The pressure inside the chamber is maintained at 2×10^{-5} mbar. The gate width of the Boxcar Averager is kept at 10 ns and the gate delay is varied in steps of 10 ns for obtaining the time resolved spectrum. Electron density of the plasma, calculated by the above method is plotted against the time delay and is shown in figure 3.13. It is observed that the density increases upto 200 ns after the laser pulse and then decreases to a lower value after a time delay of about 280 ns. The signal strength after this delay is too low to be observed. The maximum electron density of about $2.8 \times 10^{17} \text{ cm}^{-3}$ corresponds to a time delay of nearly 200 ns at a distance of 2mm from the target. The electron density variation observed in the

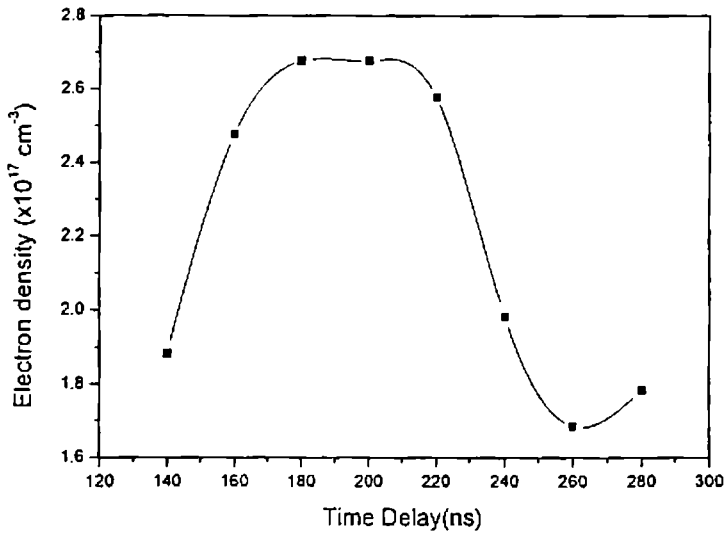


Figure 3.13: Electron density variation with time delay for SiC plasma

present case is similar to the observations for plasma generated in aluminium [37]. The main source of production of electrons, except that originating directly from the target, is due to collisions in the plasma. This means that during the initial time delay, there are large number of collisions which results in the production of electrons thereby increasing the number density of electrons. Thus the formation of plasma occurs after the duration of the laser pulse through collisions. We see that after the plasma density reaches a maximum at around 200 ns, it is found to decrease rapidly thereafter. The decrease in the density after a definite time delay is due to different electron loss mechanisms, i.e., the recombination and plasma radial expansion. The plasma expansion model studied by Kools et al [38] and Pietsch [39], describes the expansion one-dimensionally at the early stages, and then three dimensionally. Therefore, we can deduce that at the initial 1-D expansion stage, the plasma moves away from the target while its volume changes slightly. In addition, the laser pulse produces relatively steady ablated particles under similar conditions. In this case, a

Chapter 3

delay of less than 220 ns is estimated for 1-D plasma expansion and after it, plasma density decreases rapidly due to 3-D expansion. Similar observations have been recorded by Lu et al. [40]. Also, when the plasma begins to cool due to expansion, the probability of recombination increases and hence the electron density decreases. Thus plasma evolution can be described as going through temporal regions, one of which is the formation phase and the other is the delay or recombination regime.

3.3.7 Electron temperature measurement

The oldest method for the determination of temperatures in Local Thermodynamic Equilibrium (LTE) plasmas is based on the fact that densities in various excited states are proportional to the products of statistical weights with the exponentials of the negative ratios of excitation energy and the thermal energy kT . The electron temperature is accordingly inversely proportional to the logarithm of the ratio of total intensities of lines arising from different upper levels, provided that none of the lines is affected by self-absorption. Quantitatively,

$$kT = \frac{E' - E}{\ln(I\lambda^3 g'f' / I'\lambda'^3 gf)} \quad (3.4)$$

where I , λ , g , f and E are the total intensity, wavelength, statistical weight, absorption oscillator strength and the excitation energy of one line, respectively. The corresponding quantities for the other line are I' , etc.

Relative line intensities from the same element and ionization stage usually do not result in accurate temperatures, not even for LTE hydrogen plasma. The principal reason for this is the relatively small separation between the upper levels of the two lines, which is normally not much larger than typical thermal energies and

may be smaller. This renders the line-intensity ratio rather insensitive to temperature changes. Considerable improvement in the sensitivity is obtained if lines from successive ionization stages of the same element are compared with each other, because the effective energy difference is now enhanced by the ionization energy, which is larger than the thermal energy. In LTE the ratio of such line intensities follows as

$$\frac{I'}{I} = \frac{f'g'\lambda^3}{fg\lambda^3} \left(4\pi^{3/2} \alpha_0^3 N_e\right)^{-1} \left(\frac{kT}{E_H}\right)^{3/2} \exp\left(-\frac{E' + E_\infty - E - \Delta E_\infty}{kT}\right) \quad (3.5)$$

Primed quantities refer to the line from the higher ionization stage, and ΔE_∞ is the reduction of the ionization energy E_∞ of the lower ionization stage. Very high electron densities are necessary to ensure LTE, e.g., more than $N_e = 10^{18} \text{ cm}^{-3}$ in the case of neutral and ionized helium for an accuracy of about 10 per cent in the line intensity calculated for a given temperature. At $N_e = 10^{17} \text{ cm}^{-3}$ this ratio would have an uncertainty of a factor of 2, giving rise to a relatively large error in temperature if the ratio were measured and the temperature calculated using the above relation. For electron densities between, say in the range $10^{15} - 10^{17} \text{ cm}^{-3}$, one should use the corona equation for the ratio of two ion densities. This procedure yields for the ratio of the ion and neutral line intensities,

$$\frac{I'}{I} \approx \frac{f'g'\lambda^3}{fg\lambda^3} \exp\left(\frac{E'_\infty - E' - E_\infty + E}{kT}\right) \frac{S}{\alpha} \quad (3.6)$$

Here E'_∞ is the ionization energy of the higher ionization stage and E_∞ that of the lower, and S and α are ionization and recombination coefficients with respect to the next higher ionization stage.

Chapter 3

The electron temperature of the plasma is calculated by taking into consideration corona equilibrium. For calculating electron temperature, the relative line intensities corresponding to Si I (390.5 nm) and Si II (412.8 nm and 413.0 nm) are taken. Plasma is generated with the laser pulse energy of about 150 mJ and in a vacuum chamber of pressure 2×10^{-5} mbar. The time resolved studies on the variation of the electron temperature is carried out by recording the spectrum with a gate width of about 10 ns and varying the width in equal steps of 20 ns using a Boxcar Averager.

Figure 3.14 shows the variation of electron temperature with time delay. It is seen that electron temperature has a maximum value of about 2.48 eV and decreases with increase in time to about 380 ns, after which the intensities of the lines are too low to be detected. Initially the plasma expands isothermally within the time duration of the laser pulse, after which, the plasma expands adiabatically. During this,

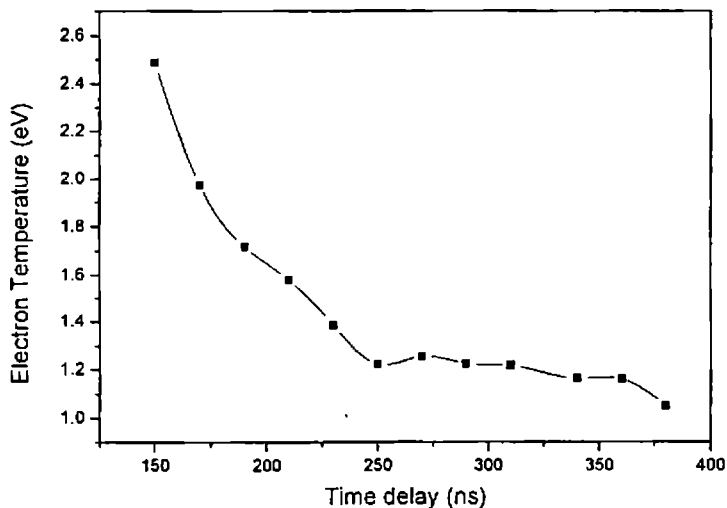


Figure 3.14: Electron temperature variation with time delay for SiC plasma

expansion, the thermal energy is converted into kinetic energy and the plasma cools down rapidly. An adiabatic expansion of the plasma occurs, and the temperature can be related to the dimensions of the plasma by adiabatic thermodynamic relation

$$T[X(t)Y(t)Z(t)]^{\gamma-1} = \text{constant} \quad (3.7)$$

where γ is the ratio of specific heat capacities at constant pressure and volume, $X(t)$, $Y(t)$ and $Z(t)$ are the dimensions of the expanding plasma in the three mutually perpendicular directions. The temperature decreases more slowly than predicted by the adiabatic equation due to the preferential expansion of plasma in one dimension during the initial stages and due to recombination effects [41].

3.4 Summary

Plasma generated at the surface of a silicon carbide target by the irradiation of a nanosecond laser has been studied. Space-resolved studies of the evolution of different species present in the plasma reveal that velocities of these species are dependent on the ionization states and the most ionized species, Si IV is found to have higher velocities in comparison to others. Electron density and electron temperature calculations show that plasma has the highest density at a time delay of around 200 ns from the laser pulse and the electron temperature decreases with increase in time delay.

Chapter 3

References:

1. W.W. Duley, *UV lasers: Effects and Applications in Materials Science*, Cambridge University Press, Cambridge (1996)
2. M. von Allmen, *Laser Beam Interactions with Materials*, Springer, Heidelberg (1987)
3. M.A. Shannon, X. Mao, A. Fernandez, W.T. Chan and R.E. Russo, *Anal. Chem.* 67 (1995) 4522
4. J.C. Miller and R.F. Haglund, Jr., *Laser Ablation Mechanisms and Application*, Springer, Heidelberg (1991)
5. X. Zhang, S.S. Chu, J.R. Ho and C.P. Grigoropoulos, *Appl. Phys. A* 64 (1997) 545
6. A.B. Brailovsky, S.V. Gaponov, and V.I. Luchin, *Appl. Phys. A* 61 (1995) 81
7. A. Miotello and R. Kelly, *Appl. Phys. Lett.* 67 (1995) 3535
8. R. Kelly and A. Miotello, *Appl. Surf. Sci.* 96-98 (1996) 205
9. J.H. Yoo et al. *Appl. Phys. Lett.* 76 (2000) 783
10. D.B. Chrisey and G. K. Hubler (Eds), *Pulsed Laser deposition of thin films*, Wiley, New York (1994) Chapter 5
11. B.C. Castle, K. Visser, B.W. Smith and J.D. Winefordner, *Appl. Spectrosc.* 51 (1997) 1017
12. H. Kurniawan, Y. Ishikawa, S. Nakajima and K. Kagawa, *Appl. Spectrosc.* 51 (1997) 1769
13. E. Mathias, M. Reichling, J. Seigel, O.W. Kading, S. Petzoldt, H. Skurk, P. Bizenberger and E. Neske, *Appl. Phys. A* 58 (1994) 129
14. R.J. de Young and W. Situ, *Appl. Spectrosc.* 48 (1994) 1297
15. M. Kuzuya, H. Matsumoto, H. Takechi and O. Mikami, *Appl. Spectrosc.* 47 (1993) 1659
16. A. Dupont, P. Caminat, P. Bournot and J.P. Gauchon, *J. Appl. Phys.* 78 (1995) 2022

17. L.M.Cabalin and J.J. Laserna, *Spectrochim Acta Part B* 53 (1998) 723
18. Y.M. Lai and N.H. Cheung, *Rev. Sci. Instrum.* 64 (1993) 1606
19. S. Amoroso, A. Amodeo, V. Berardi, R. Bruzzese, N. Spinelli and R. Velotta, *Appl. Surf. Sci.* 96 (1996) 175
20. S. Nakamura, K. Midorikawa, H. Kumagai, M. Obara and K. Toyoda, *Jpn. J. Appl. Phys.* 35 (1996) 101
21. M.Milan and J.J. Laserna, *Spectrochim. Acta part B* 56 (2001) 275
22. W. K. Choi, in *Silicon-baser materials and Devices Vol. I Materials and Processing*, edited by H S Nalwa (Academic, San Diego, 2001), Chap 1
23. S. Trusso, E Barletta, F Barreca and F Neri, *Appl. Phys. A* 79 (2004) 1997
24. S. Trusso, F. Barreca and F.Neri, *J. Appl. Phys.* 92 (2002) 2485
25. R.C. Weast, *CRC Handbook of Chemistry and Physics*, CRC Press, Inc. Florida (1988)
26. R.W.B. Pearse and A.G. Gaydon, *The Identification of Molecular Spectra*, Chapman & Hall Ltd, London (1965)
27. *Handbook of Chemistry and Physics*, CRC Press, Boca Raton 1995
28. S.H. Nam and S.M. Park, *J. Appl. Phys.*, 95 (2004) 8425
29. Michael A. Capano, *J. Appl. Phys.*, 78 (1995) 4790
30. R.K.Singh, O.W. Holland and J. Narayan, *J. Appl. Phys.* 68 (1990) 233
31. W. Marine, M. Gerri, J.M.Scotta d'Aniello, M. Sentis, Ph. Delaporte, B. Forestier and B. Fontaine, *Appl. Surf. Sci.* 54 (1992) 264
32. F.E. Irons, R.W.P.McWhirter and N.J.Peacock, *J. Phys. B* 5 (1972) 1975
33. R.M. Gilgenbach and P.L.G.Ventzek, *Appl. Phys. Lett.* 58 (1991) 1597
34. Hans R. Griem, *Plasma Spectroscopy*, McGraw-Hill Book Company, New York, 1964
35. W. L. Wiese, *Plasma Diagnostic Technique*, R H Huddleston and S.L. Leonard (Eds.), Academic Press, New York, 1965
36. G Bekefi, *Principles of Laser Plasmas*, John Wiley and Sons, New York, 1976

Chapter 3

37. J.T. Knudtson, W.B. Green and D.G. Sutton, *J. Appl. Phys.*, 61(1987) 4771
38. J.C.S. Kools, T.S. Baller, S.T. DeZwart and J. Dieleman, *J. Appl. Phys.* 71 (1992) 4547
39. W. Pietsch, *J. Appl. Phys.* 79 (1996) 1250
40. Y. F. Lu, Z. B. Tao and M.H. Hong, *Jpn. J. Appl. Phys.* 38 (1999) 2958
41. S.S. Harilal, *Ph.D. Thesis*, Cochin University of Science & Technology, 1997

Chapter 4

Laser Produced Plasma from Copper Target - Spectral Studies

5.1 Introduction

Material ablation by short laser pulses is the basic process in many laser technologies such as pulsed laser deposition or laser sputtering. For a sufficient understanding of these processes and for an effective technology optimization, especially for increasing efficiency and productivity, experimental determination of the nature, quantity and properties of ablated particles and their transformation into high-energetic plasma jet is necessary. The transformation from hot vapour to high energetic plasma jet is directly coupled with the expansion of laser induced plasma in the vacuum. Laser energy is primarily absorbed by the electron gas. The electrons with their high thermal velocity try to expand in free space dragging behind the sluggish ions [1]. Ion fluxes produced by high-power lasers from solid targets are the subject of continuing interest in regard to basic research of laser-plasma interaction with profound applications in various fields. They can be potentially useful in large heavy ion accelerators [2] as well as in modifying material properties through ion implantation [3]. The development of laser-ion sources also creates prospect for the construction of compact tabletop particle accelerators, with applications in nuclear physics and medicine [4]. Despite the extensive experimental work that has been performed, various effects of laser beam interaction with metallic surfaces are still not

Chapter 4

satisfactorily explored. Most of the published works are done with IR lasers, and only a few experiments employed lasers in the visible and UV region [5].

In laser ablation of metal targets, the plume is significantly ionized and the ions present have high kinetic energy (up to ~ 100 eV) [6,7]. The kinetic energy distribution of the ejected particles results from the interactions occurring in the plume and is affected primarily by the high density vapour which is formed very close to the ablated target surface. A study of laser plasma at the advanced stage of its expansion gives information about the kinetic energy distribution of the emitted particles, and makes it possible to follow the changes occurring during the variation of experimental parameters.

Pulsed laser deposition offers several attractive features such as the relatively easy preservation of stoichiometry and good structural quality of the deposited film, even when the film is grown at a relatively low temperature. This is attributed to the large kinetic energy of the ablated atoms and molecules upon arrival at the substrate surface. This kinetic energy is obtained in the actual laser ablation process as a result of the laser-matter interaction. However, the precise shapes of the velocity, or kinetic energy, distributions of the depositing particles are the result of various interactions occurring after desorption. Due to the high vaporization rate, there will be a region near the surface where the gas density is sufficiently high for collisions to occur between the desorbed particles. There has been considerable effort, both theoretically and experimentally, on the problem of a gas cloud created by transient desorption from a solid surface [8]. The kinetic energy distributions of ions produced by ablating Si, Ge and Cu targets by high-fluence excimer laser pulses have been demonstrated [9]. Average kinetic energies of Cu^+ ions of the order of 1-30 eV have been observed in the excimer laser produced plasma from copper targets [10]. The ablation depth per pulse and the flux and energy distributions of the ions in the plume of laser ablated copper has also been studied with special emphasis on the growth of thin films [11].

The expansion of a laser-ablated plume in different ambient gases has been investigated theoretically using a two-fluid gas-dynamic model and experimentally with time-of-flight mass spectrometry by Bulgakov and Bulgakova [12]. Simple gas-dynamic considerations based on the analogy between an ablation plume and a supersonic underexpanded gaseous jet was found to explain a number of effects of the interaction between the plume and background gas. Dynamics of a dense, laser-produced vapour plume has been analytically studied by Anisimov et al.[13] and the analysis is based on the special solution of gas dynamic equations that describes the expansion of an ellipsoidal gas cloud into vacuum. The 'flip-over effect' suggested in this model has been used for the interpretation of the time-of-flight spectra of atoms in laser ablation, and for the description of the shape of vapour cloud expanding into an ambient gas. In the theoretical model suggested by Singh and Narayan [14] for simulation of laser-plasma-solid interaction, the laser-generated plasma is treated as an ideal gas at high pressure and temperature, which is initially confined in small dimensions and is suddenly allowed to expand in vacuum. The three dimensional expansion of this plasma gives rise to the characteristic spatial thickness and compositional variations observed in laser-deposited thin films of multicomponent systems.

The successful deposition of stoichiometric thin films by the method of pulsed laser deposition demands the characterization of the ablation plume with temporal, spatial and angular resolutions. When laser plasma is considered under the context of thin film deposition, there exists two different angular distributions which are (i) the source angular distribution and (ii) the film thickness distribution. The highest energies of ablated particles occur in directions close to the target normal and with increasing angle of emission the average energy as well as the total ion flux decreases strongly [15,16].

Chapter 4

Geohegan and Purezky [17] describe the broadening of the time-of flight profile in Yttrium plasma at high pressure levels due to collision with the background gas molecules. In vacuum, they found narrow velocity profile for ionic species. At high ambient pressure, the plasma plume has a large angular spread due to scattering, which is negligible in vacuum. Gas phase collisions inside the plasma play a major role in determining the spatial, temporal and angular distribution of ablated species. When the particle densities are high enough, collisions induce the formation of thermalization layer called Knudsen layer with a few mean free paths from the target surface where negative velocities develop among the particles[18-20]. In order to have momentum conservation, a positive flow velocity also develops for the species. In the presence of collisions in the plasma and KL formation the half-range Maxwellian velocity distribution for various species in collisionless plasma gets modified into a full-range Maxwellian in a centre of mass system. A Knudsen layer can also be defined as the layer at which the change in velocity distribution occurs. The backward moving particles are either re-condensed or reflected from the target surface [21]. The Knudsen layer formation is followed by a more forward peaked particle flux with an unsteady adiabatic expansion of the plasma.

Recently, there has been a report on the characterization of collinear double pulse laser-induced plasma from copper and zinc at several ambient gas pressures by spectrally and temporally resolved imaging technique [22]. This double pulse configuration leads to a significant increase of the plume volume and to a different spatial distribution of the emitters, compared to the case of a single pulse of the same total energy.

The characterization of laser-induced plasmas (LIPs) has been recognized as essential for the understanding and use of these complex and interesting sources of radiation and materials. Amongst the various techniques which are convenient tools to detect various transient species with optical transition in visible spectral region, the

optical emission spectroscopy has definite advantages pertaining to high spatial and temporal resolution without perturbation of the plasma. Multari et. al. [23] has studied the variation of neutral atom and ion emission distributions for different laser focusing conditions by using an acousto-optic tunable filter placed in front of an intensified CCD detector. Castle et. al.[24] used a similar detector to obtain wavelength-integrated and spectrally-resolved images of LIP where as neutral atom and ion emissions were selected by Aragon et. al. [25] using interference filters.

4.2 Experimental

The experimental set up used for this study is the same as that described in previous chapters. The plasma is produced in a chamber by irradiating a copper target with the fundamental output of the Q-switched Nd: YAG laser with pulse width 9 ns and repetition rate 10 Hz. During the experiment, pressure inside the chamber could be varied. The optical emission spectrum is recorded by a monochromator-PMT assembly using a computer interfaced Boxcar averager in the wavelength range 350-650 nm. From the recorded spectrum, different emission lines are identified by comparing the spectrum with standard emission data. The emission spectrum contain signature of Cu I, Cu II and Cu III when the pressure inside the chamber is 2×10^{-5} mbar. Emission lines from the ionized species of nitrogen have also been recorded, when the ambient pressure in the chamber is increased to 1×10^{-3} mbar. Since the intensities corresponding to various transitions are very low, we selected only those emission lines which showed a considerable intensity. The main emission lines chosen for detailed investigations are 521.8 nm emission corresponding to Cu I and 490.7 nm corresponding to Cu II.

4.3 Results and Discussion

4.3.1 Spatial variation of Cu I

The temporal profile of the emission corresponding to Cu I species is analyzed with spatial resolution. Monochromator is fixed at the wavelength of 490.7 nm corresponding to Cu I species and the PMT output is given to a digital storage oscilloscope. The intensity of emission and the time delay are recorded by imaging different sections of the plasma into the entrance slit of the monochromator. These experiments are performed at rotary vacuum at a pressure of about 150×10^{-3} mbar. The temporal profile of the signal for different distances from the target surface is recorded for different energies of the laser pulse. Figures 4.1, 4.2, 4.3 and 4.4 show the variations in intensity and time delay of the temporal profiles with distance for 100 mJ, 150 mJ, 200 mJ and 250 mJ of laser energy, respectively. The intensity distributions of the emission lines are found to be sensitive to laser fluence:

Spectral emission intensity is observed to decrease with increasing distance from the target surface for all laser energies probed. The intensity decreases upto a distance of 2 mm, beyond which it remains a constant. However, for laser energies of 200 mJ and 250 mJ, it is observed that the intensity of the Cu I species increase suddenly at close proximity to the target. Due to the high electron densities of plasma nearer to the target, the ions and other species in the plasma collide. Maximum intensity is found at a distance of 1mm from the target for a laser pulse energy of nearly 250 mJ. The increase in intensity of Cu I is mainly due to the collisional recombination of Cu II species with the free electrons.

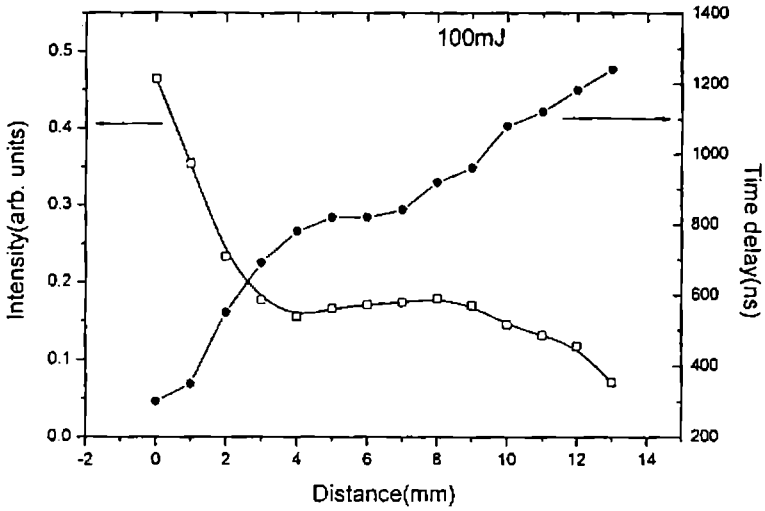


Figure 4.1: Variation of intensity and time delay of Cu I emission with distance for 100 mJ laser pulse

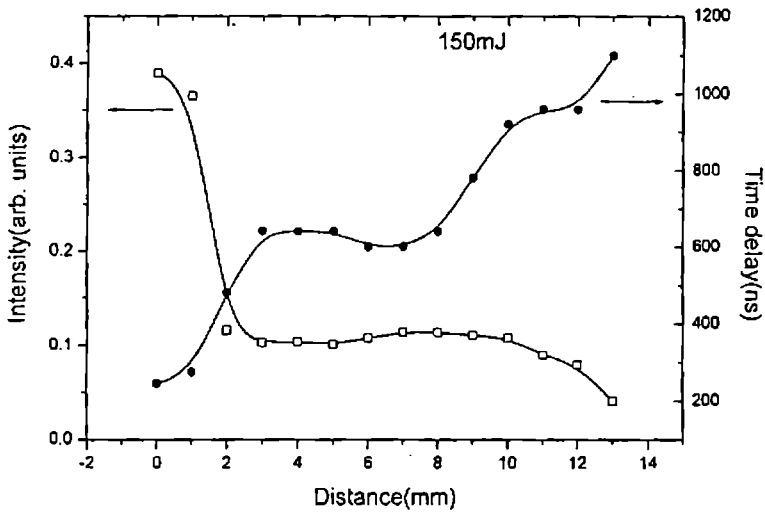


Figure 4.2: Variation of intensity and time delay of Cu I emission with distance for 150 mJ laser pulse

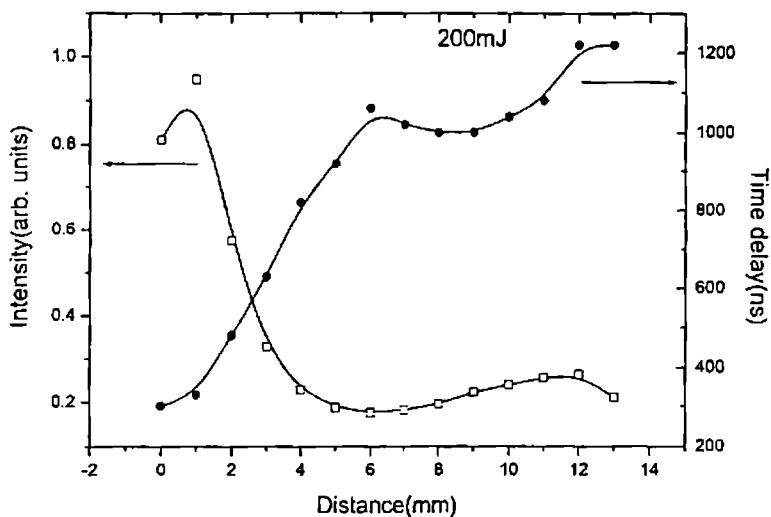


Figure 4.3: Variation of intensity and time delay Cu I emission with distance for 200 mJ laser pulse

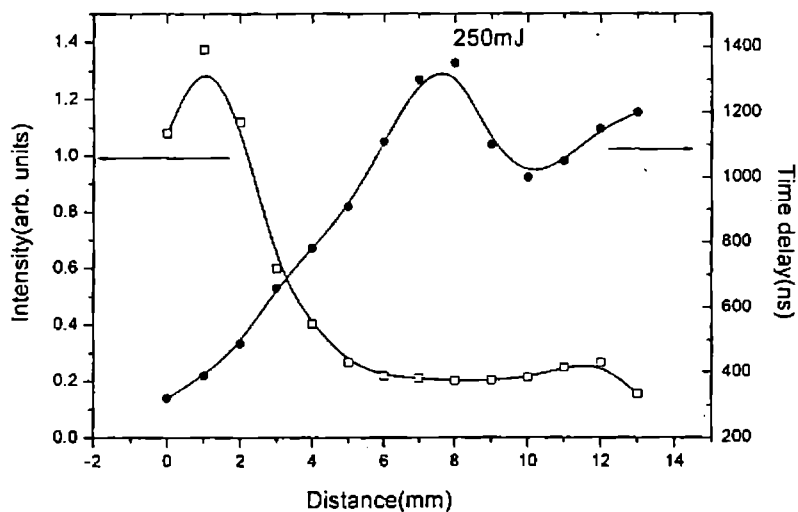


Figure 4.4: Variation of intensity and time delay of Cu I emission with distance for 250 mJ laser pulse

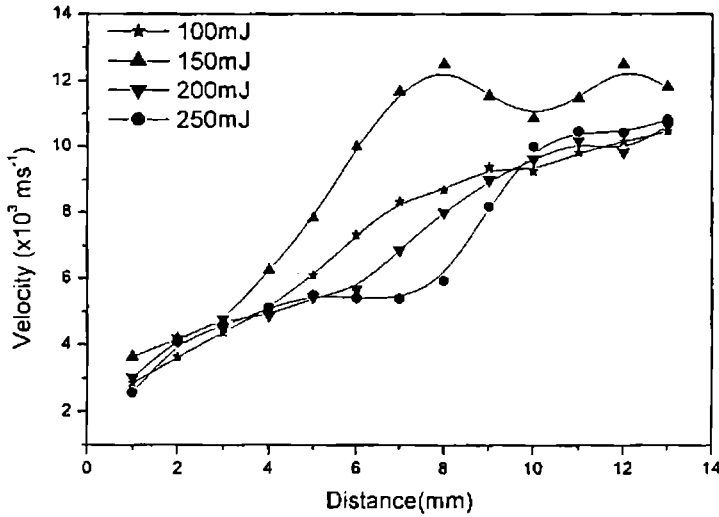


Figure 4.5: Variation of velocity of Cu I species with distance for different energies of the laser pulse

As is evident from the figures, time-delay of the emitted neutral copper species shows a monotonic increase close to the target, which then remains constant upto a certain distance, beyond which there is an increase with distance. This sudden change in the time-delay, shows that there is a considerable change in the expansion velocities of the plasma front for the neutral species of copper around these distances from the target. The velocity of the species is determined by observing the time when the plasma emission is strongest at a particular distance from the target. The emission of Cu I is chosen for this purpose, as this line is long-living and not appreciably self-absorbed. Since distances from the target are small and plasma signal is not sharp peak but a broad noisy maximum, judging the exact time of maximum plasma emission is tricky, especially at larger distances from the target. As a result, the derived velocity can be taken only as a rough estimate of the real plasma expansion velocity. However, it is difficult to expect a sharply defined expansion velocity for

the plasma plume. Rather, a distribution of velocities is more plausible, and our result give a rough measure of the averaged plasma expansion velocity. An initial expansion velocity of the order of several kilometers per second is indicated by the experimental data plotted in the figure. Figure 4.5 shows the variation in velocity of the neutral copper species with distance for different fluences of the laser. Measuring the time of radiation onset yields directly the plasma front axial velocity, which is defined as the expansion velocity of ablation surface perpendicular to the target. The velocity of the neutral copper species is found to increase with distance from the target. But in the region between 5-9 mm from the target surface, the variation in velocity deviates from this regular trend. Detailed experimentation is necessary to confirm the observed deviation in velocity.

4.3.2 Spatial variation of Cu II

The production of metal ions during ablation is important since the chemistry of these species differs markedly from the neutral forms. Evaporation techniques using thermal sources produce primarily neutral metals in the gas phase and result in the deposition of oxygen deficient films. It may be possible to enhance the formation of metal oxides within the plasma by producing ionic forms of these metals during ablation. The ionization potential for Cu^+ (7.726 eV) is greater than the laser photon energy [26]. But, production of Cu^+ is mainly due to mutli-photon ionization, as the laser beam is tightly focussed. The presence of significant emission from neutral atoms indicates the plasma produced is not fully ionized. The copper plasma is developed during nanosecond laser pulse on the basis of these atom/ion collisions and multiphoton absorption[27].

Figure 4.6 gives the typical temporal profile of Cu II line corresponding to a wavelength of 490.7 nm, at different distances from the target. The temporal profile of the emission line has three different peaks, of which the first and second peaks are

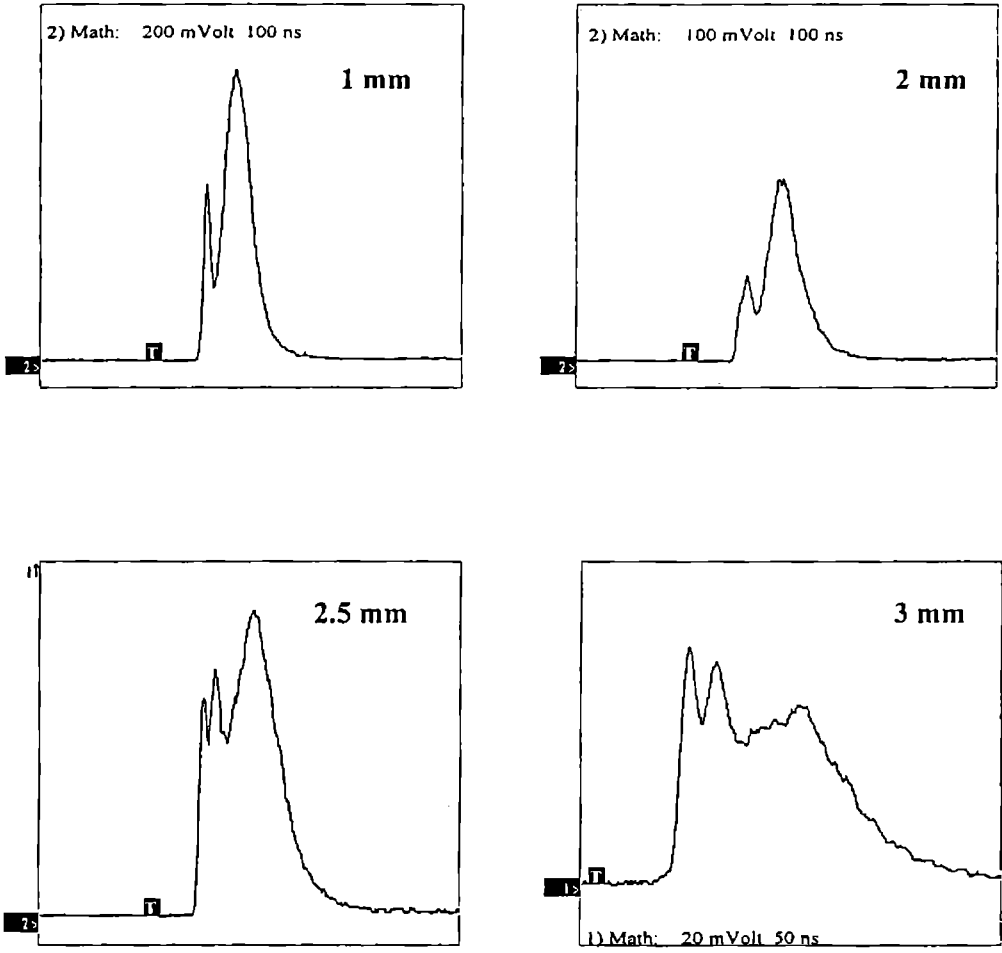


Figure 4.6: Typical temporal profiles of Cu II species at 1mm, 2 mm, 2.5 mm and 3mm distance from the target

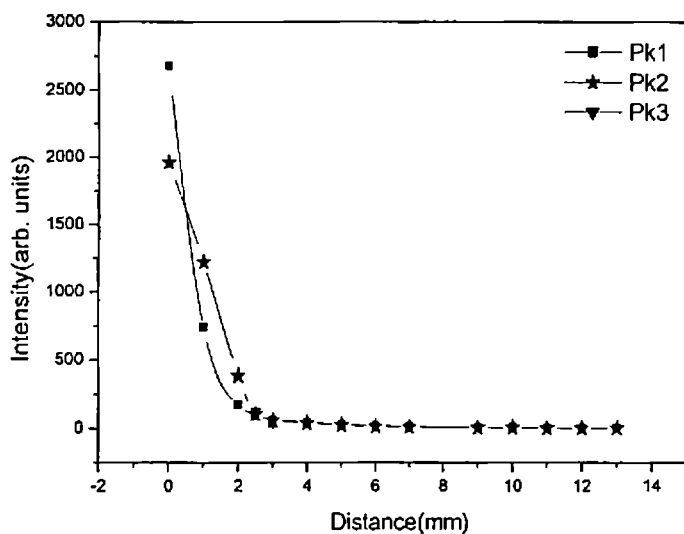


Figure 4.7 : Intensity variation with distance for Cu II species

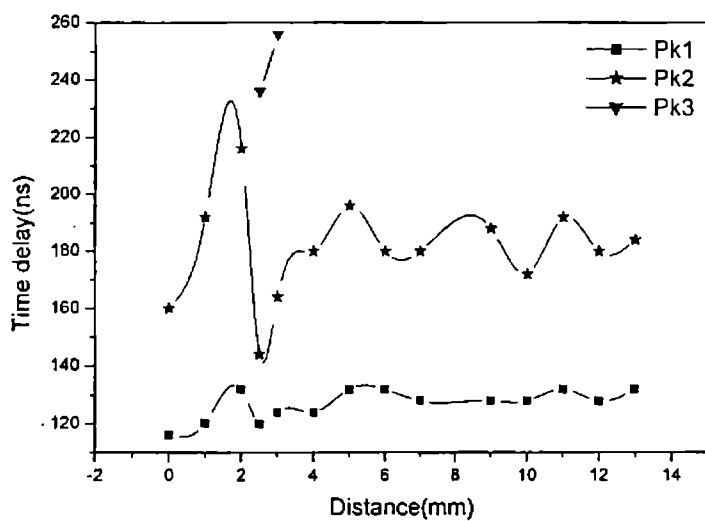


Figure 4.8 : Spatial distribution of time-delay for the different peaks of Cu II species

seen at all distances investigated during the course of this study, but the third peak is observed only at a distance of 2.5 mm and 3 mm from the target surface. The detailed investigation of this region is explained in the next section. Figure 4.7 gives the variation in the intensity of emission of Cu II species with distance. The intensity is found to decrease considerably with distance from the target.

The emission line corresponding to the first ionized species of Cu is recorded with the pressure in the chamber at 0.01 mbar and a laser energy of 150 mJ per pulse. Variation in the time-delay of the peak emission is plotted in figure 4.8 for the various distances from the target surface. The time-scales at which the three peaks appear is seen clearly from the figure. The first and the second peaks remain for the entire distance considered for the study, where as the third peak remains only for a specific distance from the target. The time delay for the first peak remains the same for different distances, but the second peak shows noticeable variation. During the appearance of the third peak, the time delay for the second peak reduces to a very low value, and after the disappearance of the third peak, the time delay for peak 2 remains the same for the different distances considered.

The expansion velocities, as calculated by the method described in the previous section, for Cu II reveals a different behaviour. The velocity is found to increase with distance for the first two peaks of the temporal profile. The increase in the velocity has a linear relation with distance. Figure 4.9 shows the variation in velocity distribution of the slow and fast components of Cu II species in the plasma with distance from the target. The velocity of the ionic species of copper atom is found to be higher than the neutral species considered in the previous section. The origin of such high velocities could be explained as follows. Firstly it should be

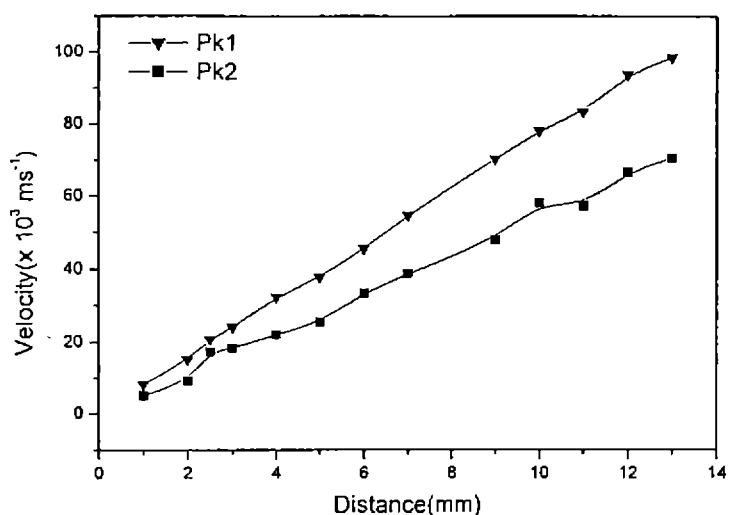


Figure 4.9 : Plot between the distance from the target and the velocity of ions

mentioned that the absorption of laser radiation by the dense plasma such as is produced when a solid target is irradiated may have a strong effect on the velocities attained. It is possible that a significant part of the incoming energy is transferred to the plasma and only a lesser amount dissipated in the solid. This occurs by coupling the light frequency with the plasma frequencies before significant expansion has occurred, i.e., when the plume is at a short distance from the target. The pulse duration is relatively long and this follows an efficient coupling with the plasma, before the pulse terminates. The partial absorption of laser energy by the ejected plasma, through an inverse bremsstrahlung process, above the target surface gives rise to an increase in the velocities and energies [28].

The expansion dynamics of laser-generated plasma has been described by semiquantitative models. The behaviour of the gas cloud moving away from the target could be treated theoretically by means of hydrodynamic equations. The

analytical models describe time- and space- dependent gas density and angular velocity distribution of the ejected particles [29]. The particle motion in the perpendicular direction x and the two lateral directions y, z with respect to the target plane can be separated into three: (i) interaction of the laser with the target leading to plasma formation, (ii) isothermal expansion, and finally (iii) adiabatic expansion of the gas cloud. The first two regimes occur during the laser pulse while the latter applies in the absence of laser pulse. In the isothermal expansion, gas-dynamic equations of mass and momentum conservation are applied.

The linear increase in velocity is in agreement with the widely accepted theory of adiabatic plasma expansion [30]. During adiabatic expansion, the x -component of velocity v_x is given by the relation,

$$v_x = \frac{x}{X(t)} \frac{dX(t)}{dt}$$

Here $X(t)$ is the dimension of expanding plasma along x -direction and corresponds to the distance at which the plasma density decreases to 60.65 %. In the case of adiabatic expansion, velocities of all the constituent species increase linearly with distance from the target. Here the thermal energy of the particles is converted to kinetic energy.

4.3.3 Pressure dependence of Cu II

Since the temporal profiles of the emission corresponding to Cu II species shows multiple peaks at certain distances from the target surface, its dependence on the pressure inside the chamber was investigated for these distances. Figures 4.10(a), 4.11 (a) and 4.12 (a) give the variation in intensity of emission corresponding to the different peaks for various pressures of the chamber at distances 2mm, 2.5mm and

Chapter 4

3mm from the target surface, respectively. Figures 4.10(b), 4.11(b) and 4.12(b) give the corresponding variation of time delay for these peaks for various pressures at distances 2 mm, 2.5 mm and 3 mm, respectively.

The intensity of the first peak, which is the fastest peak, formed at a distance of 2 mm from the target surface, increases with increase in pressure of the chamber. However, the first peak at distances 2.5 mm and 3 mm remain at the same intensity with increase in pressure. The intensity of the second peak increases with pressure to a maximum value and then decreases at a distance of 2 mm. At 2.5 mm away from the target surface, there is an additional component originating, which shows a complimentary variation in intensity with the second peak observed. The intensity of the second peak increases to a maximum value at a pressure around 0.2 mbar and then decrease with pressure, while the intensity of the third peak (slowest peak) decreases to a minimum value around 0.2 mbar and then increases with increase in pressure. At 3 mm from the target surface, the intensity of the second peak remains a constant, where as the third peak increases sharply with pressure and then decreases. This behaviour is similar to the second peak at a distance of 2 mm from the target. The maximum value of the intensity for the distance of 2 mm is at a pressure of about 40-50 mbar, where as that for 3 mm it is around 15-20 mbar. The second peak could not be detected, when the pressure was increased more than 1 m Bar at distances 2.5 mm and 3 mm.

The time-delay for the emitter at these distances and pressure also show similar variations. Time delay is the same for the first peak in the temporal profile, at different pressures considered, for the three distances from the target surface. It is also seen that time delay of the second peak at a distance of 2 mm is same as that for third peak at distances 2.5 mm and 3 mm from the target. The time delay for peak 2(pk 2) at 2mm and peak 3(pk 3) at 2.5 mm and 3 mm, is found to remain a constant

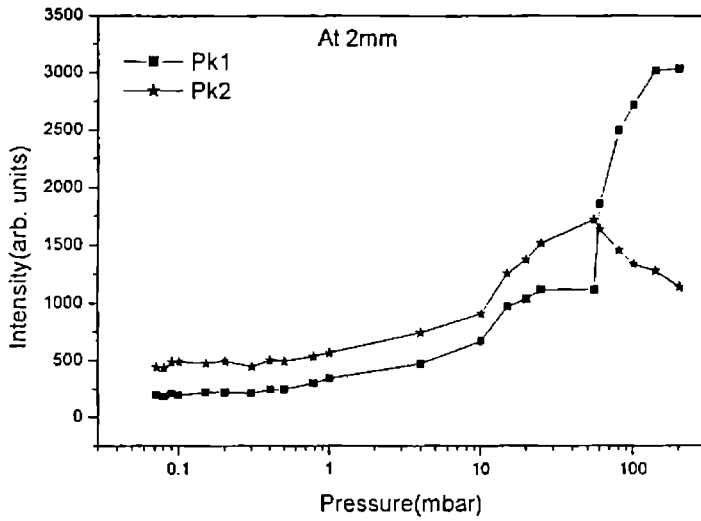


Figure 4.10 (a) : Variation of the intensities for different pressures for the two peaks (pk 1 and pk2)

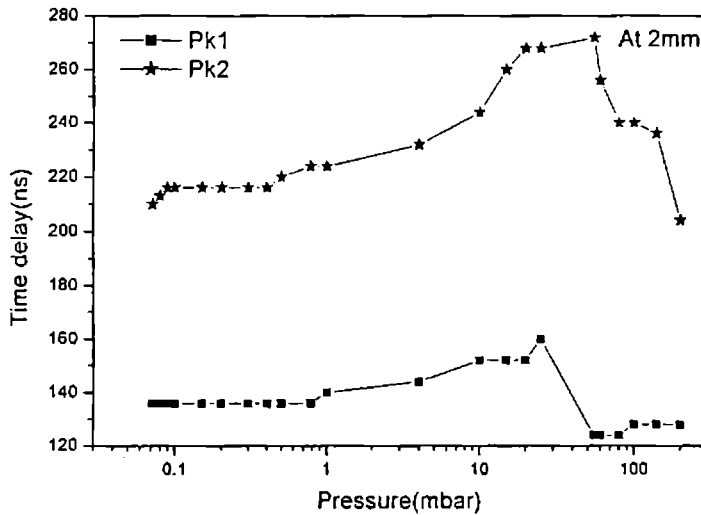


Figure 4.10 (b) : Variation of the time delay for different pressures for the two peaks (pk 1 and pk2)

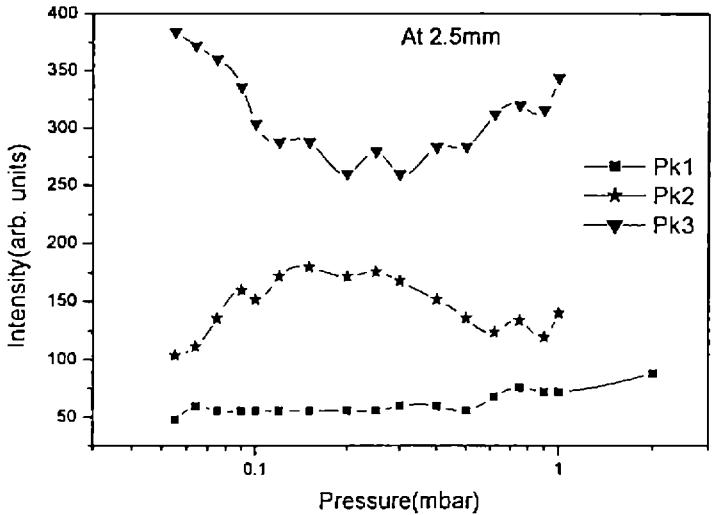


Figure 4.11 (a) : Variation of the intensities for different pressures for the three peaks (pk 1, pk 2 and pk 3)

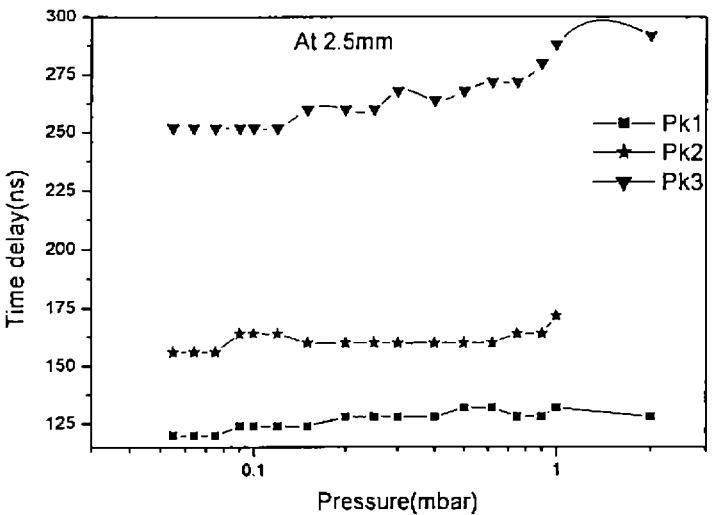


Figure 4.11 (b) : Variation of the time delay for different pressures for the three peaks (pk 1, pk 2 and pk 3)

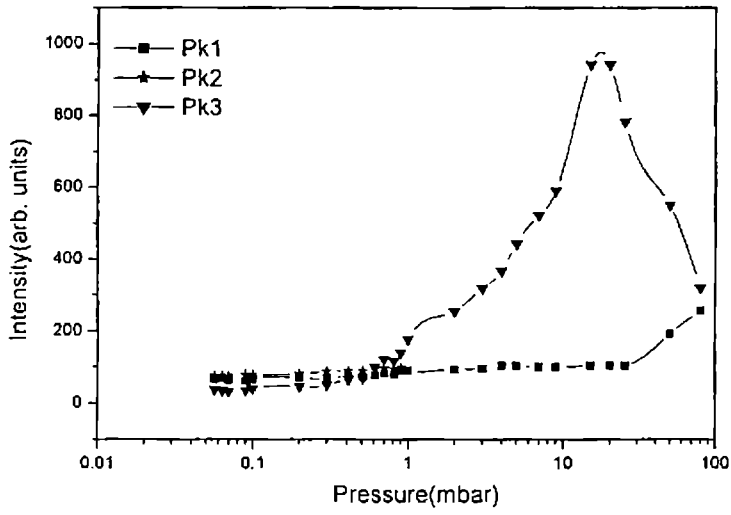


Figure 4.12 (a) : Variation of the intensity for different pressures for the three peaks (pk 1, pk 2 and pk 3)

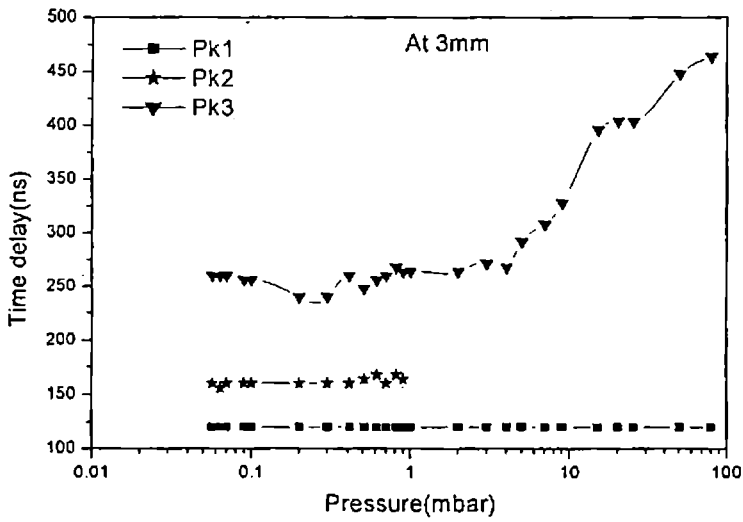


Figure 4.12 (b) : Variation of the time delay for different pressures for the three peaks (pk 1, pk 2 and pk 3)

Chapter 4

The various complex processes in the laser plasma such as plasma instabilities, chemical reactions, gas phase collisions and formation of Knudsen layer, make the temporal profiles difficult to analyse. A twin peak distribution in the temporal profile of silver atoms in vacuum has been investigated [31]. There are also reports on the twin peak distribution in the temporal profiles of ions which exist only at a particular distance from the target. The appearance of the double peak depends critically on ambient pressure and it has been reported due to the onset of Rayleigh-Taylor instability at the plasma boundary [32]. These peaks were observed in the case of singly ionized species and were absent for highly ionized species. A simple ballistic behaviour of particles cannot explain such observations which indicate the complex nature of the behaviour of constituents in the laser generated plasma.

During the expansion, plasma acts like a piston and it expands into the ambient with supersonic velocities and a shock front is generated. The pressure of the expanding plasma and the ambient pressure, equalizes at certain distances forming a well defined boundary. At this boundary, there exists a turbulent mixing of the ablation plume with the ambient gas and triggers the onset of Rayleigh-Taylor instabilities and other nonlinear processes at the boundary. The partial ionization of the vapour due to temperature increase near the shock wave front can also result in an acceleration of the flow [33]. The addition of kinetic energy to the laser-induced flow through absorption of incident laser energy will result in a moderate deceleration of the shock wave velocity than the predicted blast wave theory. Simultaneously, the part of the ablated species that collide with background gas will lose their kinetic energy. Thus, the plume itself might be split as observed by Harilal et.al.[34].

4.3.4 Ionization of the ambient molecule

The recorded spectrum of the emissions from copper plasma also contained signature of ambient ionization at high pressure in the chamber. The spatial variation of these

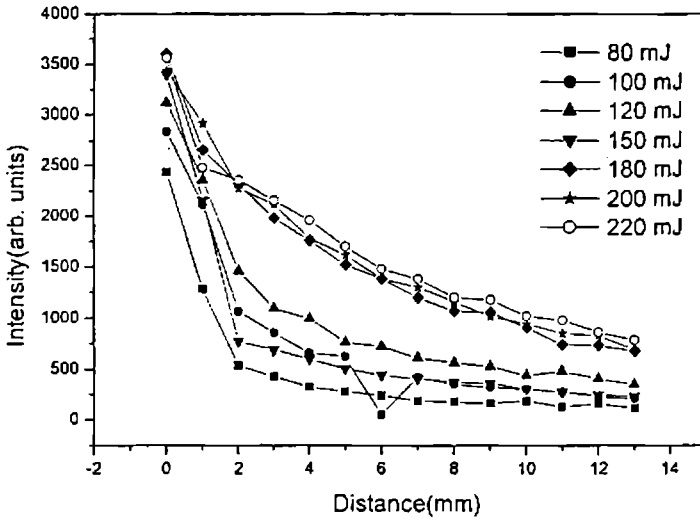


Figure 4.13 (a): Variation of the intensity of emission of 391.7 nm line corresponding to N_2^+ with distance for various laser energies.

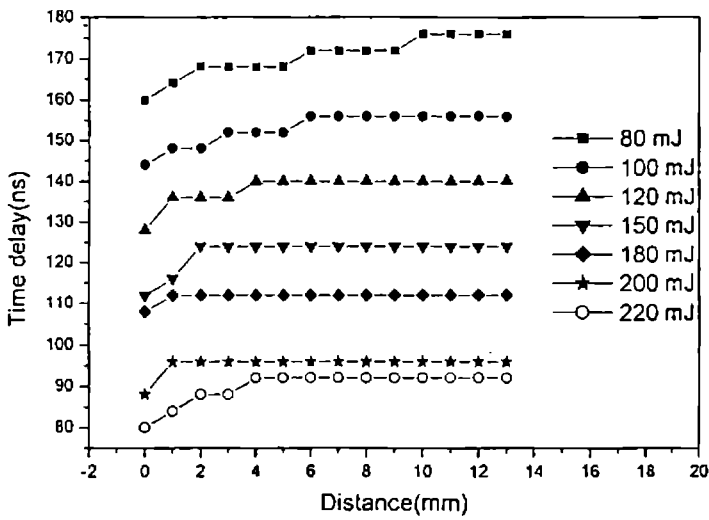


Figure 4.13 (b): Variation of the time-delay of emission of 391.7 nm line corresponding to N_2^+ with distance for various laser energies

Chapter 4

emissions corresponding to the N_2^+ transition at 391.2 nm has been investigated for different fluences of the laser pulse. Figures 4.13(a) and (b) represent the variations in intensity and time-delay for various energies of the laser pulse for different distances from the target surface. The intensities of emission are found to decrease with increase in distance from the target surface. The intensity of emission is high for higher fluences and the time delay decreases for higher fluences and remains the same for various distances from the target. These emissions corresponding to the ionization of the ambient molecule has been investigated in detail. They are found to be originating as a result of the prompt electrons produced in the plasma and by the subsequent ionization of the ambient gas molecules. Ambient ionization of various gases present in the chamber has been reported earlier by Riju et.al.[35].

There are different mechanisms by which the ambient molecules may be excited and ionized. One of the possible ways is by the absorption of ultra violet radiation arising in the plasma core. For these ionizations energies of the photons should be very high, as the ionization potentials of the ambient gases are high. Another possibility for the ionization of ambient molecules is through the direct multiphoton absorption of laser light resulting in gas breakdown. But for the case of nitrogen, for multiphoton ionization to occur, atleast 12 photons are required and hence this option could be ruled out. Another probability, which has gained lot of interest in recent years, is the ambient excitation and ionization by collisions between the ambient species and the electrons produced during the laser ablation. The energy of the prompt electron pulse is much higher than the first ionization energy of the ambient species and it is very likely that the species become ionized due to collisions [36]. Hence the observation of the ionized species could be confirmed due to presence of prompt electrons.

4.4 Summary

In this chapter, the evolution of the neutral and first ionized atoms of Cu has been investigated. Space-resolved studies of these species for different energy fluences reveal that intensities of the neutral species is found to increase and then decrease. This increase is mainly attributed to collisional recombination among the ions with electrons in plasma. Space resolved studies of the ionic species show a decrease in the intensity distant from the target. Temporal profiles show signatures of different velocity components for the plasma species. Ambient gas molecules present in the chamber is also found to be ionized and this is due to the interaction with the prompt electrons generated in the plasma.

Chapter 4

References:

1. A. Lenk, B. Schltrich and T. Witke, *Appl. Surf. Sci.* 106(1996) 473-477
2. H. Haseroth and C.E. Hill, *Rev. Sci. Instrum.* 67 (1996) 1328
3. F. P. Boody, R. Hopfl and H. Hora, *Laser Part. Beams* 14 (1996), 443
4. T. Ditmire, J. Zweiback, V.P. Yarovsky, T.E. Cowan, G. Hays, and K.B. Wharton, *Nature* 398 (1999), 489
5. Z. Andreic, V. Henc-Bartolic and H.J. Kunze, *Phys. Scripta*, 47(1993) 405-412 and references therein.
6. S.C. Miller, R.F. Haglund (eds.) *Laser Ablation: Mechanism and Applications*, Springer, Berlin 1991.
7. S.V. Gaponov, B.M. Lu, B.A. Nesterov and N.N. Salashchenko, *Sov. Tech. Phys. Lett.* 3 (1997) 234.
8. J.C.S. Kools, T.S. Baller, S.T. De Zwart and J. Dieleman, *J. Appl. Phys.* 71(1992) 4547 and references therein.
9. Y. Franghiadakis, C. Fotakis and P. Tzanetakis, *Appl. Phys. A* 68 (1999) 391
10. S. Amoroso, V. Berardi, R. Bruzzese, N. Spinelli, X. Wang, *Appl. Surf. Sci.* 127-129 (1998) 953
11. R. Jordan, D. Cole, J.G. Lunney, K. Mackay and D. Givord, *Appl. Surf. Sci.* 86 (1995) 24
12. A.V. Bulgakov and N.M. Bulakova, *J. of Phys. D: Appl. Phys.* 31(1998) 693
13. S. I. Anisimov, B.S. Luk'yanchuk and A. Luches, *Appl. Surf. Sci.* 96-98(1996) 24
14. R. K. Singh and J. Narayan, *Phys. Rev. B* 41 (1990) 8843
15. T.N. Hansen, J. Schou and J.G. Lunney, *Europhys. Lett.* 40 (1997) 441
16. T.N. Hansen, J. Schou and J.G. Lunney, *Appl. Phys. Lett.* 72 (1998) 1829
17. D. B. Geohegan and Puretzky, *Appl. Phys. Lett.* 67 (1995) 197
18. R Kelly and R W Dreyfuss, *Surf. Sci.* 198 (1998) 263
19. R Kelly and D Braren, *Appl. Phys. B* 160 (1991) 169

20. R Kelly, *Nucl. Instr. Meth. Phys. Res. B* 46 (1990) 441
21. R C Issac, K V Pillai, S S Harilal, G K BVarier, C V Bindhu, P Gopinath, P Radhakrishnan, V P N Nampoori and C P G Vallabhan, *Appl. Surf. Sci.* 125 (1998) 227
22. G. Cristoforetti, S. Legnaioli, V. Palleschi, A. Salvetti and E. Tognoni, *Appl. Phys. B* 80 (2005) 559
23. R.A. Multari, L.E.Foster, D.A. Cremers and M.J. Ferris, *Appl. Spectrosc.* 50 (1996) 1483
24. B.C. Castle, K. Visser, B.W. Smith and J.D. Winefordner, *Appl. Spectrosc.* 51 (1997) 1017
25. C. Aragon, F. Penalba and J.A. Aguilera, *Appl. Phys. A* 79 (2004) 1145
26. W. A. Weimer, *Appl. Phys. Lett.* 52 (1998) 2171
27. R. E. Russo, *Appl. Spectrosc.* 49 (1995) 14A
28. A. G. Guidoni, R. Kelly, A. Mele and A. Miotello, *Plasm. Sourc. Sci. Tech.* 6 (1997) 260
29. R. Kelly and A. Miotello, *Nucl. Instrum. Methods B* 91 (1994) 682
30. R K Singh, D W Holland and J Narayan, *J. Appl. Phys.* 68 (1990) 233
31. R.C.Issac, P.Gopinath, G.K.Varier, V.P.N.Nampoori and C.P.G.Vallabhan, *Appl. Phys. Lett.* 73 (1998) 163
32. Abhilasha, P.S.R.Prasad and R.K.Thareja, *Phys. Rev. E* 48 (1993) 2929
33. K.R.Chen, J.N. Leboeuf, R.F. Wood, D.B. Geohegan, J.M. Donato, C.L. Liu and A.A.Puretzky, *J. Vac. Sci. Technol.* 14 (1996) 1111
34. S.S. Harilal, C.V.Bindhu, M.S. Tillack, F. Najmabadi and A.C.Gaeris, *J.Phys.D: Appl. Phys.* 35 (2002) 2935
35. R.C. Issac, G.K. Varier, P. Gopinath, S.S.Harilal, V.P.N. Nampoori and C.P.G.Vallabhan, *Appl. Phys. A* 67 (1998) 557
36. R C Issac, Ph.D Thesis, Cochin University of Science & Technology, 1998

Chapter 4

Chapter 5

Studies on Hard X-ray Emission from Laser Produced Plasma

5.1 Introduction

The recent developments in high-power laser technology, especially the chirped pulse amplification technique, have led to a new class of short-pulse, high power lasers [1]. Short-pulse laser facilities operating in the terawatt range are now commercially available and a few lasers working at the 100 TW level are now in operation. A 1 PW laser was built in the Lawrence Livermore Laboratory [2] and while it has been dismantled for the construction of the Megajoule National Ignition Facility, a few petawatt facilities are in construction in Europe, Japan and the USA.

After the focusing of such high-power laser beams into focal spots of a few micrometers in diameter, the laser intensity reaches 10^{18} - 10^{20} W cm⁻² and intensities higher than 10^{21} W cm⁻² are expected in the near future. At such intensities, the typical quiver velocity of an electron in the laser field is very close to the speed of light, c , and the plasma irradiated by the laser beam is highly relativistic. In this regime, the dynamics of the electrons in the laser electric and magnetic fields and in the high-frequency and low-frequency electric and magnetic fields generated in the plasma leads to the acceleration of a large number of electrons to relativistic energies, up to

Chapter 5

tens and even hundred of mega-electron volts. Moreover, the typical current and current density in the target can be as high as 10^7 A and 10^{12} A cm⁻²[3].

The propagation of this intense electron beam inside the target leads to individual as well as collective phenomena. The energetic particles produced during laser-plasma interactions generate, via electromagnetic interaction with plasma particles, energetic electromagnetic radiation typically in the hard x-ray and γ -ray region and to a number of nuclear reactions producing neutrons, positrons and radioactive nuclei. The most important mechanism responsible for the conversion of the particle kinetic energy in electromagnetic radiation is the bremsstrahlung. Collective phenomena include the generation of intense magnetic fields, together with space-charge and inductive electric fields. These fields modify the propagation of the electron beam in the target and a significant fraction of the accelerated electrons can be focused and even guided over 'long' distances. The space-charge electric field also accelerates ion beams inside or outside the target at multi-mega-electronvolt energies.

When an intense short pulse laser is focused onto the surface of a solid target, the laser energy is absorbed within a thin skin layer. This results in the creation of dense, high temperature plasma. The physics, especially the dynamics, of such 'solid' like plasmas is the subject of great interest and is probed by various techniques [4,5]. The hot electrons in the plasma can be sub divided into two groups: thermal and suprathermal electrons. Correspondingly, the x-ray radiation generated during this interaction also has two components: thermal (soft) x-ray emission produced due to the interaction of thermal electrons with ions [6] and hard x-ray radiation produced due to the stopping energetic, fast electrons inside the solid target [7]. The fast electrons and hard-x-ray radiation are expected to last no longer than the duration of the driving short laser pulse. The interaction of high-power femtosecond laser pulses with matter is now established as a powerful technique of generating short intense x-

ray pulses with photon energies extending from a few hundreds of electron volts to the MeV region [8].

Collisional absorption mechanisms are inefficient at the intensities considered. In fact, analytical studies and numerical simulations show that in this regime collisionless processes including resonance absorption [9], vacuum heating [10] and anomalous skin-layer heating [11] play a key role in the absorption of laser energy by the target. It has been shown that these absorption processes lead to non-thermal electron distribution functions. In particular, high-intensity, ultrashort laser heating gives rise to the production of a substantial fraction of highly energetic electrons and a relatively cold background plasma. Energetic electrons give rise, via collisions with ions, to emission of high energy (up to MeV region) photons in a continuum spectrum while the background plasma accounts for keV or sub-keV line or continuum emission.

X-ray photons are emitted either by radiative de-excitation and recombination processes or by electron-ion collisions (bremsstrahlung). In particular, the duration of the X-ray pulse depends upon the transient properties of these radiative relaxation processes and upon the lifetime of energetic electrons produced during the laser-matter interaction processes. On the other hand, the properties of the radiation also depend upon the type of target used. Mass-limited targets consisting of very thin foils, in contrast with thick targets, give significant advantages in the production of short X-ray pulses.

Measurements of hard x-ray radiation provide direct information on fast electrons and possible energy deposition depth inside the solid target. Extensive investigations are presently under way the world over of the interaction between matter and intense femtosecond laser pulses with energy flux density of the order of 10^{14} Wcm⁻² and higher. This is associated with both the fundamental aspects of the

Chapter 5

behaviour of matter in ultrastrong laser fields and various applications such as the development of new sources of X-ray radiation, the study into canalized propagation of laser pulses in waveguide structures, and the laser generation of shock waves. Ultrashort X-ray generation by laser-produced plasma has also been proved to be attractive for wide range applications including time-resolved diffraction and spectroscopy studies of transient chemical and physics phenomena [12]

Novel, efficient X-ray sources have been created by supersonically heating a large volume of Xe gas and a laser-induced bleaching wave quickly ionizes the high Z-gas, and the resulting plasma emits X-rays. By this method, the production of hard x-rays is improved significantly as less energy is lost to kinetic energy and sub-keV x-rays [13]. One possible way to get higher x-ray emission is to use a prepulse [14,15]. A prepulse plays an important role by forming gaseous plasma, called the preformed plasma, before the incidence of an intense main pulse. Use of an independent ultrashort pulse as a prepulse makes it easier to adjust the parameters of the preformed plasma. By introducing an independent 100 fs prepulse, a more than 20-fold enhancement in K-shell emission from aluminium plasma has been achieved [16].

The spatial and temporal evolution of the X-ray emitting plasma has been studied by high resolution X-ray spectra, pump-probe reflection measurements, ion and electron energy measurement and so on. The time-resolved soft x-ray absorption of photoexcited silicon by means of pump-probe spectroscopy, using a picosecond soft x-ray pulse from femtosecond laser produced plasma as a probe has been measured by [17]. The x-ray conversion efficiency and emission duration has been measured by a time-resolved transmission grating spectrometer and the interaction of a high intensity sub-picosecond laser pulse with a preformed plasma was investigated by Pelletier et al.[18] The temporal and spectral profiles of the hard x-rays generated by focusing terrawatt laser on copper target and their dependence of the laser energy

have been studied by Yoshida et al.[19] using a charge coupled device and an x-ray streak camera. The K_{α} and K_{β} line emissions have also been observed along with the hard x-rays. Most of the studies have concentrated on high resolution spectra, but there is a great need to look at the total X-ray yields. X-ray yields from intense, ultra short laser driven plasmas from aluminium and silicon have been carried out by Banerjee et.al.[20] Hard x-ray yield from femtosecond laser interactions with both solid and micron-scale droplet targets have been studied and the inferred electron temperature has been found to be consistent with particle-in-cell simulations by Donnelly et al.[21] This chapter deals with the hard X-ray generated on the surface of a copper target by the irradiation of a Ti:Sapphire femtosecond laser available at the Tata Institute of Fundamental Research, Mumbai, India.

5.2 Experimental

The details of the experimental methods and the instruments used for the purpose of study of the emission from the plasma produced by the irradiation of a femtosecond laser on a copper target has been given in chapter 2. The femtosecond laser used was a custom built Chirped Pulse Amplification (CPA) system (Continuum) that uses seed pulses from a Coherent Mira Seed Ti:Sapphire laser which is pumped by a coherent innova-90/6 plus argon ion laser. The seed pulses at 806 nm, having a bandwidth of about 22 nm, are stretched and fed to a regenerative amplifier and later to a multi pass amplifier, both of which are pumped by 532 nm radiation from a 10 Hz, Surelite III-10 (Continuum) nanosecond Nd:YAG laser. The amplified pulse can finally be compressed to a duration of 100 fs. The maximum output from the laser is about 50 mJ/pulses. The femtosecond laser was focused with a lens of focal length 30 cm on a copper target kept in a chamber with a pressure of about 10^{-3} mBar. The solid target was in the form of a disc and was continuously rotated and translated using a stepper motor drive. A thin half-wave plate was introduced in the beam path to switch the polarization of the beam between horizontal (p) and vertical (s). The measurement

Chapter 5

technique is pulse height analysis common to X-ray spectroscopy. A single photon can deposit enough energy in the scintillator crystal to allow a determination of the photon energy. A large number of single photon events is then collected, resulting in a distribution which represents the X-ray spectrum. A thallium doped sodium Iodide (NaI (Tl)) scintillation detector was used for collecting hard x-ray emission in the range 30-500 keV. NaI (Tl) detectors are routinely used for gamma-ray spectroscopy because of their excellent photon yield, large interaction cross-section for γ -ray detection and reasonably good resolution. They are used to measure radiations in the range 10 keV – 10 MeV. The amplified signal was fed to a multi channel analyzer through an ADC. The pulses are height-analyzed in the MCA and are counted in different channels according to their heights. This provides the energy spectrum of the x-ray emission from the plasma.

The NaI (Tl) crystal is normally enclosed in an aluminium casing and is of about 2 inch size. This crystal is quite susceptible to the background radiation coming from the radioactive elements in concrete walls, cosmic rays, etc. To improve the signal to noise ratio, a time-gate is employed. A delay gate generator is triggered by a part of the laser pulse that produces plasma, which generates a time window of variable width. The emission is recorded only in this time window enabling almost back-ground free collection.

Pile-up effect is a major problem as far as detection of the x-ray is concerned. If two pulses are produced by the detector are overlapped, the electronics will not be able to decide the accurate pulse-height. Also, when more than one x-ray photon is incident on the crystal at the same time, such that the detector is insensitive to identify them individually, it also leads to the pile-up. The pile-up of the first kind is avoided using a spectroscopy amplifier with a low dead time to shape the pulses properly. The second kind of pile-up is reduced by using lead apertures to cut down

drastically the count rates. Further, the detectors are kept at a distance of about one meter from the plasma to reduce the solid angle for collection.

Calibration of the detector is an essential aspect of any experiment as it decides the absolute photon energy corresponding to each pulse height. Well defined emission lines from radiation sources like Co^{57} , Cs^{137} , Co^{60} , etc are normally used for calibration in gamma-ray spectroscopy. Since the best spectrometer systems show nonlinearities over a wide range of channels, it is better to use calibration peaks at various points along the measured energy range. The NaI (TI) detector was calibrated using Cs^{137} . There are two emission lines in the range considered viz. 36.6 keV and 661.6 keV. The channel numbers of the multi-channel analyzer is calibrated accordingly.

5.3 Results and Discussion

The plasma generated at the target surface is found to emit highly energetic electrons. The hot electrons generated in the laser plasma radiate via bremsstrahlung and these electrons are heated to extreme energies and the radiation emitted is also of similar energies. This radiation falls in the hard x-ray regime of the electromagnetic spectrum. Studying the hard x-ray bremsstrahlung therefore provides important information about the hot electrons that generate the radiation and their distribution in plasma. By knowing the temperature of the different hot electrons in the x-ray emission, the different absorption and acceleration mechanisms in the plasma could be explained.

The Na I (TI) detector coupled to photomultipliers is placed at a distance of about half a meter away from the target surface detected this and the signal was amplified and given to the multi-channel analyzer through an analog to digital converter as mentioned in the previous section and the energy spectrum is recorded.

Chapter 5

The solid angle subtended at the detector is around $40 \mu\text{S}$. In order to minimize the probability for pile up, the count was reduced by introducing a lead aperture in front of the detector. The lead aperture used was of 3 mm diameter and 16 mm thick. These factors take care of the piling up of the radiation by the detector. The recorded spectrum is a time integrated spectrum and it is recorded for long duration of times. In the present case, the spectrum was recorded for thirty minutes time. The spectrum recorded is a pulse height spectrum accumulated over 18000 shots by the detector. The X-ray spectrum is recorded for different polarizations of the incident laser beam. The angle of observation (the position of the detector) is also varied during the course of study.

The recorded spectra (figures 5.1-5.6) are continuous without any distinctive line structure. This indicates that x-ray emission is due to hot electron bremsstrahlung emission when hot electrons propagate in targets, as suggested by Kmetec [12]. The spectra is recorded in the 50-600 keV region from the plasma formed on a copper target at an intensity of about $2 \times 10^{16} \text{ W cm}^{-2}$, with p- and s- polarized light incident at 45° and observed at angles 45° , 90° and 135° with respect to the target surface. The angle of observation of 90° means that the detector is placed perpendicular to the target surface, i.e., it is in the direction of the expanding plasma, as the plasma expands perpendicular to the target surface and is not dependent on the angle of irradiation of the laser on the target.

The bremsstrahlung emission temperature can be measured by fitting an $\exp(-E/kT)$ to the tail of the photon distribution. The emission spectrum observed for the various configurations as mentioned above show different temperatures. The maximum temperature, 152 keV is obtained for p-polarization and for an angle of observation of 90° . It is seen that in the case of p-polarization, there are two components for the temperature, 152 keV and 45 keV. This clearly indicates that there are two different temperature components for the hot electrons emitted from the

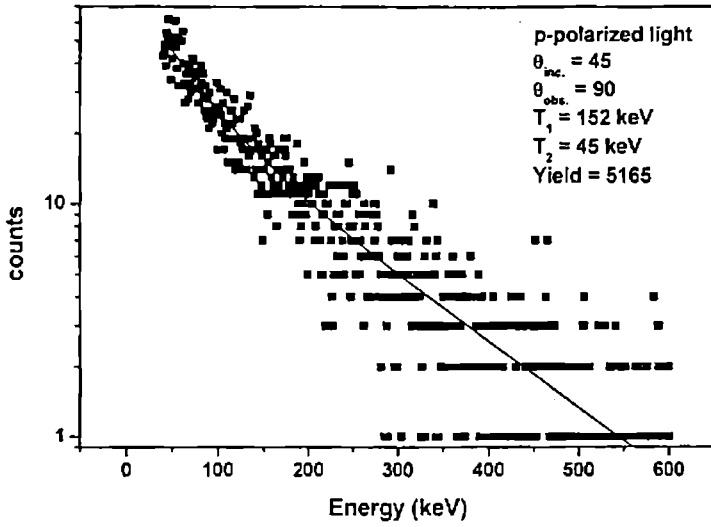


Figure 5.1: The X-ray spectrum for the incident p-polarized laser and angle of observation of 90° .

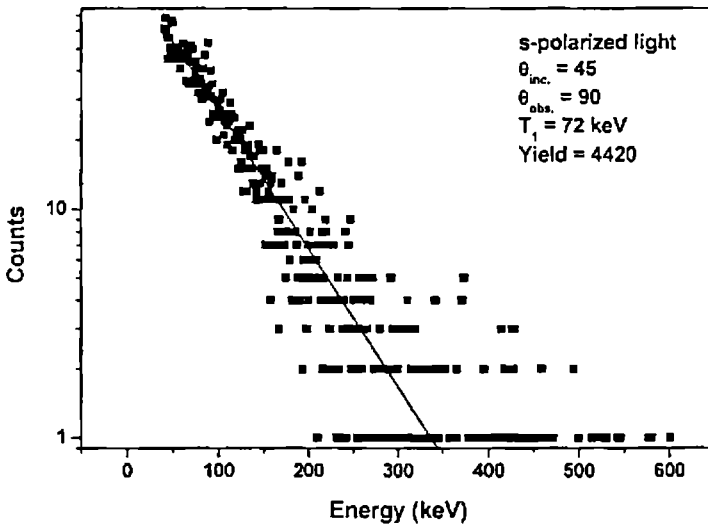


Figure 5.2: The X-ray spectrum for the incident s-polarized laser and angle of observation of 90° .

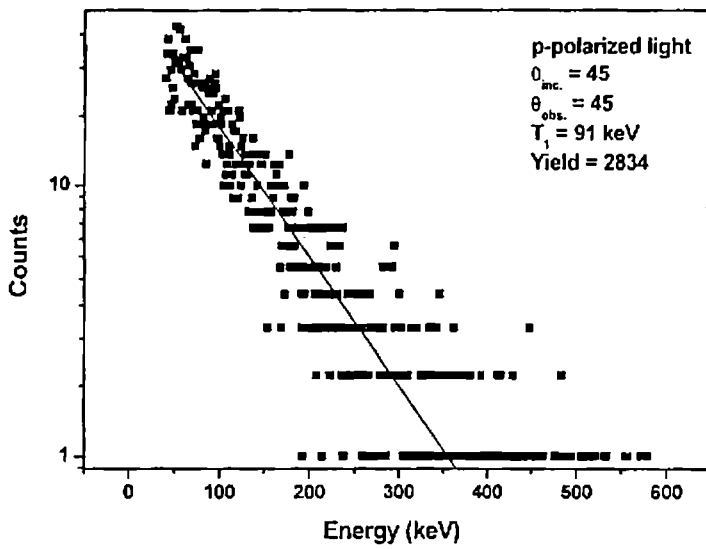


Figure 5.3: The X-ray spectrum for the incident p-polarized laser and angle of observation of 45° .

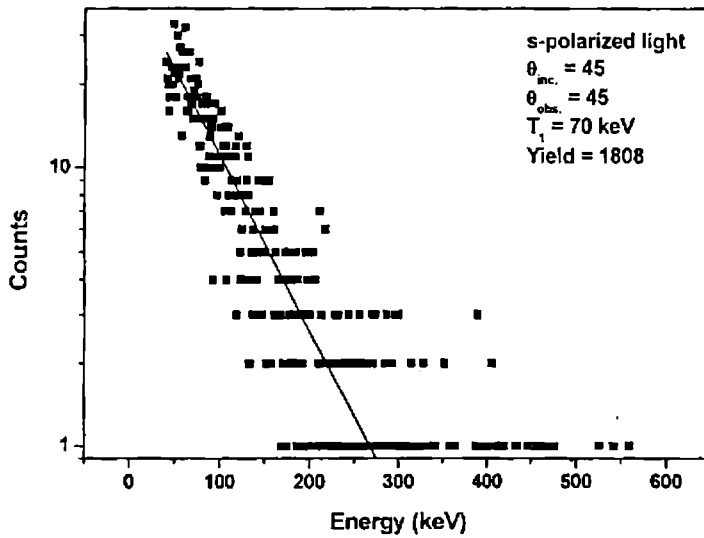


Figure 5.4: The X-ray spectrum for the incident s-polarized laser and angle of observation of 45° .

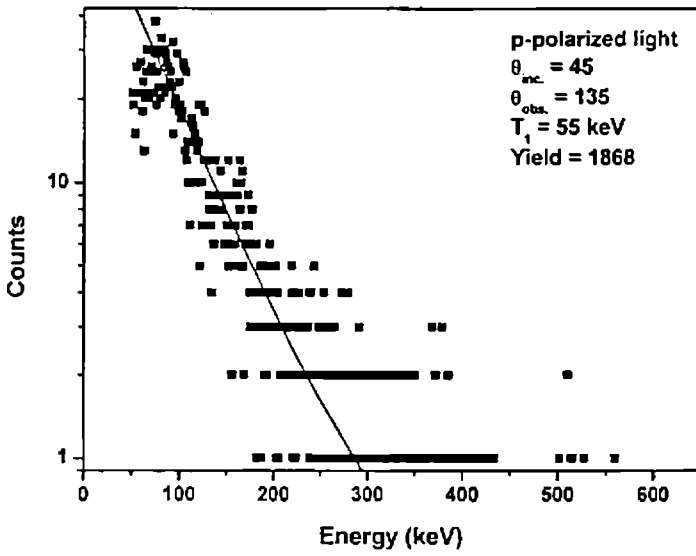


Figure 5.5: The X-ray spectrum for the incident p-polarized laser and angle of observation of 135° .

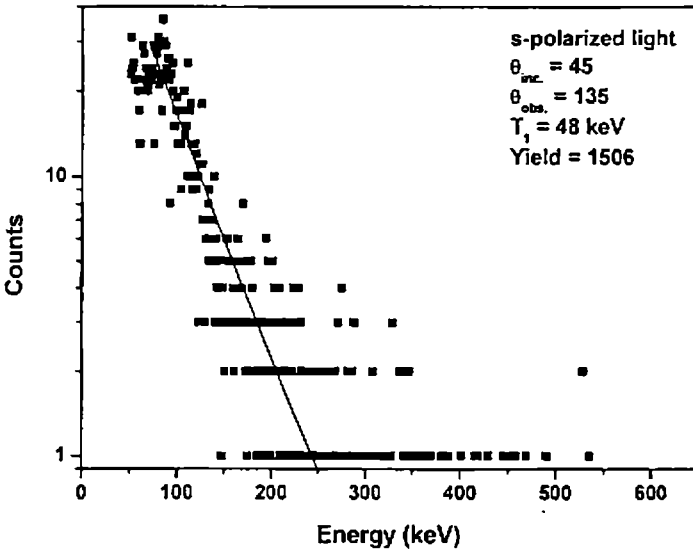


Figure 5.6: The X-ray spectrum for the incident s-polarized laser and angle of observation of 135° .

Chapter 5

plasma. But the temperature deduced for the plasma created by the s-polarized laser beam has only one component and the temperature is of the order of 72 keV. Similar values of the temperature calculated from the fit to the experimental data are given in the graphs for different polarizations and angle of observation. The yields of the x-rays are also mentioned in the graph for each case. Similar x-ray spectra have also been observed by Zhang et al [22] in copper targets for the p-polarized light with pre-pulse and without pre-pulse.

The absorption mechanisms in the femtosecond interaction regime show that X-ray emission strongly depends on the polarization of the incident laser light. The production of hot electrons in the plasma generated by high intensity lasers have been studied using computer simulations [23]. Laser radiation can be absorbed by collisionless processes, particularly by 'resonance absorption'. This is so called because it depends upon the electromagnetic fields resonantly exciting a large amplitude plasma wave which is then damped to transfer energy to the plasma. The dispersion relation for an electromagnetic wave propagating through plasma is

$$\omega^2 = \omega_p^2 + k^2 c^2$$

The local value of ω_p increases as the wave penetrates to higher density plasma until $\omega_p = \omega$. The surface at which $\omega_p = \omega$ is called the critical surface. At higher densities, k is imaginary and the wave decays evanescently since it cannot penetrate beyond the critical surface. Since $\omega_p = \omega$ at the critical surface, electromagnetic and plasma frequencies are identical there, and the electromagnetic wave resonantly excites a plasma wave, thus transferring energy to the plasma. However, this apparently simple absorption process is complicated by the plasma wave being longitudinal and the electromagnetic wave being transverse. If the electromagnetic wave enters the plasma at normal incidence, its electric field is tangential to the critical surface and cannot excite a plasma wave. A plasma wave is excited only if the electromagnetic wave

enters the plasma obliquely and with the correct polarization (called the p-polarization) for its electric field to have a component directed into the plasma.

The hot electron temperature in laser produced plasmas at higher incident laser intensity, scales weakly with both laser wavelength and laser intensity [24]. At high laser power the self-consistent steepening of the plasma density profile in which the laser penetrates to densities greatly exceeding the critical density results in resonant absorption being the dominant absorption mechanism. At the same time the electron-heating mechanism of resonant absorption allows the steepened profile to persist. In the quasi-equilibrium state this model predicts that the characteristic hot-electron energy, T_H , is given approximately(in keV) by

$$T_H \sim 14 (I\lambda^2)^{1/3} T_c^{1/3}$$

where I is the laser intensity in units of 10^{16} W/cm², λ is the laser wavelength in micrometers, and T_c is the background electron temperature in keV at the critical density.

There is a simple way to show the dependence of the resonance absorption on laser polarization. By expressing the plasma dielectric constant in terms of the electron density,

$$\epsilon = 1 - \left(\frac{\omega_p}{\omega_L} \right)^2 = 1 - \frac{n_e}{n_c}$$

The Poisson equation in a plasma, $\vec{\nabla} \cdot (\epsilon \vec{E}) = 0$, can be written as follows:

$$\vec{\nabla} \cdot \vec{E} = - \frac{\vec{\nabla} \epsilon \cdot \vec{E}}{\epsilon} = \frac{\vec{\nabla} n_e \cdot \vec{E}}{n_c - n_e}$$

Chapter 5

On the other hand, $\bar{\nabla} \cdot \bar{E} = -4\pi e \delta n_e$, where δn_e is the electron density perturbation of the plasma wave. By equating the right member of the last two equations, we have

$$\delta n_e = \frac{\bar{\nabla} n_e \cdot \bar{E}}{4\pi e (n_e - n_c)}$$

The last equation shows in particular that 's' polarized laser radiation, for which $\bar{\nabla} n_e \cdot \bar{E} = 0$, cannot drive langmuir waves, while for 'p' polarized radiation, for which $\bar{\nabla} n_e \cdot \bar{E} \neq 0$, the electron density perturbation of the plasma wave increases when the critical density is approached[25]. Resonance absorption has been studied extensively in the 1970s and 1980s with two dimensional PIC codes in order to understand the origin of fast electrons generated in nanosecond laser-plasma interactions. With the advent of short pulses, hot electrons are very much back in fashion because they generate hard x-rays as they travel through the cold part of the target behind the hot plasma where they are generated. But, resonance absorption ceases to work in its usual form in very steep density gradients. If we consider a resonantly driven plasma wave at the critical density with a field amplitude E_p , in a sharp-edge profile, there will be little field swelling and E_p will be roughly the same as the incident laser field E_0 . Electrons will therefore undergo oscillations along the density gradient with an amplitude[26]

$$X_p \approx e E_0 / m_e \omega_0^2 = v_{os} / \omega_0$$

where v_{os} is the quiver velocity, e is the charge and m_e is the mass of the electron and ω_0 is the frequency of the electromagnetic radiation. The resonance breaks down if this amplitude exceeds the density scale length L i.e. if $v_{os} / \omega_0 L > 1$.

Under these conditions, it is no longer useful to speak of electrons being heated by a plasma wave, since this wave is destroyed and rebuilt afresh each cycle. This simple fact was pointed out by Brunel [27], who proposed an alternative mechanism in which electrons are directly heated by the p-polarized component of the laser field. This mechanism known as vacuum heating is especially important when the quiver amplitude of the electrons is large and the plasma expansion is negligible. Very intense laser radiation, obliquely incident on a metallic surface or a sharply bounded overdense plasma, pulls electrons into the vacuum and drives them back into the plasma with a velocity

$$v_q = \frac{eE_L}{m\omega_L}$$

Since the electric field inside the plasma is zero, one can see that a large part of the kinetic energy acquired by the electrons in the vacuum is lost when electrons re-enter the plasma. This mechanism is more efficient than the usual resonance absorption for $v_q/\omega_L > L$, L being the density scale length. Since the absorption due to the Brunel effect is proportional to v_q/c , it plays an important role at relativistic laser intensity and is of particular interest in femtosecond interactions where sharply bounded plasmas are achieved. This, along with the space charge formed in the plasma, results in an acceleration of electrons greater than in resonant absorption. This might be the cause for the generation of the higher temperature component in the spectrum. Gibbon and Bell [28] found a highly complex transition between resonance absorption and vacuum heating depending upon the irradiance and scale length. For high irradiances and short scale lengths, the absorption saturates at around 10-15 %, but for intermediate values, the absorption can be as high as 70 %.

Chapter 5

The simplest and most obvious way to absorb electromagnetic laser energy into a plasma is collisionally. The electrons respond to the electromagnetic fields of the laser beam by oscillating at the laser frequency. The major absorption mechanism in the case of s-polarized excitation is through collisions between moving electrons and relatively stationary ions (inverse bremsstrahlung). As the collisional cross-section reduces drastically with increasing particle velocity, this absorption becomes less effective above $10^{15} \text{ W cm}^{-2}$.

We have observed that there is an increase in the temperatures of the hot electrons for the two polarizations considered and it showed the similar behaviour for the different angle of observations considered. The temperatures obtained in the case of x-rays produced with s-polarized laser are comparatively lesser than that produced by p-polarized laser. The major reason for this enhancement of the temperature is due to the different absorption mechanisms for the different polarizations of the laser pulse. The absorptions by resonant absorption and the vacuum heating for the p-polarized laser light, transfers major part of the electromagnetic energy to the electrons generated in the plasma, resulting in higher temperatures. The difference in the absorption for the two polarizations has been confirmed by the reflection studies performed for them by Teubner et al [29]. The reflected laser energy and the x-ray yield were measured for s and p- polarized laser radiation. The reflectivity was found to be more for the s-polarized case rather than the p-polarized light and the relative increase of the x-ray yield for p-polarized over s-polarized light had a maximum at an angle of incidence of 45° . If the absorption of the laser radiation were due to collision absorption, the x-ray signal would be expected to be a function of the absorbed intensity only and independent of the angle of incidence and polarization for constant absorption. Since this is not observed, non collisional, angle- and polarization dependent absorption process such as resonant absorption must contribute to the total absorption.

5.4 Summary

The hard X-ray generated from the plasma produced by the interaction of an intense femtosecond laser on a copper target is studied for different polarizations of the laser beam. The absorption mechanisms for the two polarizations viz. p- and s-polarizations are entirely different. The main absorption mechanism in the case of p-polarization is non collisional , resonant and by Brunel heating and it is collisional absorption for the case of s-polarization. The temperature of the hot-electrons produced in the plasma is high for the p-polarized case when compared to the s-polarized case.

Chapter 5

References:

1. M. D. Perry and G.A.Mourou, *Science* 264 (1994) 917
2. G.A. Mourou, C.P.J. Barty and M.D.Perry, *Phys. Today* 51 (1998) 22
3. F. Amiranoff, *Meas. Sci. Technol.* 12 (2001) 1795
4. E.M. Cambell, *Phys. Fluids B* 4 (1992) 3781.
5. M.Chaker, J.C. Keiffer, J.P.Matte, H. Pepin, P. Audebert, P. Maine, D. Strickland, P. Bado and G. Mourou, *Phys. Fluids B* 3 (1991) 167
6. M.M. Murnane, H.C. Kapteyn, S.P. Gordon and R.W. Falcone, *Appl. Phys. B: Lasers Opt.* 58 (1994) 261
7. P. Audebrt, J.P.Geindre, J.C.Gauthier, A.Mysyrowicz, J.P.Chambaret and A. Antonetti, *Europhys. Lett.* 19 (1992) 189
8. D. Giulietti, L.A.Gizzi, A.Giulietti, A. Machhi, D. Teychenne, P. Chessa, A. Rousse, G. Cheriaux, J.P. Chambaret and G.Darpentigny, *Phys. Rev. Lett.* 79 (1997) 3194
9. R.P.Godwin, *Appl. Optics* 33 (1994) 1063
10. F. Brunel, *Phys. Rev. Lett.* 59 (1987) 52
11. A.A.Andreev, et. al., *Sov Phys. JETP*, 74 (1992) 963
12. J.D Kmetec, C. L. Gordon III, J.J.Macklin, B.E.Lemoff, G.S. Brown and S.E.Harris, *Phys. Rev. Lett.* 68 (1992) 1527
13. C.A. Back et.al. , *Phys. Rev. Lett.* 87 (2001) 275003
14. D. Kühlke, U. Herpers and D. von der Linde, *Appl. Phys. Lett.* 50 (1989) 1785
15. D.G. Stearns, O.L.Janden, E.M.Cambell and J.Scofield, *Phys. Rev. A* 37 (1988) 1684
16. H.Nakano, T. Nishikawa and N.Uesugi, *Appl. Phys. Lett.* 79 (2001) 24
17. H. Nakano, Y. Goto, P Lu, T.Nishikawa and N.Uesugi, *Appl. Phys. Lett.* 75 (1999) 2350
18. J.F. Pelletier, M.Chaker and J.C. Kieffer, *J. Appl. Phys.* 81 (1997) 5980

19. M. Yoshida, Y. Fujimoto, Y. Hironaka, K.G.Nakamura, K. Kondo, M. Ohtani and H Tsunemi, *Appl. Lett.* 73 (1998) 2393
20. S. Banerjee, G.R.Kumar, A.K. Saha, L.C. Tribedi, *Optics Commun.* 158 (1998) 72
21. T.D. Donnelly, M.Rust, I Weinr, M.Allen, r a Smith, C A Steinke, S Wilks, J. Zweiback, T.E. Cowan and T Ditmire, *J. Phys. B: At. Mol. Opt. Phys.* 34 (2001) L313
22. P. Zhang, J. T. he, D.B. Chen, Z.H. Li, Y. Zhang, J.G. Bian, Wang, ,Z.L.Li, B.H. Feng, X.L.Zhang, D.X.Zhang, X.W. Tang and J. Zhang, *Phys. Rev. E* 57, (1998) R3746
23. K.Estabrook and W.L. Kruer, *Phys. Rev. Lett.* 40 (1978) 42
24. D.W. Forslund, J.M. Kindel and K.Lee, *Phys. Rev. Lett.* 39 (1977) 284
25. D. Giulietti and L. Gizzi, *La Rivista del Nuovo Cimento*, 21(10) (1998) 1
26. P. Gibbon and E Förster, *Plasma Phys. Control. Fusion* 38 (1996) 769
27. F. Brunel, *Phys. Rev. Lett.*, 59 (1987) 52
28. P. Gibbon and A.R. Bell, *Phys. Rev. Lett.* 68 (1992) 1535
29. U Teubner, J. Bergmann, B. van Wonterghem and F.P. Schäfer, *Phys. Rev. Lett.*, 70 (1993) 794

Chapter 5

Chapter 6

Conclusion and Future Scope

The interaction of laser radiation with plasma has been a subject of great interest ever since the invention of the laser in 1960. Progress in femtosecond laser technology has provided new impacts in the field of laser-plasma interaction. With the development of chirped pulse amplification and new broadband solid state laser materials, femtosecond laser pulses with peak power in the terawatt range and focused intensities greater than 10^{20} W cm⁻² can be generated with relatively small-scale, table-top laser systems. The electric field strength corresponding to such high intensities are comparable with coulomb field in atoms. As a result, atomic, molecular or any condensed form of matter is ionized very rapidly and turned into a plasma during interaction with the laser pulse. Plasma generated by such kind of a laser is a source of highly energetic electrons which generates X-rays and γ -rays.

Plasma generated by nanosecond laser irradiation contains both neutral and ionized species along with electrons. Evolution of these species has lot of applications as far as pulsed laser deposition of thin films is concerned. This thesis deals with the optical emission spectroscopic studies of the plasma generated on the surface of silicon carbide and copper targets with the irradiation of a Q-switched Nd:YAG laser. Space-resolved studies of the plasma show that in the case of SiC plasma, intensity of Si IV species is the highest in comparison with other species and it decreases with

Chapter 6

distance from the target surface. Highly ionized species are found to move faster than lower ionized species. Si IV is found to have minimum time delay and hence maximum velocity. Velocities of different species increase with laser fluence, because more electromagnetic energy is coupled to the species present in plasma. Electron density of the plasma increases to a maximum value and then decreases with time. As the density increases, it shields the laser from reaching the target and hence plasma production is reduced, thus lowering the density. As the plasma expands adiabatically, electron temperature is found to decrease with time.

Multiple peak temporal profiles are observed in the case of Cu II species in plasma generated from Cu target in certain pressure ranges. It signifies the presence of particles with velocity component directed towards the target due to shock production. This is mainly due to gas phase collisions in plasma resulting in the formation of Knudsen layer. The second and third peaks observed for Cu II species are found to transfer the energy from one component to the other for pressures in the range 0.08 - 0.8 mbar at a distance of 2.5 mm from the target surface. Signature of this transition is observed as a change in the spectral intensity. Temporal profile of Cu I species possess only a single peak structure. At high pressure, the plasma expansion follows the shock wave model whereas at reduced pressure it follows unsteady adiabatic expansion. Thus by optical emission spectroscopy, dynamics of atoms in laser generated copper plasma are studied.

Interaction of the ultra-short intense femtosecond laser on copper target yields highly energetic electrons. The hot electrons generated in the laser plasma radiate via bremsstrahlung and these electrons are heated to extreme energies and the radiation emitted lie in the hard x-ray regime of the electromagnetic spectrum. Studying hard x-rays bremsstrahlung provides information about the hot electrons produced. Hard x-rays detected are in the energy range of 50-600 keV. It is observed that the temperature of hot electrons determined using x-ray emission is different for

s and p polarizations of the incident laser beam. This can be attributed to the different absorption mechanisms taking place for the polarization state of the laser in the femtosecond regime.

Many more work can be carried out in laser produced plasma. The results presented in the thesis are mainly related to nanosecond laser based work. Interesting results may emerge on using picosecond / femtosecond laser systems, which will provide wealth of knowledge related to laser produced plasma.

~~There has been increasing~~ interest in energetic electrons generated in ultra-intense laser plasma interactions. Some of the applications are in medical imaging, microscopy, ultra fast probing of atomic structure, bench top particle accelerators, etc. Fast Igniter (FI) scheme of inertial fusion energy is an upcoming application of ultra intense laser plasma interactions. In the FI scheme, fuel is compressed with long pulses and then ignited with ultra intense laser pulses. Fuel heating and ignition are realized by energetic electrons generated in this interaction. Energetic electrons, which are usually generated around the critical density, have to propagate in overdense plasmas before reaching and heating the compressed core. The propagation of relativistic electrons in an overdense plasma is a key issue in the FI scheme.